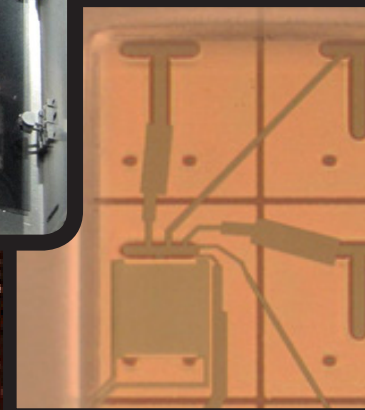
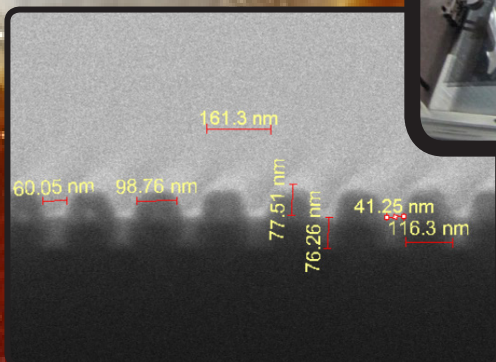
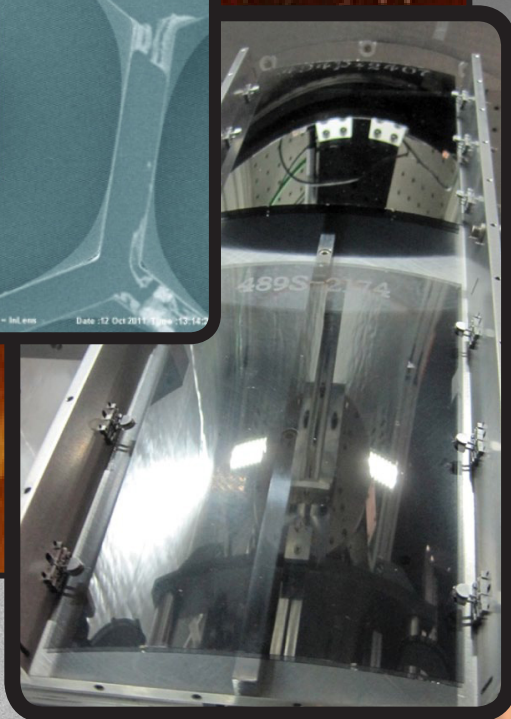
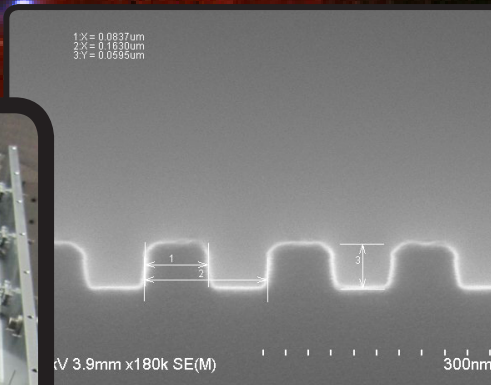
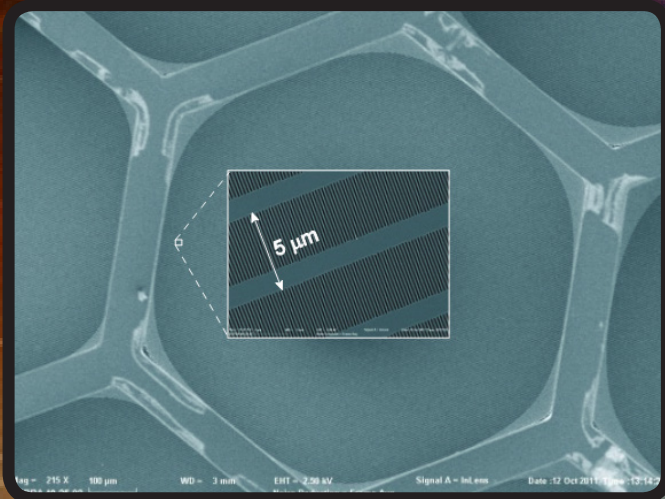


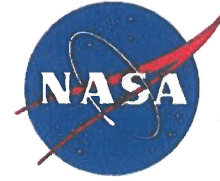
National Aeronautics and Space Administration

Technology Development Roadmap



For a Near-term Probe-class X-ray Astrophysics Mission

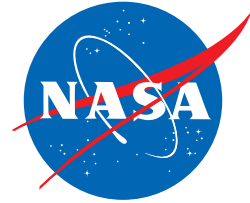
July 2013



Technology Development Roadmap Signature Page

Approved by:	<u><i>Rob Petre</i></u> Robert Petre X-ray Mission Concepts Study Scientist NASA Goddard Space Flight Center Code 662.0	<u>7/26/2013</u> Date
Approved by:	<u><i>Gerald Daelemans</i></u> Gerald Daelemans X-ray Mission Concepts Study Manager NASA Goddard Space Flight Center Code 440.0	<u>7/29/2013</u> Date
Approved by:	<u><i>Mansoor Ahmed</i></u> Mansoor Ahmed PCOS Program Manager NASA Goddard Space Flight Center Code 440.0	<u>7/29/2013</u> Date
Approved by:	<u><i>Mark Clampin</i></u> Mark Clampin PCOS Program Chief Technologist NASA Goddard Space Flight Center Code 667.0	<u>8/1/13</u> Date
Approved by:	<u><i>Thao Pham</i></u> Thao Pham PCOS Program Technology Development Manager NASA Goddard Space Flight Center Code 550.0	<u>7-29-13</u> Date
Concurrence by:	<u><i>Richard Griffiths</i></u> Richard Griffiths PCOS Program Scientist NASA Headquarters	<u>8-6-13</u> Date
Concurrence by:	<u><i>Lia LaPiana</i></u> Lia LaPiana PCOS Program Executive NASA Headquarters	<u>8/13/13</u> Date

National Aeronautics and Space Administration



Technology Development Roadmap

A Technology Development Roadmap for a Near-term Probe-Class X-ray Astrophysics Mission

Submitted to

Astrophysics Division
Science Mission Directorate
NASA Headquarters

and

Physics of the Cosmos Program Office
Astrophysics Projects Division
NASA Goddard Space Flight Center

Prepared by

Gerard Daelemans, PCOS X-ray Study Manager, NASA/GSFC
Robert Petre, PCOS X-ray Study Scientist, NASA/GSFC
Jay Bookbinder, X-ray Scientist, SAO
Andrew Ptak, X-ray Scientist, NASA/GSFC
Randall Smith, X-ray Scientist, SAO

July 2013

Contents

Executive Summary.....	1
1 Objectives.....	3
1.1 Background	3
1.2 AXSIO	4
1.3 Summary of Near-term Technology Requirements.....	5
2 Technical and Management Approach.....	7
3 Detailed Technology Roadmaps.....	9
3.1 X-Ray Mirror Technology Development Roadmap	9
3.2 Microcalorimeters Technology Development Roadmap.....	24
3.3 Off-Plane X-ray Spectrometer (OP-XGS) Technology Development Roadmap.....	38
3.4 Critical-Angle Transmission X-ray Grating Spectrometer Technology Development Roadmap.....	48
3.5 Gratings Charge-Coupled Device (CCD) Detector Technology Development Roadmap.....	55
3.6 Technology Development Costs—Summary	61
4 Longer-term Technology Needs	65
4.1 Introduction.....	65
4.2 Optics Technology	65
4.3 Detector Technology.....	69
4.4 Gratings Technology	71
5 Technology Development Management	73
6 Risk Management.....	75
7 Conclusions.....	77
Acknowledgements.....	79
Acronyms	81
References	85

Figures

- Figure 3.1–1. The hierarchical structure of a segmented design is shown. Left: mirror segment; Center: mirror module, and; Right: telescope mirror assembly. Nominally, a mirror segment is 200 mm × 200 mm; a mirror module contains ≈100 co-aligned mirror pairs (primary and secondary); and a telescope mirror assembly comprises of order 10–100 aligned and integrated modules..... 10
- Figure 3.1–2. Left and middle: In the glass slumping process, a thin float-glass sheet slumps under its own weight as the temperature ramps gradually to ~ 600°C, replicating the mandrel’s precise figure. Right: Histogram of the figure quality of 32 pairs of consecutively produced mirror segments gives a mean imaging quality of 6.5-arcsec HPD (two reflections), satisfying the allocation for making a 10-arcsec telescope. 14
- Figure 3.1–3. This schematic illustrates the mirror alignment process. The entire operation is a closed-loop operation that is controlled by a computer. After a mirror segment is installed on one of the hexapods, the software takes over to bring it into optimal alignment in a matter of minutes. 16
- Figure 3.1–4. This schematic illustrates the way each mirror segment is bonded to the module housing. a) Each mirror is bonded at six locations to the housing to give it the ability to withstand launch loads; b) a zoomed-in view of a bond; c) further zoomed-in details of a bond, consisting of three adhesive bonds: P0, P1, and P2. The nano-actuator, distance-measuring microscope, and computer are equipment used to perform the bonding and are not part of the finished mirror module..... 18
- Figure 3.1–5. Comparison of mirror characteristics before (left panels) and after (right panels) bonding. The comparison shows that the bonding process has largely preserved the figure. The difference in HPD between the free-standing mirror is about 2 arcsec..... 19
- Figure 3.1–6. This image shows alignment error as a function of time and indicates the times when P1 and P2 bonding take place. The jump of alignment error at the time of P2 bonding could be due to a number of possible causes (e.g., adhesive shrinkage during cure, causing the pins to move, or a temperature differential between the mirror segment and the structure to which the mirror is bonded). On average, the alignment error is at about 5 arcsec, which is acceptable for building a 10-arcsec telescope mirror assembly. A major objective of this effort is to understand jumps like this to minimize them and perfect the bonding process..... 20
- Figure 3.2–1. This image shows one possible configuration of the XMS focal plane array. .24
- Figure 3.2–2. This image shows a close-packed array of small pixels on a 75-micron pitch, read out with micro-strip. 27
- Figure 3.2–3. This plot shows the TDM multiplexing predicted and measured energy resolution as a function of the number of multiplexed rows using TES microcalorimeters with an energy resolution of 2.5 eV..... 28

- Figure 3.2–4. Left: The resulting MnK spectra from an 8-pixel CDM experiment using flux-couple code division multiplexing. Right: Fluxed coupled CDM circuit when just two TESs are coupled.....30
- Figure 3.2–5. This annotated photograph shows the layout of a CDM chip that incorporates 4-, 8-, and 16-row CDM readouts.....31
- Figure 3.2–6. Left: This image of a 6-pixel macro-pixel, seen from the back (looking through the nitride membrane), shows six absorbers, a single TES, and the links between them. Right: This image shows the characteristic pulse shapes that distinguish the 6 pixels. Resolutions across the 6 pixels ranged from 5.4 eV to 7.8 eV. A single pixel of the same heat capacity and TES properties would have had a resolution of about 4 eV.....32
- Figure 3.2–7. A proof-of-concept ACD for XMS, consisting of 121 TESs wired in parallel. Future iterations will cover the surface with four channels similar to this one. The prototype had a sensitivity threshold well below 6 keV, far below the level needed for detection of minimum ionizing particles, which will deposit 120 keV traversing 0.3 mm of Si.33
- Figure 3.2–8. This image shows the SRON Netherlands Institute for Space Research (SRON)/Goddard design for the focal-plane assembly for IXO/XMS. Demonstrating a flight-worthy design of these electrical, thermal, and mechanical interfaces is an important aspect of TRL-6.34
- Figure 3.3–1. Left: The off-plane grating mount. Right: Three gratings, placed many meters from the focus are shown projected onto the focal plane to elucidate the nature of the arc of diffraction which is detected by an array of CCDs depicted as squares.....39
- Figure 3.3–2. Measured diffraction efficiencies at graze angles of 2 (top row), 1.5 (middle row), and 1 (bottom row). Measurements of individual orders are shown in the left column as absolute efficiencies, which include the reflectivity of Au. Summed order efficiencies are shown in the right column. The thin, solid black line shows the total absolute efficiency of all orders, including zero order; the thick, solid black line shows the total relative efficiency which factors out the effect of the Au reflectivity.....41
- Figure 3.3–3. Scanning Electron Microscope images of the pre-master fabricated at LightSmyth. Left: Rectangular groove profile etched into the single crystal silicon substrate. Right: The silicon substrate appears black with an 80 nm coating of gold appearing gray.....42
- Figure 3.3–4. Left: Image of the first order Mg K line. Right: Histogram of all CCD counts. The red line is a best fit Gaussian to the data with a FWHM of 0.011 Å (R=900). .43
- Figure 3.3–5. Nanopositioning alignment fixture for populating off-plane grating modules. 44
- Figure 3.4–1. This schematic shows a CATXGS (not to scale). (a) Shown here is a perspective view of optical design, with X-rays incident onto the FMA from the right. (b) A side view of optical design is shown here. X-rays are focused by the telescope module onto the focus F. CAT gratings intercept a fraction of the X-rays and diffract them, predominantly at angles centered around the blaze direction. Representative paths for longer (red) and shorter (blue) wavelength rays diffracted in one order are shown. The CAT grating has high diffraction efficiency in many orders.....49

Figure 3.4–2. This image shows a CAT grating array and mounting concept and grating membrane structure.50

Figure 3.4–3. This scanning electron micrograph of the bottom of a 31 × 31 mm² deep reactive-ion etched CAT grating shows the hexagonal L2 mesh etched from the bottom and the much finer L1 supports etched from above. Inset: This zoomed-in view show the L1 lines and the 200 nm-period CAT grating bars. ... 51

Figure 3.5–1. This SEM cross-section of integrated imaging detector and readout circuitry is fabricated with MIT Lincoln Laboratory 3-D circuit integration technology. ...58

Figure 4.2–1. (a) Left – Schematic cross-section of thin piezoelectric film X-ray mirror. A low DC voltage applied across the top and bottom electrodes (green) produces a strain in the piezo film (light blue) parallel to the mirror surface (both in the plane of the page and out of the page). This produces localized bending in the structure, primarily over the extent of the individual top electrode. (b) Right – a test cylindrical mirror, 10 cm x 10 cm, with 49 piezo cells each 1 cm². The electrode side is facing up66

Figure 4.2–2. Differential deposition process67

Figure 4.2–3. The image on the left is from a flat single crystal silicon mirror 100mm in diameter and 25mm thick. The image on the right is from the same mirror after it has been light-weighted to 0.40mm thickness, a factor of more than 60 reduction. The differences between these two images show that the figure is preserved at the sub-arc-second level. The similarities between them demonstrate the validity of making extremely lightweight mirrors by polishing and light-weighting single crystal silicon, which is abundantly and inexpensively available because of the semiconductor industry.69

Figure 4.3–1. This figure shows the Moore’s Law plot for the number of TESs in a fully functioning instrument, and extrapolates the current rate of evolution for the next couple of decades.70

Tables

Table 1.3–1. Near-term Technology Needs	5
Table 3.1–1. Parameters of a “Generic” Module Used for Technology Development.....	11
Table 3.1–2. Imaging Error Allocation to, and High-Level Description of, the Three Major Steps in Constructing a Segmented X-ray Telescope.....	12
Table 3.1–3. A Brief Summary of the Elements of This Technology Development Program: Issues and Solutions That Will Be Investigated as Part of This Effort	13
Table 3.1–4. Key Parameters of the X-ray Probe Mirror Assembly	22
Table 3.1–5. X-ray Mirror Technology Development Schedule and FY13 Costs	23
Table 3.2–1. X-ray Microcalorimeter Technology Development Tasks Schedule and FY13 Costs	37
Table 3.3–1. Off-Plane Gratings Technology Schedule and FY13 Costs	47
Table 3.4–2. CAT Gratings Technology Development Schedule and FY13 Costs	54
Table 3.5–1. CCD Grating Detector Technology Development Schedule	59
Table 3.6–1. Total FY13 Costs for the X-ray Astrophysics Probe Technology Development.....	63

Executive Summary

This document presents a roadmap, including proposed budget and schedule, for maturing the instrumentation needed for an X-ray astrophysics Probe-class mission. The Physics of the Cosmos (PCOS) Program Office was directed to create this roadmap following the December 2012 NASA Astrophysics Implementation Plan (AIP). Definition of this mission is called for in the AIP, with the possibility of selection in 2015 for a start in 2017.

The overall mission capabilities and instrument performance requirements were defined in the 2010 Astronomy and Astrophysics Decadal Survey report, *New Worlds, New Horizons in Astronomy and Astrophysics* (NWNH), in connection with the highly ranked *International X-ray Observatory* (IXO). In NWNH, recommendations were provided regarding the size of, and instrumentation needed by, the next large X-ray observatory. Specifically, the key instrumental capability would be an X-ray calorimeter spectrometer at the focus of a large mirror with angular resolution of 10 arc seconds (arcsec) or better. If possible, a grating spectrometer should also be incorporated into the instrument complement.

In response to these recommendations, four instrumentation technologies are included in this roadmap. Three of these are critical for an X-ray mission designed to address NWNH questions: segmented X-ray mirrors, transition edge sensor calorimeters, and gratings. Two approaches are described for gratings, which represent the least mature technology and thus most in need of a parallel path for risk reduction. Also, while current CCD detectors would likely meet the mission needs for grating spectrum readout, specific improvements are included as an additional approach for achieving the grating system effective area requirement. The technical steps needed for these technologies to attain technology readiness levels (TRL) of 5 and 6 are described, as well as desirable modest risk reduction steps beyond TRL-6. All of the technology development efforts are currently funded through the NASA Physics of the Cosmos (PCOS) Strategic Astrophysics Technology (SAT) program; some through the end of FY13, others though FY14. These technology needs are those identified as critical for a near-term mission and briefly described in the 2012 NASA X-ray Mission Concepts Study. This Technology Development Roadmap (TDR) provides a more complete description of each, updates the status, and describes the steps to mature them.

For each technology, a roadmap is presented for attaining TRL-6 by 2020 at the latest, and 2018 for most. The funding required for each technology to attain TRL-5 and TRL-6 is presented and justified through a description of the steps needing completion.

The total funding required for these technologies to reach TRL-6 is relatively modest, and is consistent with the planned PCOS SAT funding over the next several years. The approximate annual cost through 2018 is \$8M. The total cost for all technologies to be matured is \$62M (including funding already awarded for FY13 and FY14). This can be contrasted to the \$180M recommended by NWNH for technology development for IXO, primarily for the maturation of the mirror technology.

The technology described in **Section 3** of this document is exclusively that needed for a near-term Probe-class mission, to start in 2017, or for a mission that can be recommended by the next Decadal survey committee for an immediate start. It is important to note that there are other critical X-ray instrumentation technologies under development that are less mature than the ones discussed here, but are essential for a major X-ray mission that might start in the late 2020s. These technologies, described briefly in **Section 4**, are more appropriately funded through the Astronomy and Physics Research and Analysis (APRA) program.

1 Objectives

The primary purpose of this document is to present a roadmap to bring to TRL-6 the enabling technology for a Probe-class X-ray astrophysics mission. This mission, if selected, could start in 2017. The key technology areas are identified, their status is summarized, and the steps needed to advance them to TRL-6 are listed. A schedule and budget for reaching TRL-6 is provided. If this mission were selected, then NASA can use this document as a planning tool to ensure the required technical maturity level is reached in a timely fashion.

In addition, this document describes the types of technologies necessary for strategic X-ray astrophysics missions which can be presented to the 2020 Decadal review. These technologies build upon earlier developments, but will require more time to develop to reasonable TRLs for a Decadal (assumed to be 5/6). This is not an exhaustive list, but we identify them now as a high priority; additional funding of these efforts will be important if they are to attain a sufficient readiness level for a mission starting in ~ 2025 .

1.1 Background

The purpose of the X-ray astrophysics Probe-class mission is to fulfill as completely as possible the high-priority scientific objectives identified for IXO in NWNH. These objectives include:

- tracing the orbits of accretion disk material close to the event horizons of black holes, a rare opportunity to study astrophysics in the strong-field limit;
- quantifying the growth and physics of galaxy clusters, the largest gravitating structures in the universe and a sensitive constraint on structure formation;
- measuring black hole spin, a fundamental property that can reveal how supermassive black holes grow;
- carrying out emission studies of hot interstellar medium of galaxies, exploring the physics of stellar feedback on galaxy structure, and absorption studies of the hot intergalactic medium, revealing the nature of the baryons missing from galaxies and from the baryon census;
- determining the evolution of active galactic nuclei (AGN) over cosmic time and their feedback on their environment, which shapes the properties of galaxies and galaxy clusters;
- measuring the equation of state of neutron stars, thereby providing new insights into nuclear physics in the high-density regime not accessible on Earth.

NWNH focused on the science objectives for X-ray astronomy, but in regard to the technology requirements noted that “Large-aperture, time-resolved, high-resolution X-ray spectroscopy is required for future progress on all of these fronts...” and in particular that “The key component of the IXO focal plane is an X-ray microcalorimeter spectrometer...”.

In an effort to identify a more cost-effective means to fulfill the IXO objectives, NASA commissioned an X-ray Mission Concepts Study in 2011. This study showed that a significant portion of IXO’s objectives could be fulfilled by a mission costing \$0.8–1.5B, a fraction of the \sim \$5B estimated by NWNH* for IXO. The key finding embodied in the study report is that such a notional mission is feasible for start within this decade, but only if technical risk is controlled by the prior development of key technology to TRL-6.

* Note that the NWNH cost estimate did not include the contingency of proposed descopes.

The study investigated four feasible notional missions, each of which could fulfill a substantial fraction of the IXO science, and described the essential technologies that would need to be brought to TRL-6 prior to their start. This roadmap covers the development of the optics, calorimeters, and gratings, consistent with the study report's executive summary:

“Lightweight optics is the central technological development that provides an order of magnitude more collecting area relative to existing observatories. It is fundamental to all of the notional missions as well as advancing X-ray Explorer-class missions in the near term. Progress in this area has been steady (now at TRL-4) given the available funding, but a more vigorous approach is warranted. Calorimeter detector technologies have advanced significantly through the development for Astro-H, but further array development is needed for the notional calorimeter missions. Other important technologies for the notional missions are identified, such as gratings development.”

The X-ray Mission Concepts Study Report also identifies the technology that would be needed for a subsequent strategic X-ray astrophysics mission. This technology is at a lower readiness level and requires long-term investment. Some of these technologies build directly upon the near-term technologies. The major goal for lightweight optics by the late 2020s is to improve the angular resolution by an order of magnitude to the arcsec level, a return to *Chandra* resolution but with much larger effective area per unit mass. For detectors, the goal is to expand the kilopixel calorimeter arrays into megapixel arrays over the next decade. Additionally, a long-term technology development roadmap could allow the replacement of currently available megapixel charge-coupled device (CCD) detectors by more versatile active-pixel sensor imagers with more than 10 megapixels.

The NASA Astrophysics Implementation Plan (AIP) (December 2012) references the Study report when it identifies an X-ray Probe-class mission as a candidate for a 2017 start. In preparation for the potential selection of an X-ray mission, the AIP advocates the development of a Technology Development Roadmap (TDR)[†] to guide investment in critical technology areas. The AIP states:

“To move forward with the required investment in critical technologies, during FY13 the PCOS [Physics of the Cosmos] Program Office [PO] will create a TDP that captures the costs and schedule needed to mature current technologies for both a probe-class mission that might be started this decade and for a larger mission that could be considered by the 2020 decadal survey for a start in the next decade. In the following years, the TDP will be used to guide X-ray technology investments, both through the SAT program that is competed through ROSES [Research Opportunities in Space and Earth Sciences] and through directed technology efforts. In the mid-decade time frame, the Astrophysics Division may engage the science community to refine the definition of a probe-class mission that pursues the IXO science objectives that might be started this decade, and later on to define a larger class mission that would be a candidate for prioritization by the 2020 decadal survey as either an international partnership or a U.S.-led mission.”

1.2 AXSIO

The Concepts Study identified four notional missions—three with a single instrument (a calorimeter, a grating spectrometer, or a wide field imager), along with one mission that combined a calorimeter and a grating spectrometer. A finding of the study, consistent with a conclusion in NWNH, is that the substantial share of the IXO science objectives can be fulfilled using a calorimeter plus a grating spectrometer. NWNH recommended that a calorimeter be maintained under all circumstances, and a grating spectrometer if at all possible. In recognition of these recommendations, the TDR addresses the instrument technology that would enable the two-instrument notional mission, the Advanced X-ray Spectroscopic and Imaging Observatory (AXSIO).

[†] The AIP referred to the creation of a Technology Development Plan (TDP), however a formal TDP only applies to missions at least in formulation, and therefore this document is referred to as a Technology Development Roadmap.

AXSIO, as described in the Concepts Study, will serve as the starting point of a definition study of a Probe-class mission intended for a mid-decade start. The technologies that need maturation include optics, calorimeter, gratings, and CCDs. While the mission parameters might evolve over the course of the study (e.g., the mirror effective area might shrink in order to reduce mission mass and cost), all of the technologies will be incorporated into the design, and the performance goals for the optics and instruments are unlikely to change.

AXSIO was developed before the Mission Concepts Study was initiated, in direct response to NWNH recommendations. AXSIO's flight mirror assembly (FMA) is based on a segmented Wolter-I (two-stage grazing incidence reflection) design with precision-slumped glass mirror segments, the same general approach as proposed for the IXO mirror. The mirror has an angular resolution requirement of 10 arcsec while providing 0.9 m² of effective area at 1 keV and 0.2 m² at 6 keV. The focal plane instrumentation consists of a 4 × 4 arcmin composite microcalorimeter array with <3 eV spectral resolution over at least the central half (see **Fig. 3.2-1**) plus a grating spectrometer with spectral resolution of 3000 over the 0.2–1.0 keV band.

1.3 Summary of Near-term Technology Requirements

Table 1.3-1 summarizes the key technologies needed to enable the X-ray probe. All are at or near TRL-4 and need to be brought to TRL-5 and, once the mission requirements are fully defined, to TRL-6.

Table 1.3-1. Near-term Technology Needs

Technology	Current Performance	Current TRL	Requirement	Notes
Slumped Glass Optics	11.5 arcsec for 3 segment pairs	4	8.5 arcsec per module	Angular resolution of 8.5 arcsec needed for a fully integrated system resolution of 10 arcsec
Kilopixel Calorimeter Arrays	2.5 eV with a 2 × 8 row multiplexing of sensors, one pixel per sensor	4	1) 2.5 eV with a 32-row multiplexing of sensors; 2) 6 eV four pixels per sensor in outer envelope	
Off-plane Gratings	$\lambda/\Delta\lambda=1300$	4	$\lambda/\Delta\lambda=3000$	
CAT Gratings	Resolution measurement expected in CY13	3	$\lambda/\Delta\lambda=3000$	
X-ray CCDs	0.3 Hz frame rate	5	15 Hz frame rate	The TRL for X-ray CCDs with the faster readout rate is 3.

Note: The purpose of this table is to show the key technology developments needed for each system.

2 Technical and Management Approach

NASA Procedural Requirement (NPR) 7120.5e, “NASA Flight Program and Project Management Requirements,” requires that the technology readiness level for all mission enabling technologies for a NASA mission be no lower than TRL-6 by the mission Preliminary Design Review (PDR). For a Probe-class mission, selected in 2015, it is anticipated that a PDR would be held no later than 2020.

For the technologies described in **Section 3**, which are now being funded through the NASA Headquarters (HQ) competed SAT program, day-to-day and year-to-year management is the responsibility of the respective Principal Investigator (PI), with oversight from the PCOS PO. Oversight includes bimonthly reporting on cost, schedule, and technical status by the PI. The PIs also provide a year-end summary of their progress to the PO. The PO, via its Technology Management Board (TMB), evaluates and verifies the readiness of each technology to proceed to the next level.

In the event that NASA HQ selects an X-ray Astrophysics Probe-class mission in 2015, technologies will receive their funding directly via a project office. Management responsibility for maturing them to level TRL-6 by the missions’ PDR then becomes the responsibility of the X-ray Astrophysics Probe Project Manager. Management activities will be consistent with the requirements established in NASA NPR 7120.5e; this includes the development of a mission specific TDP (which this document is not) that addresses all NASA Procedure Requirements (NPR) documents for a TDP.

For technologies that do not directly enable the X-ray Astrophysics Probe, funding to their respective PIs will continue to be competed through either the NASA APRA or SAT programs.

3 Detailed Technology Roadmaps

3.1 X-Ray Mirror Technology Development Roadmap

3.1.1 Introduction

A robust mirror technology is essential for a successful implementation of future X-ray astronomical missions. Robustness means that, in addition to meeting requirements dictated by science, such as angular resolution and effective area, it must also meet appropriate budget and schedule requirements. This subsection outlines a roadmap to develop a mirror technology that will meet the near-term objective of enabling a Probe-class X-ray mission in the mid-2010s as well as a strategic mission in the 2020s.

The state of the art of X-ray optics is represented by the three X-ray missions currently in operation: *Chandra*, *XMM-Newton*, and *Suzaku*. Each of these three X-ray telescopes occupies its own unique optimum position in terms of angular resolution and effective area per unit mass—*Chandra* for its exquisite (0.5 arcsec) angular resolution, though at a very low effective area per unit mass ($\sim 0.5 \text{ cm}^2/\text{kg}$); *Suzaku* for its extremely large effective area per unit mass ($\sim 20 \text{ cm}^2/\text{kg}$), though at a cost of poor angular resolution ($\sim 120 \text{ arcsec}$); and *XMM-Newton* for its moderate angular resolution ($\sim 10 \text{ arcsec}$) and effective area per unit mass ($\sim 3 \text{ cm}^2/\text{kg}$). Future X-ray telescopes will necessarily represent a significant advance in angular resolution and/or effective area per unit mass. The objective of this mirror technology development is to achieve *XMM-Newton*'s angular resolution at *Suzaku*'s effective area per unit mass. In achieving both of these technical objectives, the production cost per unit effective area must be minimized to enable the utilization of this technology by missions of all kinds, ranging from small Explorer missions, to medium Probe-class missions, to large strategic missions.

3.1.1.1 Strategic Considerations

In order to effectively meet the three-fold requirements of angular resolution, effective area per unit mass, and low cost, the following strategy has been adopted from the outset:

1. Adopt a segmented optical design. In this approach any mirror assembly, no matter its size, can be divided into many modules, each of which is either substantially similar or identical to others, enabling efficient management of spares and mass production.
2. Use commercially available equipment. This approach minimizes capital equipment investment and thereby reduces the mirror assembly construction cost and production time.
3. Use commercially available materials. Use of commodity-type materials, such as the Schott D263 glass sheets or single-crystal silicon, minimizes the cost of raw material.
4. Develop procedures with demonstrated consistency, repeatability, reliability, and efficiency. Each procedure involved in producing segmented X-ray optics will be repeated hundreds to thousands of times. It is essential that they are empirically repeatedly verified and optimized in reliability and efficiency. A high level of analytical understanding of each procedure must be attained so that it can be demonstrated that it has achieved the maximum efficiency possible.

3.1.2 Objectives

The objective of this development program is to produce optics scalable to an X-ray mission of any size, from small Explorer missions like NuSTAR to strategic missions like AXSIO, which can be implemented before this decade is out, to strategic missions in the 2020s and beyond. Although these mission concepts differ significantly in their capability, cost, and scope of science topics to be addressed, their X-ray mirror assemblies are very similar. The main difference lies in the number of mirror modules they require. The commonality among them is that they each will share three basic requirements: 1) as high an angular resolution as possible; 2) as large an effective area as possible for a given mass; and 3) the construction of the mirror assembly must fit within a budget and a schedule.

As shown in **Fig. 3.1–1**, the construction of any mirror assembly is reduced to three well-defined steps: 1) fabrication of mirror segments; 2) alignment and integration of a large number of mirror segments to make modules; and 3) alignment and integration of modules into the final mirror assembly. The last step—alignment and integration of modules into the mirror assembly—has been carried out for many past missions. As such, it does not require technology development.



Figure 3.1–1. The hierarchical structure of a segmented design is shown. **Left:** mirror segment; **Center:** mirror module, and; **Right:** telescope mirror assembly. Nominally, a mirror segment is 200 mm × 200 mm; a mirror module contains ≈100 co-aligned mirror pairs (primary and secondary); and a telescope mirror assembly comprises of order 10–100 aligned and integrated modules.

Therefore, the mirror technology development in this context consists of the following specific components:

1. Mirror segment fabrication
 - a. Substrate fabrication
 - b. Coating
2. Integration of mirror segments
 - a. Mirror segment alignment
 - b. Permanent bonding of mirror segments to module housing

As context for developing the various techniques, the original parameters of the Constellation-X mission, as conceived in 1998, have been used. **Table 3.1–1** lists the key parameters of a “generic” module that will be built to demonstrate technical readiness. **Table 3.1–2** presents a high-level error budget that will guide this technology development. The three major components of this technology as listed in **Table 3.1–2**—segment fabrication,

segment integration into modules, and module integration into assembly—are largely independent in the development paradigm. They can be independently developed and verified, each meeting its own precisely defined error budget and other requirements. This approach has several distinct and significant advantages:

- Techniques can be developed in parallel. Resources can be applied quickly when they are available. In cases where insufficient resources are available to pursue the three steps in parallel, they can be pursued serially.
- The interfaces among the three steps are well defined such that, when warranted, a new technique can be introduced into one step without adversely affecting the others. For example, if a better (cheaper, faster, or higher angular resolution) method is found for making mirror segments, it can be incorporated as long these mirror segments meet geometry and thickness requirements.
- At any given time these steps can be easily prioritized, depending which one is the largest contributor to the mirror assembly image quality. Resources can be applied optimally toward reducing the largest error contributor.

Table 3.1–1. Parameters of a “Generic” Module Used for Technology Development

Focal length	8400 mm
Module inner radius	100 mm
Module outer radius	250 mm
Mirror segment height	200 mm
Module axial height	450 mm (200 mm primary + 200 mm secondary + 50 mm gap between the aft end of primary and the forward end of secondary)
Number of mirror shells	~60
Angular span of module	30 degrees
Arc length of the smallest (largest) mirror segment	52 (130) mm
Mirror segment thickness	0.4 mm
Mirror segment areal density	1 kg/m ² (0.4 mm Schott D263 glass with density of 2.5 g/cm ³)
Estimated mass of fully populated module	840 kg (525 kg from mirror segments and 315 kg from module structure)

All of these parameters pertain to the original Constellation-X mission parameters as defined circa 1998.

Table 3.1–2. Imaging Error Allocation to, and High-Level Description of, the Three Major Steps in Constructing a Segmented X-ray Telescope

Major Step	Description	Objectives	
		10-arcsec Requirement	5-arcsec Goal
Mirror Segments	Each mirror segment must be good enough in every aspect: focal length, figure, and micro-roughness. It must be individually, completely, and independently measured and verified to meet all requirements.	< 7	< 3.5
Mirror Modules	Each mirror module is tested and verified to meet both performance and environmental requirements. With the segmented design, these modules are relatively small in size and can be tested with existing equipment or easily constructed facilities.	< 5	< 2.5
Flight Mirror Assembly	Each module must be accurately aligned and located to a superstructure. Mechanical, thermal, and other factors that can potentially degrade image quality must be quantified, including launch shifts, gravity release, and detector pixel size.	< 5	< 2.5
Mirror Assembly Image Quality (Half-Power Diameter)		< 10	< 5

The two examples of angular-resolution requirements may entail different methods for making mirror segments, as well as for aligning, testing, and qualifying mirror modules.

3.1.3 Development of Technical Elements

Under the three major components are several technical elements, each of which needs to be developed and perfected. **Table 3.1–3** is a breakdown of these elements and presents succinct description for each of them, including the issues being addressed.

3.1.3.1 Mirror Substrate Fabrication

Through the thermal forming (“slumping”) process, a mirror substrate replicates the figure of a forming mandrel while preserving the substrate’s original excellent micro-roughness. The substrate must meet figure, micro-roughness, and dimensional requirements. In addition, its edges must be smooth and free of micro-fractures that could propagate over time and result in breakage. The making of a substrate is a three-step process: 1) preparation of the mandrel surface, 2) slumping, and 3) cutting.

Table 3.1–3. A Brief Summary of the Elements of This Technology Development Program: Issues and Solutions That Will Be Investigated as Part of This Effort

Technology Elements	Issues	Proposed Solutions
Forming Mandrel Fabrication	Mandrel production cost; mandrel production schedule	Apply a precision wire-electric discharge machining (EDM) machining technique on commercially available and inexpensive single-crystalline silicon to make segmented mandrel blanks before fine polishing, reducing mandrel contour generation cost and time by a factor of 10 and reducing the mandrel cost by a factor of two
Mirror Substrate Fabrication	Middle spatial frequency ripples dominating imaging performance of 6.5 arcsec HPD	Use an industrial homogenizer to minimize boron nitride particle agglomeration; use a more aggressive buffing technique to remove agglomerates
Coating	Stress of magnetron-sputtered thin film causing severe figure distortion	Use atomic layer deposition (ALD) to create thin film of much lower stress; achieving simultaneous conformal coating of both sides of the mirror, resulting in stress cancellation
Mirror Segment Measurement	Figure distortion caused by gravity and frictional forces, and by thermal gradients across mirror segment	Implement a kinematic mount with minimal friction at each constraint; enclose segment in a thermal enclosure during measurement
Alignment	No significant technical issue	Further improve closed-loop operation to minimize the amount of time needed to bring a mirror into alignment
Bonding	Adhesive joints causing local and global figure distortion, and alignment shift; changing over long term and in vacuum	Use precision machining to minimize adhesive bond gaps; identify the best adhesives to achieve smallest bond gaps with acceptable stability
Design and Construction of Mirror Modules	Achieve mechanical design to minimize mass of module housing structure; match coefficients of thermal expansion between housing and mirror segments; achieve thermal design to provide required stable thermal environment with minimal power consumption	Conduct extensive finite element analysis, both thermal and mechanical, to optimize module housing design and to minimize material and fabrication cost
Testing and Qualification of Mirror Modules	Measure point-spread function; measure effective area versus energy; understand environment test results	Use an existing X-ray beam line with standard equipment; refine calibration of both relative and absolute flux; use spacecraft environments model from IXO designs

Elements highlighted blue have been accomplished and no longer represent technical challenges. The emphasis of this effort will be on other elements.

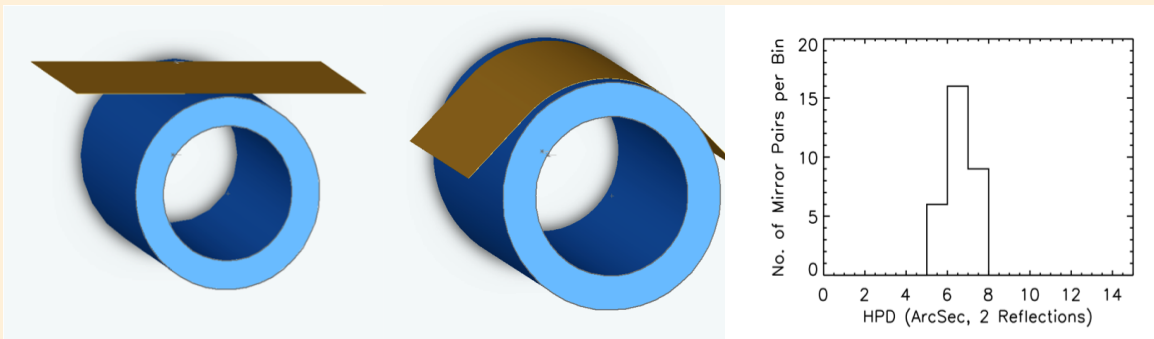


Figure 3.1-2 Left and middle: In the glass slumping process, a thin float-glass sheet slumps under its own weight as the temperature ramps gradually to $\sim 600^{\circ}\text{C}$, replicating the mandrel's precise figure.

Right: Histogram of the figure quality of 32 pairs of consecutively produced mirror segments gives a mean imaging quality of 6.5-arcsec HPD (two reflections), satisfying the allocation for making a 10-arcsec telescope.

The invention and perfection of the precision glass slumping process is one of the most significant achievements in the last decade (Zhang et al. 2003, 2011). Substrates are consistently made with 6.5-arcsec half-power diameter (HPD) (Fig. 3.1-2).

Starting with the receipt of a qualified and pristine forming mandrel, the first step of the slumping process is the application of a boron nitride release layer on the mandrel surface. Over the past decade, a “spray-bake-buff” process has been developed that coats the mandrel surface with a thin and uniform boron nitride layer that preserves the mandrel figure and provides the necessary release. Once the release layer is prepared, the mandrel and a sheet of glass are placed into an oven (Fig. 3.1-2), with a highly optimized temperature cycle that initially ramps up to approximately 600°C and then ramps back down to room temperature. The entire temperature cycle takes approximately 30 hours.

The purpose of future work in the slumping is to perfect the “spray-bake-buff” release layer application process. This process currently has two drawbacks. The first is that it takes 12 weeks from the receipt of the mandrel to the time when the release layer is smooth enough to produce 6.5-arcsec substrates. The goal is to reduce this time to 4 weeks to reduce cost. The key to reducing this time is the buffing method. Slightly more abrasive pads will be used to speed up the buffing process without introducing unacceptable scratches that could be imparted to the substrate during slumping.

The second drawback is that boron-nitride particulates are responsible for the ripples on the substrates that dominate the 6.5-arcsec HPD image. The ripples are caused by agglomeration of boron-nitride particulates during the spray process. Two methods will be used to reduce the size and the number of those agglomerates. During the spray process, an industrial homogenizer will be used to minimize or prevent the formation of agglomerates. During the buffing process, a more aggressive approach to remove them will be adopted. A moderate reduction in the size and the number of agglomerates could improve the HPD of the substrates to about 3.5 arcsec, thereby enabling the production of 5-arcsec telescopes.

The slumping process starts with an oversized glass sheet. At the completion of the slumping process, the formed glass shell needs to be trimmed to the precise design dimension. No work is planned for the next few years on cutting. It is mentioned here only for completeness.

3.1.3.2 Coating: Atomic Layer Deposition (ALD)

For the typical X-ray telescope mirror assembly covering the energy band below 10 keV, iridium is the best reflective coating. In comparison with gold, iridium increases the effective area of the same telescope mirror assembly by nearly 30% across the entire band. The drawback of iridium is that its magnetron-sputtered film stress is several times higher than that of similarly sputtered gold film, causing unacceptable distortion of the mirror segments. Over the last few years, a set of techniques has been developed to balance the coating stress of iridium using a layer of similarly coated chromium. While this technique works, it requires a delicate balance between the relative thicknesses of the two films. While this technique serves as fallback position, ALD is the preferred technique for coating these extremely thin X-ray mirror substrates.

Although it has not been used in coating astronomical X-ray optics, ALD has come of age (Maula et al. 2010). Its main advantage over magnetron sputtering is that it is totally conformal. Magnetron sputtering is a ballistic process in which the iridium atoms travel in straight lines to deposit themselves on the substrate surface. In contrast, ALD relies on diffusion and chemisorption processes to enable chemical reactions to take place on the substrate surface that leave behind a layer of iridium atoms. As a result, in a given coating run, ALD can coat a very large number of substrates; in general, this is not possible with magnetron sputtering unless the magnetron is made proportionally large. This means ALD can simultaneously coat both sides of a thin substrate with exactly the same thickness. As such, any film stress is cancelled exactly, resulting in a zero net stress on the substrates and preserving the substrate figure. Preliminary experiments have resulted in the successful ALD-coating of small glass wafers (100 mm in diameter and 0.4 mm thick) with 20 nm of the iridium film. The film has a density of 98% bulk and preserves the 4-Å micro-roughness of the float glass surface.

A series of experiments will be conducted to characterize the relatively low stress associated with ALD-coated thin iridium film in comparison with magnetron-sputtered iridium film. Then small coupons will be used to measure the extent to which the stresses of the two sides can be made to cancel each other. Finally, full-size mirror substrates will be prepared for ALD coating. The last step of the investigation will be to optimize the coating chamber's temperature and other parameters to achieve the maximum coating rate.

3.1.3.3 Measurement of Mirror Segments

Accurate and efficient measurement of all aspects of the mirror segment at every step of the process is imperative. Sufficient equipment and knowledge have been accumulated over the last decade to enable the building of 5-arcsec telescope mirror assemblies. Three challenges that the measurement process has posed and that have been addressed are: 1) how to support the extremely thin and flexible mirror segments for measurement; 2) how to measure the figure of a nearly cylindrical surface of the parabolic and hyperbolic mirrors; and 3) how to eliminate thermal disturbance caused by laboratory lighting and the presence of human beings during measurement.

Taking advantage of the near cylindrical geometry of the mirror segment, the gravity distortion is minimized by standing the mirror on one end, allowing the mirror to fully relax and hold its natural figure, while at the other end it leans against another surface so that the mirror's optical axis is close to the vertical direction. These three contact points also serve to dampen any acoustic and mechanical vibrations that are easily excited in the lightweight mirror.

A cylindrical lens system (Lehan et al. 2009, Chan et al. 2011) that converts the plane wavefront of a commercially procured Fizeau phase-measuring interferometer into a cylindrical wavefront that can be retro-reflected off the mirror under measurement has been designed, built, tested, and calibrated. Extensive ray-tracing has demonstrated that, because of the relatively small azimuth span of the parabolic/hyperbolic mirror under measurement, the wavefront error due to the intrinsic parabolic or hyperbolic shape is negligible. As such, this measurement system has enabled accurate and efficient measurement of the mirror figure. In particular, the Fizeau interferometer, using

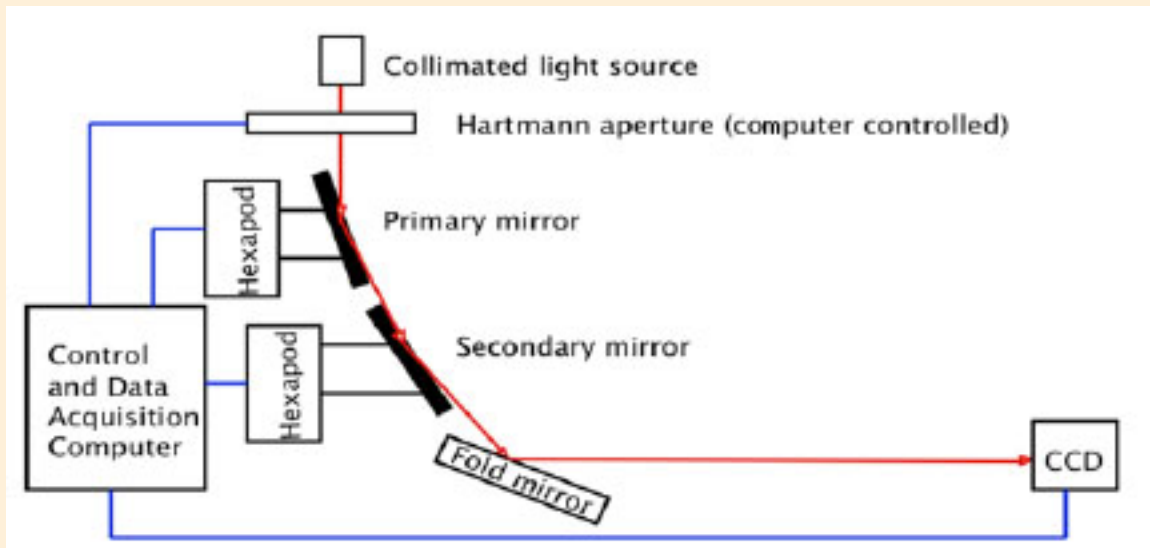


Figure 3.1–3. This schematic illustrates the mirror alignment process. The entire operation is a closed-loop operation that is controlled by a computer. After a mirror segment is installed on one of the hexapods, the software takes over to bring it into optimal alignment in a matter of minutes.

a laser source with a short (~ 150 micrometers, or μm) coherence length, is capable of measuring bare thin glass substrates.

A laboratory environment has been designed and built that thermally isolates the mirror segment under measurement from the room lighting and human body heat that can severely distort the mirror segment due to non-uniform radiative heating. This thermal isolation has enabled a high degree of figure measurement repeatability.

As of March 2012, measurement repeatability of better than 1 arcsec HPD has been achieved, which is sufficient to fully support the work of developing the technology of making 10-arcsec telescope mirror assemblies. With minor investment in this area in the next two years, the measurement repeatability will be further improved to 0.25 arcsec to prepare for future work of making better telescope mirror assemblies.

3.1.3.4 Integration of Mirror Segments into Modules

The highest priority of the mirror technology development program over the next two years is the perfection of a process to assemble individual mirror segments into mirror modules. The assembly process has proven to be a formidable challenge for three reasons: 1) the mirror segment is extremely flexible and susceptible to distortion by even tiny forces; 2) every adhesive, be it epoxy or otherwise, suffers from shrinkage during cure and is susceptible to long-term movement that is aggravated by temperature and moisture variation over time; and 3) the mirror segment, being small in thermal mass, is extremely sensitive to convection and radiative heating and susceptible to thermal distortion.

The chosen approach takes advantage of the accurate figure of the formed mirror segments. This figure is sufficiently accurate so that simply aligning the segments and mounting them in an undistorted state provides the required angular resolution (Chan et al. 2010; Evans et al. 2010). There is no need to manipulate the shape of segments to adjust the figure or the focal length (Craig et al. 2011; Freeman et al. 2010). This approach addresses the problems

posed by epoxy shrinkage by minimizing any epoxy bond line size and thickness. It does not require the precision machining of a structure for each mirror. This approach has the following salient features:

1. It realizes each mirror segment's full potential. When better mirror segments become available, this technique could be used to assemble them, leading to mirror modules with higher angular resolution.
2. Each segment is aligned and mounted independently of all others, preventing any cross talk between mirrors aligned and bonded at different times. Because each module would contain hundreds of mirror segments, its completion would necessarily take weeks. Any influence between mirror segments could be disastrous.
3. The number of mounting points (constraints) is a natural compromise between mechanical survival and optical performance. In other words, this approach does not impose additional requirements on the number of constraints for additional purposes (i.e., trying to improve the mirror segment figure).
4. Each mirror segment is in its natural and stress-free state, and thus does not impart any stress to the housing other than its own weight, which is known and whose effects can be addressed easily. This is an extremely important feature because, should a mirror segment introduce some unpredictable stress to the housing, the housing, which must be necessarily lightweight, could deform in unpredictable ways as more and more mirror segments are installed, creating an unmanageable systems problem.

3.1.3.5 Alignment

Alignment means translating and orienting the mirror segment so that, together with other mirror segments, it can form the best possible image with the largest possible photon collecting area. The alignment process is illustrated in **Fig. 3.1–3**. The mirror segment is placed on a kinematic mount, which is then placed on a hexapod to manipulate the mirror segment in all of its six degrees of freedom. The entire process is monitored and checked with a beam of light, an aperture, and a charge-coupled device (CCD) camera that are used to generate a Hartmann map after each movement. The Hartmann map is used to determine the next iteration (Saha et al. 2011). This move-and-measure process is a closed-loop operation controlled by a computer. It can align a mirror segment in a matter of minutes. This alignment process has been fully implemented and tested and requires no further development. Any work done over the next two years would be to increase its user friendliness and efficiency.

3.1.3.6 Bonding

The bonding process, which is the crux of the assembly process, begins after the Hartmann tests have determined that the mirror segment has achieved optimum alignment. It must fulfill several requirements. First, it must mechanically fasten the mirror such that it can withstand launch loads. Extensive analysis, in combination with experimental tests, has determined that each mirror segment needs to be firmly bonded at six locations, three on each side, as shown in **Fig. 3.1–4(a)**. This bonding configuration has the added advantage of minimizing gravity distortion when the mirror is tested in a horizontal X-ray beam. Second, the bonding process must not move the mirror segment. Third, the bonding process, when completed, must not distort the mirror segment. In summary, the bonding process must over-constrain the mirror segment, yet it must not disturb its alignment nor distort its figure. A three-step process, illustrated in **Fig. 3.1–4**, has been developed that meets these requirements.

The bonding process connects an optically precise and delicate mirror segment to an imprecise module housing. The process and mechanism shown in **Fig. 3.1–4(c)** have been designed to establish this connection accurately, efficiently, and inexpensively. It has three adhesive bonds, designated P0, P1, and P2, all shown in red.

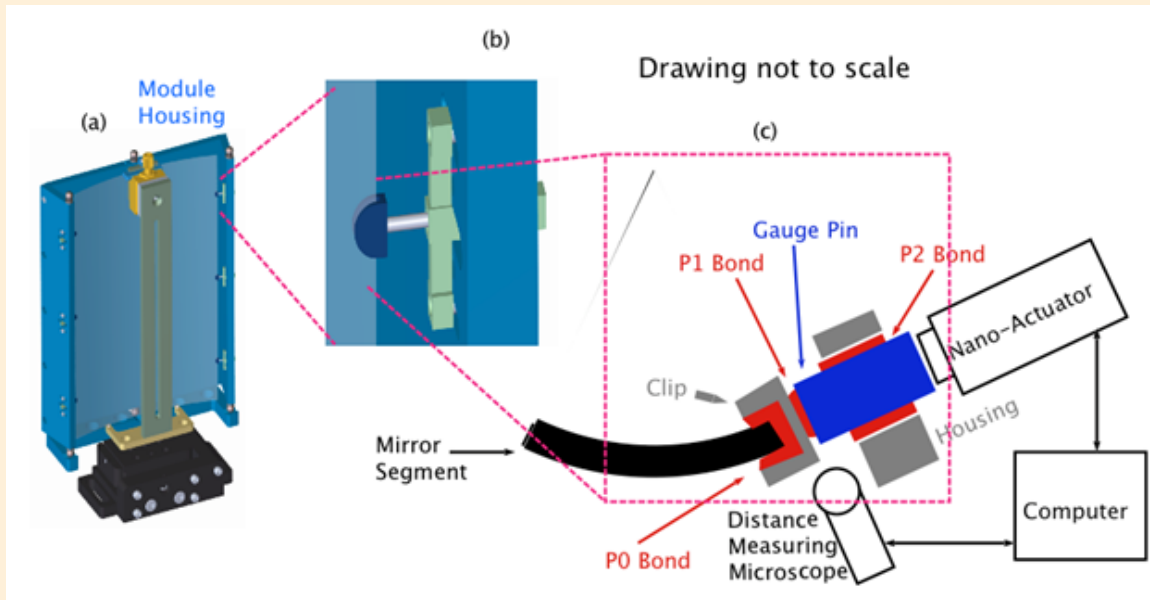


Figure 3.1-4 This schematic illustrates the way each mirror segment is bonded to the module housing. a) Each mirror is bonded at six locations to the housing to give it the ability to withstand launch loads; b) a zoomed-in view of a bond; c) further zoomed-in details of a bond, consisting of three adhesive bonds: P0, P1, and P2. The nano-actuator, distance-measuring microscope, and computer are equipment used to perform the bonding and are not part of the finished mirror module.

P0 Bonding. The first step of the bonding process, which takes place as part of the mirror segment qualification process, is the attachment of six U-shaped clips to the edges of the mirror segment. These clips serve as the interface between the housing and the glass, performing the important function of diffusing and distributing stress. Once the segment is qualified optically, the six clips are attached with an adhesive. After the adhesive cures, the mirror segment is measured again to ensure that the clips and their bonding have not caused unacceptable distortion. Experience has shown that several factors are crucial in preventing any distortion: 1) the U-shaped gap should be as small as possible to minimize the amount of adhesive needed to fill it; 2) the mirror segment should be as centered as possible inside the U gap, such that there is approximately an equal amount of adhesive on either side of the mirror segment to balance any stress that the adhesive exerts on the mirror; and 3) the material of which the clips are made should have the same coefficient of thermal expansion (CTE) as the glass. This is important because the mirror segment and the clips need to be thermal-cycled to an elevated temperature to ensure full cure and to minimize the probability of adhesive creep that could cause alignment and figure change over time.

P1 Bonding. After the P0 adhesive bonds have fully cured at an elevated temperature and the figure of the mirror segment has been verified, the mirror segment is delivered to an alignment facility to be aligned and bonded into a module housing. The first step there is to attach a gauge pin to each of the six clips. Each gauge pin is inserted into a bushing that is part of the housing structure, shown in gray in Fig. 3.1-4(c). The interior of the bushing is lapped to be extremely smooth and holds the gauge pin with a clearance on the order of several micrometers. The gauge pin, which is very smooth and precise in diameter, can slide with minimal friction. A small bead of adhesive is applied to the head of the gauge pin. Surface tension causes the adhesive to wet and cover the entire end surface of the pinhead. The pin is then pushed using a nanoactuator until the adhesive comes into contact with the clip. (The entire operation is monitored with a microscope that measures the gap between the tip of the pin and the

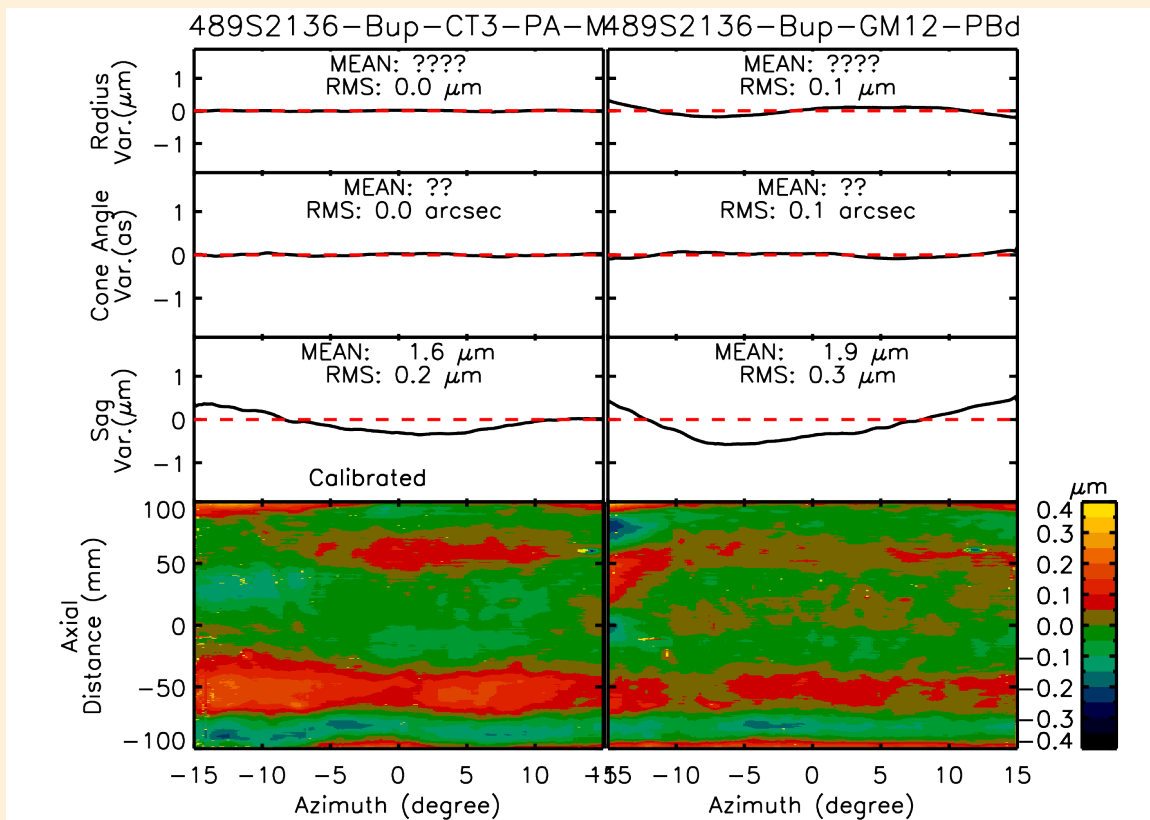


Figure 3.1-5. Comparison of mirror characteristics before (*left panels*) and after (*right panels*) bonding. The comparison shows that the bonding process has largely preserved the figure. The difference in HPD between the free-standing mirror is about 2 arcsec.

clip surface to which the pin is to be bonded.) As it cures, the adhesive shrinks and pulls the gauge pin inside the bushing. Shrinkage of the adhesive, which happens only in the direction in which the pin can slide, does not affect either the alignment or the figure of the mirror segment because the force the pin and adhesive can exert on the mirror is rather small, measured to be on the order of tens of micro-Newtons.

P2 Bonding. After the adhesive that attaches the pin to the clip has fully cured, a small amount of adhesive is wicked into the clearance between the pin and the bushing to lock the pin. This adhesive must be very thin and have very low viscosity so that the capillary action can take place easily with the minimal clearance. As it cures, the adhesive has the potential to wriggle or otherwise move the pin, causing alignment change. The magnitude of the alignment change depends on the clearance. During the last several months, this clearance has been reduced from about 50 μm to less than 5 μm , resulting in significantly reduced alignment change. Further reduction to achieve a clearance of about 2 μm , which simulations have shown to be adequate for making 5–10 arcsec mirror modules, will be accomplished by precision lapping the bushing and polishing the gauge pin.

The entire mirror segment bonding process has been designed to permanently attach the mirror segment to the housing at six locations with minimal disturbance, in terms of either force or displacement. Over the past year, the process has been continuously improved to reduce potential forces on, and displacements of, the mirror segment. Two parallel sets of bonding trials have been conducted with results compared. In the first set, the bonding process is conducted in front of a Fizeau interferometer that can measure figure change. In the second set, the bonding

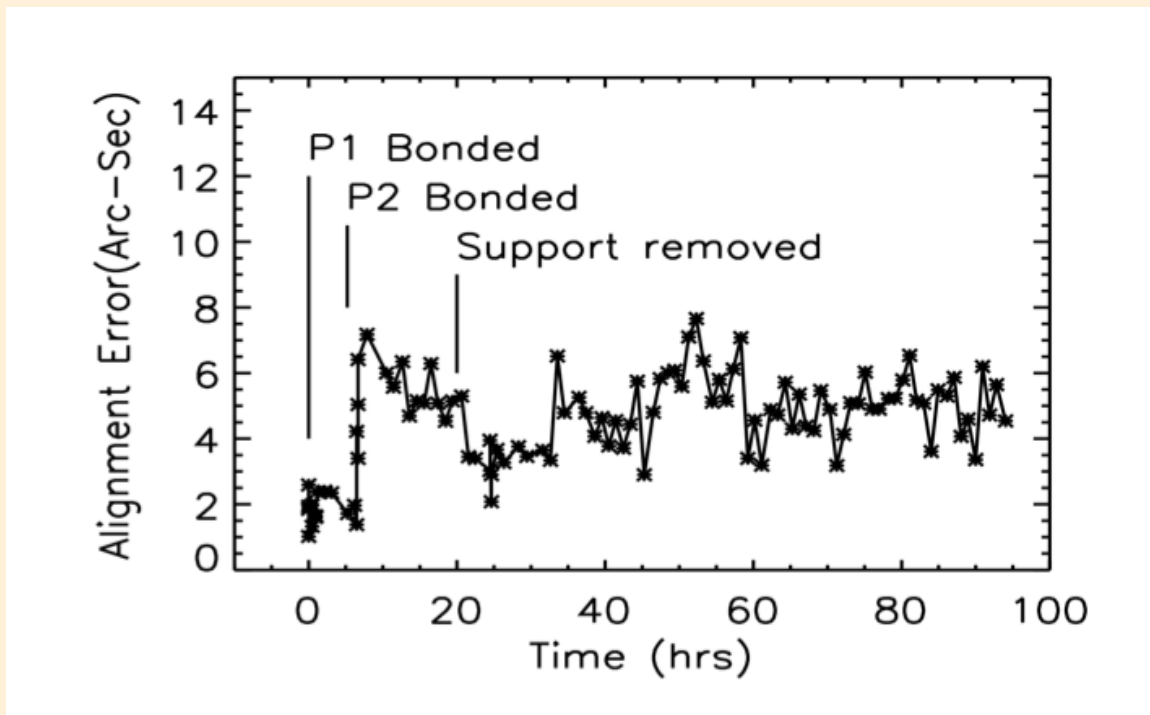


Figure 3.1-6 This image shows alignment error as a function of time and indicates the times when P1 and P2 bonding take place. The jump of alignment error at the time of P2 bonding could be due to a number of possible causes (e.g., adhesive shrinkage during cure, causing the pins to move, or a temperature differential between the mirror segment and the structure to which the mirror is bonded). On average, the alignment error is at about 5 arcsec, which is acceptable for building a 10-arcsec telescope mirror assembly. A major objective of this effort is to understand jumps like this to minimize them and perfect the bonding process.

trials are conducted in the alignment beam, where any change in mirror segment alignment can be instantly measured and recorded. Recent results are summarized in **Figs. 3.1-5** and **3.1-6**, which show both the significant accomplishments and the problems that must be solved in the next two years to make this technology ready for building 8.5-arcsec telescope mirror assemblies.

Figs. 3.1-5 and **3.1-6** show success in permanently bonding mirror segments and preserving both their figure and alignment to a level that is almost acceptable for making an 8.5-arcsec telescope mirror assembly; however, they also show that the bonding process introduces figure and alignment errors. For example, in **Fig. 3.1-5**, the average sag of the mirror segment changes by $0.3 \mu\text{m}$ as a result of the bonding process, which translates into a 2-arcsec contribution to the imaging error. **Fig. 3.1-6** show the bonding of P2 causes a jump of 4 arcsec in alignment error. Numerous trials of the bonding process have shown that both of these features are repeatable. These features have been correlated with the use of adhesive and temperature variation before and after bonding. A primary task that will be undertaken is to minimize the size of all the adhesive bonds and improve the thermal stability of the bonding environment.

The highest priority in the next two years is the continued improvement of the mirror bonding process. More resources, both intellectual and financial, will be devoted to this part of the development program than to any other part because this is the linchpin between good individual mirror segments and a good mirror module. This

work will be to first perfect each of the three bonding steps (P0, P1, and P2) and then automate the entire bonding process to minimize human involvement. Automation is necessary for two reasons. First, the presence of humans near the mirror segments and mirror modules creates a thermal disturbance. Given the small thermal mass of the mirror segment relative to its surface area, a small amount of radiative thermal flux can severely distort its figure. Second, the task of bonding requires a level of mental concentration and manual dexterity that is difficult for a person to sustain over a long period of time, which would be required for building the many modules for a spaceflight mission.

3.1.4 Demonstration for X-ray Probe

The segmented glass mirror technology is expected to reach TRL-5 by the end of 2014. The difference between TRL-5 and TRL-6 lies in specificity and fidelity. TRL-5 is somewhat generic, demonstrating that all of the technological components have been shown to work and meet generic performance, environment, as well as notional budgetary and schedule requirements. TRL-6, however, means that all specific requirements imposed by a specific mission and mission design must be met. **Table 3.1–4** list all of the requirements specific to AXSIO (assumed to be representative of an X-ray probe-class mission). The intent is to build a mirror module that meets all of these requirements. In principle, such a module could be used for spaceflight, if it is desirable.

The demonstration of TRL-6 is anticipated to take two years, assuming adequate funding. At the end of the two-year period, the following will have been achieved:

1. Have at least one mirror module that meets performance requirements after environmental tests;
2. The module(s) will have passed all environment tests at levels that are defined for an X-ray probe's specific spacecraft design and launch vehicle;
3. The process of constructing these modules will allow for an accurate and reliable cost and schedule estimate for building the entire mirror assembly. As such, all of the technical and budgetary risks associated with building a flight mirror assembly will have been retired.

Given that the mirror assembly construction and calibration would most likely be on the critical path of the X-ray probe implementation schedule, it is necessary for the TRL-6 work to be completed before the end of Phase-A so that all of the flight implementation work can start at the beginning of Phase-B. This is somewhat earlier than other components of the mission, which, in principle, do not have to reach TRL-6 until the end of Phase-B.

3.1.5 X-ray Mirror Schedule and Costs

Table 3.1–5 shows the schedule for the slumped glass mirror technology development tasks as well as the yearly estimated costs.

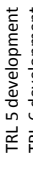
Table 3.1–4. Key Parameters of the X-ray Probe Mirror Assembly

Top-level requirements derived from science capability	
Mirror effective area at 1 (6) keV	0.9 (0.2) m ²
Angular resolution (HPD)	10 arcsec in 0.1–7 keV band
First level requirements derived from preliminary mission design	
Focal length	10,000 mm
Outer diameter	1800 mm
Mirror assembly height in axial direction	500 mm
Second level requirements derived from top and first level requirements	
Mirror segment height (P or H only)	200 mm
Number of mirror shells	227
Third level requirements derived from third level requirements	
Total number of mirror modules	36 (12 inner, 24 outer)
Inner (outer) radius of inner module	170 (535) mm
Number of shells in inner module	145
Inner (outer) radius of an outer module	535 (900) mm
Number of shells in an outer module	82
Mass allocations that meet all above requirements	
Total mass of mirror assembly	~600 kg
Mass of mirror segments	~300 kg
Mass of structure	~300 kg
Mass of an inner module	~18 kg total (~10 for mirror segments, ~8 for structure)
Arc length of the smallest (largest) mirror segment of inner module	~88 (~278) mm
Mass of an outer module	~10 kg (~6 for mirror segments, ~4 for structure)
Arc length of the smallest (largest) mirror segment of outer module	~140 (~236) mm
Mirror segment areal density	<1 kg/m ²
Mirror segment geometric thickness (assuming D263 glass or silicon density ~2.5 g/cm ³)	~0.4 mm

Table 3.1–5. X-ray Mirror Technology Development Schedule and FY13 Costs

Task		2013	2014	2015	2016	2017	2018	2019
Substrate	Slumped Glass	Mature technique at 6" Level for each pair of substrates to meet 10" mission requirements						
	Coating							
Mirror Segment	Magnetron Sputter	Experiments to determine which of the two is better; Downselect one to pursue	Develop the selected method to meet 10" mission requirements					
	Atomic Layer Deposition							
Alignment		Improve thermal control to 0.5 degrees C over a week	Improve thermal control to 0.1 degrees C over a week					
	Bonding	Improvement of edge-bonding to meet 10" mission requirements	Investigation & downselect between edge-bonding and kinematic bonding					
Module Design, Analysis, Testing		Achieve TRL-5 for making modules meeting 10" mission requirements						
				Achieve TRL-5 for making modules meeting 5" for mission performance margin				
Budget Estimate		\$1.9M	\$2.3M	\$2.3M	\$4.0M	\$4.0M	\$4.0M	

 SAT already awarded
 New funding required

 TRL 5 development
 TRL 6 development
 Risk reduction/performance margin increase

3.2 Microcalorimeters Technology Development Roadmap

3.2.1 Introduction

The ability to perform broad-band imaging X-ray spectroscopy with high spectral and spatial resolution was an essential capability of the IXO mission concept. The enabling transition-edge sensor (TES) technology that was the basis for the IXO X-ray Microcalorimeter Spectrometer (XMS) instrument then became the baseline for the XMS of the *Advanced Telescope for High Energy Astrophysics (Athena)*, and is now the baseline for the XMS for an X-ray probe calorimeter mission. The configuration of the focal plane array is shown in **Fig. 3.2–1**.

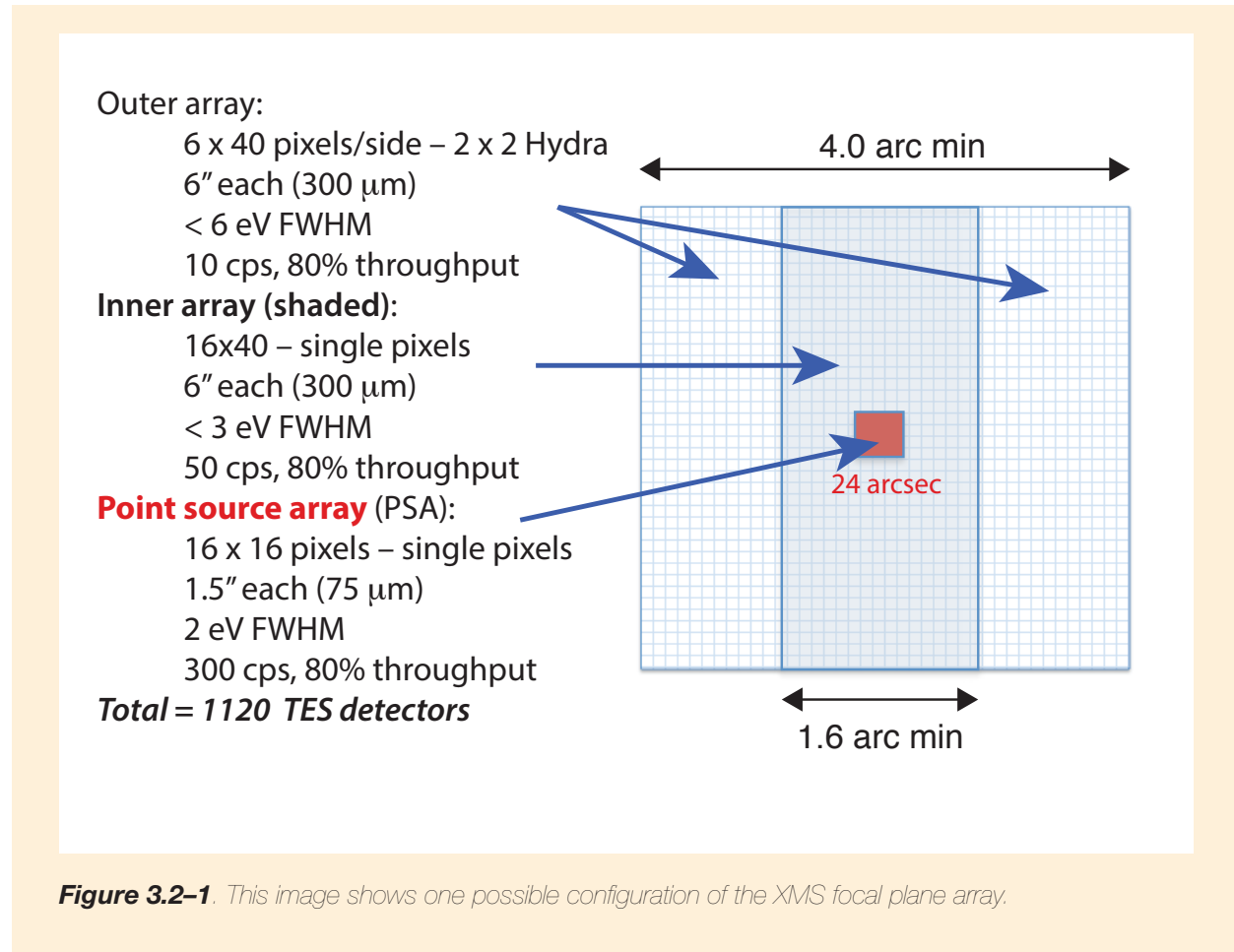


Figure 3.2–1. This image shows one possible configuration of the XMS focal plane array.

This configuration scales back from the previous IXO XMS design in that it has approximately half the number of TESs and is therefore cheaper to read out and acquire data from. A point source array (PSA) has been introduced at the center of the array. This is a valuable new attribute, motivated by the development of this type of array design for solar physics, allowing extremely good energy resolution and high count-rate capability when looking at point sources focused at the center of the focal plane array. The main array of 40 × 40 pixels consists of single pixels with better than 3 eV energy resolution and 4-absorber Hydras (4 pixels connected to a single TES), with better than 6 eV energy resolution. All absorbers in the main array are the same size, and all pixels in the main array are fabricated on a single silicon substrate.

The TRL for the fabrication and readout of the main array is comparable to that of previous XMS designs. There is a small difference in that the individual pixels are assumed to be on the same substrate as the Hydras. This is not expected to introduce any new technical hurdles because the absorber fabrication and silicon-etching processing are the same for both styles of pixel. The fabrication of the PSA is at a similar TRL as the main array, but the readout requires further extensions of present capabilities and is thus currently at a lower TRL than for the main array.

The other main components of this XMS are the particle anti-coincidence veto and the focal plane assembly that houses the detectors and cryogenic components of the readout. The TRLs of all these detector components and a roadmap for advancing them through this decade are outlined in **Section 3.2.3**. The plan to advance the TRL of the main array and its readout to TRL-5 by 2015 is described in **Section 3.2.3**, as is a technology development roadmap for the other components.

3.2.1.1 Background

An X-ray microcalorimeter measures the heat from the thermalization of an individual X-ray photon. At low temperatures, with low total heat capacity and a sensitive thermometer, extremely high energy resolution can be obtained. A superconducting TES thermometer is operated in the narrow temperature range between the onset of resistance and the fully normal state. The leading groups use a superconductor/normal-metal bilayer and tune the critical temperature (T_c) by choice of the layer thicknesses, typically aiming for $T_c \sim 0.1$ K. Resistance changes are measured by monitoring the current through a voltage-biased TES using a superconducting quantum interface device (SQUID) ammeter. The use of multiplexed SQUID readout enables kilopixel-scale arrays to be instrumented with of order 50 electronics channels. The “detector system” is the integration of the TES array and its SQUID readout. This is the technology unit that is the subject of this development roadmap. The cooling system is not addressed because options exist that are already sufficiently advanced.

3.2.1.2 Strategic Considerations

The designation of a TRL is not an absolute judgment; it depends on the intended end use. For low TRL, the range of applications can be extremely broad, but it narrows as a technology ascends the ladder to TRL-9. For the mid-range TRLs, the technology should be evaluated based on a family of related instruments with similar requirements. For this roadmap, the name of that family of instruments is XMS. XMS is the working name for the TES instruments of several mission concepts that have been developed as part of the parallel NASA effort to achieve some of the science goals of IXO at lower cost. Of all of these notional instruments, the *Athena* XMS is the least demanding of the TES detector-system technology. However, each of the others has a core that is similar to the *Athena* 32×32 array (0.25 mm pixels, 3 eV FWHM, 50 events/s/pixel) that is augmented by technology enhancements that extend the capability of the instrument. Detailed technology roadmaps were developed for the XMS of both Constellation-X and IXO (Kilbourne and Dorise 2010). Now that there are several XMS concepts, a working XMS development roadmap for the near-term has to serve two purposes: 1) It needs to promote the technology readiness of the core array technology; 2) It must also facilitate the advancement and integration of new technologies, such as the PSA, identified as enabling substantial simplifications or enhancements.

3.2.2 Objectives

Advancing a TES calorimeter system in an XMS-like configuration to TRL-6 requires technical development on multiple fronts. One of the main design drivers of the current X-ray probe focal plane array design is to allow for a large number of pixels while still limiting the number of readout channels. This is highly beneficial in terms of reducing the cost and complexity of the electronics. The key individual components of the XMS that require further development are described in detail in **Section 3.2.3**:

1. The main array: both the inner and outer arrays, with different pixel sizes.
2. The small-pixel point source array: small pixels capable of accommodating high count-rates.
3. Hydras: position-sensitive pixels that effectively couple multiple pixels to a single thermometer.
4. Multiplexing approaches: various approaches involving “time-division” and “code-division” multiplexing that will evolve sequentially. This will advance the capability of reading out multiple TESs through a single electronics chain, while maximizing the spectral resolution. The multiplexed read-out for all the different pixels types need to be developed.
5. Anti-coincidence detector: decreasing the particle background with minimal impact on the system complexity and efficiency. Such a focal plane assembly represents the TRL-6 demonstration.

These components must then be integrated into a focal plane assembly that meets the XMS performance requirements and survives environmental qualification.

3.2.3 Technical Status

3.2.3.1 Main Array

The requirements for the AXSIO main array define the main technology-development roadway and the placement of the TRL-5 milestone on that road. The reference design consists of an array of molybdenum gold (Mo/Au) TES thermometers with close-packed bismuth gold (Bi/Au) thermalizing X-ray absorbers on a 0.30 mm pitch. Each pixel is fabricated atop a silicon-nitride membrane that provides a controlled thermal link to the heat sink. In the baseline time-division multiplexing (TDM) concept (Chervenak et al. 1999), the outputs from the dedicated input SQUIDS of individual TES pixels are coupled to a single amplifier, and multiplexing is achieved by sequential switching of these input SQUIDS.

An energy resolution of 3 eV full width half maximum (FWHM) at 7 keV is required for the single pixels in the main array, with a high-resolution live time of no less than 80% at a counting rate of 50 events/s/pixel, and a bandpass of 0.1–12 keV. The integrated core XMS detector-system technologies reached TRL-4 in March 2008 with the successful demonstration (Kilbourne et al. 2008) of multiplexed (2 columns × 8 rows) readout of 16 different pixels (in an 8×8 array) similar to those in the current XMS reference design. Reaching this milestone showed that the baseline technology approach is fundamentally sound. The detector pixels were sufficiently uniform to permit good performance under common bias, and the modest degradation of the detector performance while multiplexed was consistent with models. Resolution across 16 multiplexed pixels ranged from 2.6 eV to 3.1 eV, and the pulse time constant was 0.28 ms. The performance approached the requirements of potential system applications (in terms of resolution, speed, pixel scale, and quantum efficiency.) However, consistent with the expectations for TRL-4, the validation was relatively low-fidelity compared with the eventual system application, because it is not possible to scale up the technologies used in the demonstration to what is needed for the flight system without further technology development. NASA and ESA technology assessments have agreed that the technology is at TRL-4.

The best energy resolution that has been achieved with single-channel readout of pixels of the size scale of the main array is 1.8 eV at 6 keV (Bandler et al. 2008). This resolution was achieved with 0.25×0.25 mm pixels that were close-packed in an 8×8 array. More recently, 32×32 arrays have been produced, with all pixels wired using microstrip wiring (Chervenak et al. 2012). This wiring has been achieved for pixels with pitch of 0.25 and 0.30 mm. For the array with a 0.30 mm pitch, the best resolution that has been measured is 1.8 eV FWHM at 1.5 keV (Eckart et al. 2012). The resolution of this array was degraded at 6 keV because of the poor quality of the bismuth in the absorbers of these devices; future generations of pixels will be able to achieve 1.8 eV resolution

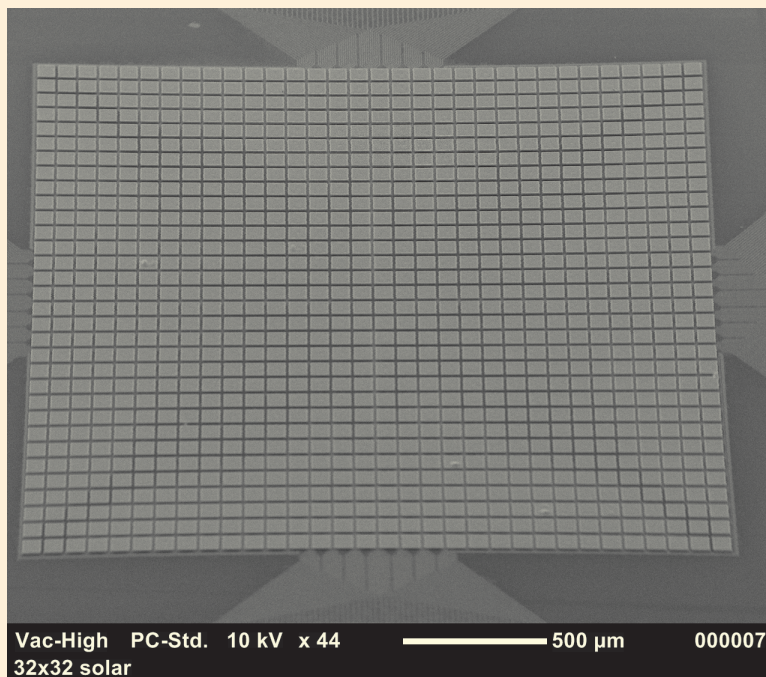


Figure 3.2–2. This image shows a close-packed array of small pixels on a 75-micron pitch, read out with micro-strip.

up to 7 keV. Although energy resolution better than 2 eV is measurable in single pixels, the energy resolution degrades when the pixels are multiplexed using TDM, and also when X-ray event record lengths are reduced in order to accommodate the count-rate requirements. Additionally, there are a number of other possible causes of energy resolution degradation in orbit that cannot be completely eliminated. An error budget has been established that takes into account the many possible sources of degradation (Kilbourne 2010). For this reason, an energy resolution requirement of 3 eV FWHM at 6 keV for all single pixels in the main array, which is consistent with the science requirements and leaves a suitable performance margin, is appropriate for this type of pixel.

Much of the ground between TRL-4 and TRL-5 has already been covered. The pixel design is well under way. The main challenge at the pixel level is process control, which is a matter of tracking and controlling the superconducting T_c of the Mo/Au TES and the heat capacity and thermalization of the Au/Bi absorber. At the array level, production of reliable 32×32 arrays with microstrip wiring is becoming routine (Chervenak et al. 2012). Concepts for array-scale heat sinking are well defined and are presently under development. The degree of heat sinking needed has been defined and determined to be achievable. The specific multiplexer architecture is based on the TDM used for the 2×8 readout demonstration, and well-defined specific changes are being implemented to increase the bandwidth, and thus improve and extend the performance of the demonstration to 16 rows (and beyond). Bandwidth and noise performance approaching requirements has been demonstrated.

3.2.3.2 Small Pixels

The PSA was introduced into the AXSIO focal plane design following the successful development of small pixels for solar physics (Bandler et al. 2010; Smith et al. 2011). It has been shown that a FWHM energy resolution of 1.6 eV is achievable at 6 keV in pixels capable of high count-rate operation (Smith et al. 2011). More recently, large-format close-packed array designs have been demonstrated (Bandler et al. 2012). An example of these arrays is shown in **Fig. 3.2–2**.

The performance of this type of pixel is consistent with the ability to operate at relatively high count rates of a few hundred counts per second, but high-count-rate performance has not yet been demonstrated. Because pulses from these pixels are much faster, they require a SQUID readout with a much higher slew-rate capability than those of the main array design, which presents a significantly greater challenge for their multiplexed readout. Therefore, there must be significant development of this type of pixel and readout to bring them to TRL-5.

3.2.3.3 Multiplexing

The AXSIO reference design is mostly based on 32-row multiplexing. The main array of single pixels utilizes 20 columns of these multiplexers, and the outer array a further 8 columns. The PSA will operate with 16-row or 32-row multiplexing, requiring 8 or 16 more columns. The greater demands on the readout for the PSA will likely necessitate the features available with flux-coupled code division multiplexing (CDM) (Irwin et al. 2010), in addition possibly reducing the number of rows per column. The readout for the main array is considered to be at TRL-4; however, a TRL assignment of 3 is more accurate for the PSA readout.

The TDM results from the 2008 TRL-4 demonstration are as shown in **Fig. 3.2–3**, where the multiplexed energy resolution is plotted as a function of the number of pixels being multiplexed.

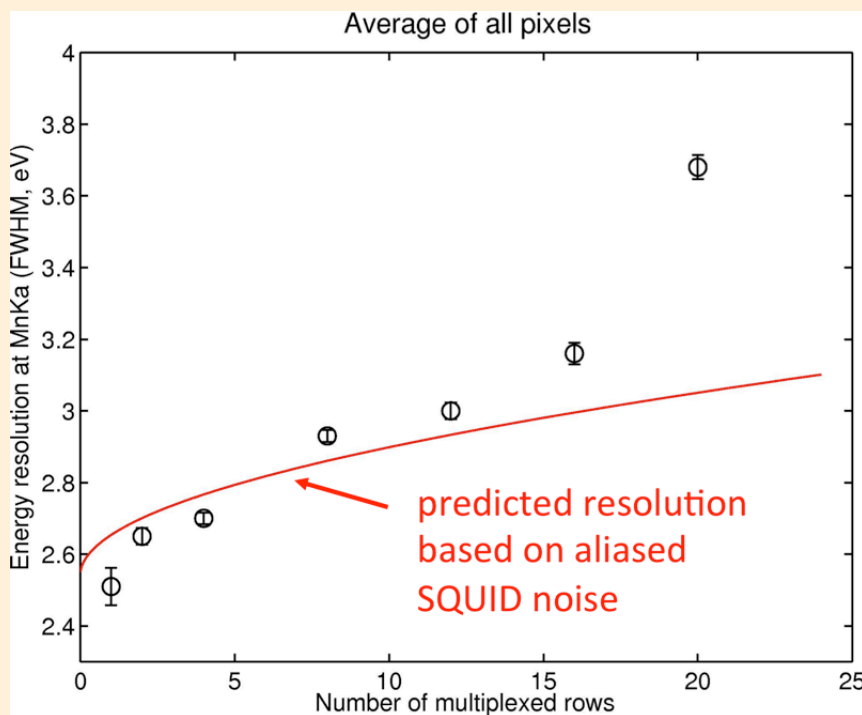


Figure 3.2–3 This plot shows the TDM multiplexing predicted and measured energy resolution as a function of the number of multiplexed rows using TES microcalorimeters with an energy resolution of 2.5 eV.

The results in **Fig. 3.2–3** show the degradation that occurred from multiplexing TES pixels that had ~2.5 eV energy resolution for 0.25 mm pixels. The detector array had a baseline energy resolution of less than 2 eV when operated with a base temperature of 50 mK. However, for these measurements it was necessary to increase the bath temperature to 70 mK in order to match the pulses to the Nyquist filters that were available—which thus degraded the performance to 2.5 eV. With the correct Nyquist inductors, the predicted resolution line in **Fig. 3.2–3** is scaled down to a level of 1.8 eV, as is expected for single-pixel XMS detectors. This energy resolution has already

been measured in individual pixels in 8×8 arrays of 0.25 mm pixels, and at 1.5 keV in 32×32 arrays of 0.30 mm pixels. With appropriate Nyquist inductors and base temperature and the same level of multiplexing capability, the observed degradation in resolution for 8- to 12-row readout would have been to approximately 2.5 eV.

There is a clear deviation of the measured energy resolution from predictions based on aliased noise of linear SQUIDs as the number of rows increases from 16 to 32. This is due to the SQUIDs no longer operating in a regime where the error signals in the flux locked loop are small enough to provide a linear SQUID response. By increasing the bandwidth, and speeding up the readout to allow higher sampling rates, it is possible to increase by a factor of four the number of rows that can be multiplexed without deviation from the expected noise-limited performance.

Since 2008 there has been good progress in improving the sampling rate. In the measurements shown in **Fig. 3.2–3**, the fastest sampling rate (time between measuring any two consecutive, sequentially read rows) was $t_{\text{row}} = 680$ ns. At 4K, in a simplified readout circuit, $t_{\text{row}} = 280$ ns has been demonstrated, and ~ 340 ns switching while reading out real X-ray detectors.

Performance can also be improved through the use of flux-actuated switches ($\sim \sqrt{2}$ improvement). These switches have now been designed and incorporated into 32-row multiplexer chips. The first generation of these chips has recently been fabricated, but they have not yet been tested.

Multiplexing performance can also be improved by lowering the level of SQUID noise and increasing the SQUID linearity. In recent years, the level of total SQUID amplifier noise, non-multiplexed, has been demonstrated to be $0.42 \mu\Phi_0/\sqrt{\text{Hz}}$, referred to the first stage SQUID in both TDM and CDM multiplexer systems. This noise is significantly lower than it was for the previous TDM results in which the total input referred was $0.65 \mu\Phi_0/\sqrt{\text{Hz}}$.

These improvements have yet to be incorporated into a full demonstration of multiplexed energy resolution of a microcalorimeter array for 6 keV X-rays. New platforms are now being developed that should soon be able to demonstrate the improved multiplexing capabilities that these technical advancements make possible. 3×32 demonstrations of multiplexing on 32×32 arrays with FWHM energy resolution of better than 3 eV at 6 keV are expected.

3.2.3.4 Code Division Multiplexer (CDM)

For the current XMS design, CDM (Irwin et al. 2010) becomes necessary. CDM is most easily understood via comparison to TDM. The circuits can look similar, but the modulation functions employed are different. TDM employs low-duty-cycle boxcar modulation functions that switch the input SQUIDs (one per TES) on and off one row at a time. In contrast, CDM uses Walsh codes, in which the coupling of the pixel signals is alternated in polarity. (In the simplest case of two-channel CDM, the sum of the signals is first measured, followed by the difference.) To extract the individual signals, multiplications by the inverse Walsh matrix are required. Because signal is measured from every detector at each sample, instead of once per frame for TDM, CDM has a \sqrt{N} amplifier noise advantage over TDM, where N is the scale of the multiplexing. CDM could be advantageous for multiplexing the main array pixels as it can lead to better energy resolution performance, and/or provide more margin in meeting the energy resolution requirements. It is necessary for fast pixels with larger slew rates (such as the AXSIO point source array) because it provides the noise margin needed to allow the coupling of the TES to the input SQUID to be reduced, allowing fast and stable readout of these large signals.

Good progress on CDM has been achieved (Stiehl et al. 2012). **Fig. 3.2–4 (a)** shows an 8-pixel CDM demonstration. The seven modulated pixels are all sub-3 eV. As is usual in CDM, pixel 0 is not switched like the other pixels, and so it has degraded resolution due to worse $1/f$ noise and pickup. It is included here only for completeness. The frame

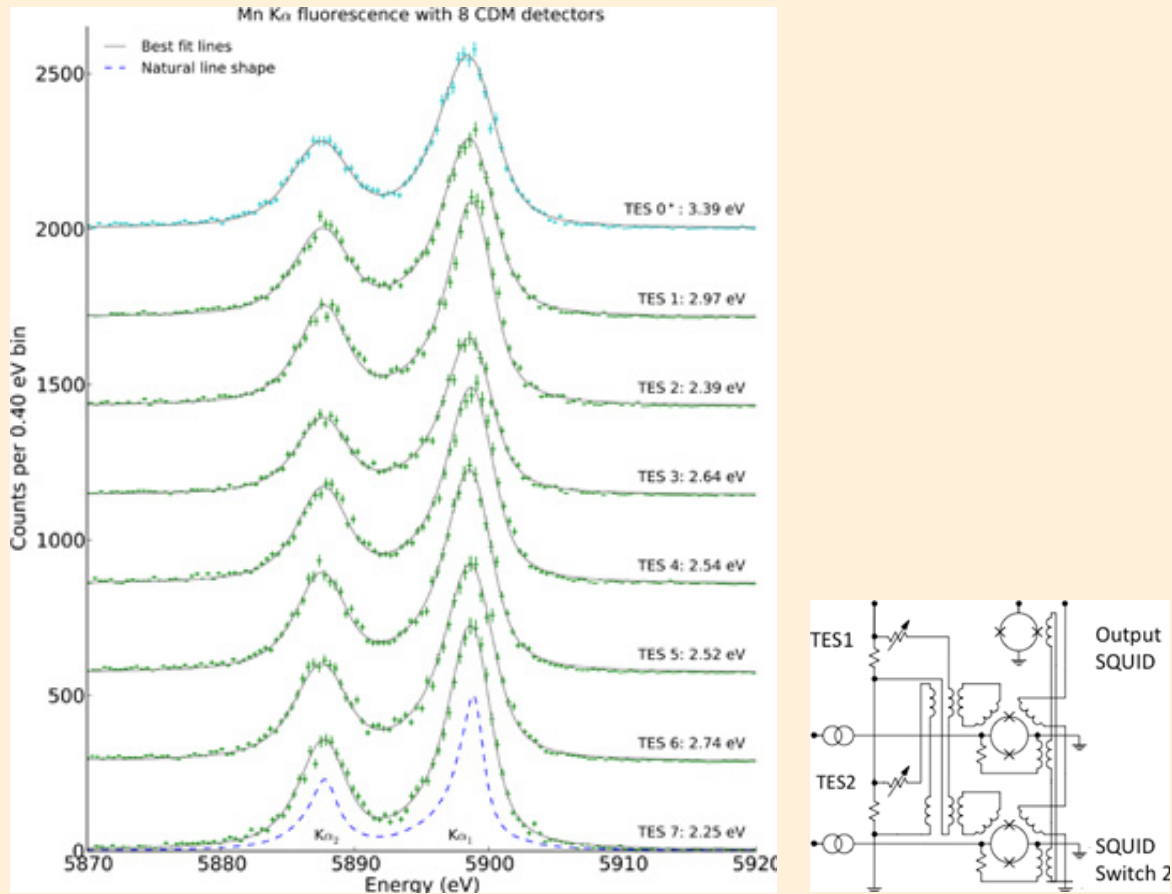


Figure 3.2-4. Left: The resulting MnK spectra from an 8-pixel CDM experiment using flux-couple code division multiplexing. **Right:** Fluxed coupled CDM circuit when just two TESs are coupled.

rate is $t_{\text{row}} = 400$ ns. For these measurements, this frame rate was limited by the inability to pass data out through the digital feedback electronics any faster than this. New room-temperature hardware necessary to speed up this frame rate is currently being implemented.

In principle, the amount of energy resolution degradation from CDM multiplexing can be reduced by up to a factor of 5.7 over TDM for a 32-row readout. A full characterization of the detector array that produced this result has not yet been completed, and only rough estimates have been made of levels of energy resolution degradation that was due to the CDM readout of between 0.2 and 0.4 eV.

The chip that produced the 8-pixel CDM results has been used to produce very similar results in 4-pixel CDM measurements, and the same chip also has a 16-channel CDM readout capability, which will be demonstrated in the near future. A new chip design will be necessary to demonstrate 32-pixel flux-coupled CDM.

Results thus far have been achieved with the Walsh matrix realized on the multiplexer (MUX) chip by fixed wiring that couples each TES to each SQUID with the polarity required by the code. There is another type of CDM multiplexing called “Current-Steering CDM” or I-CDM. In this version of CDM, the current signals for the N TESs attached to a single SQUID are switched in polarity using superconducting switches. I-CDM

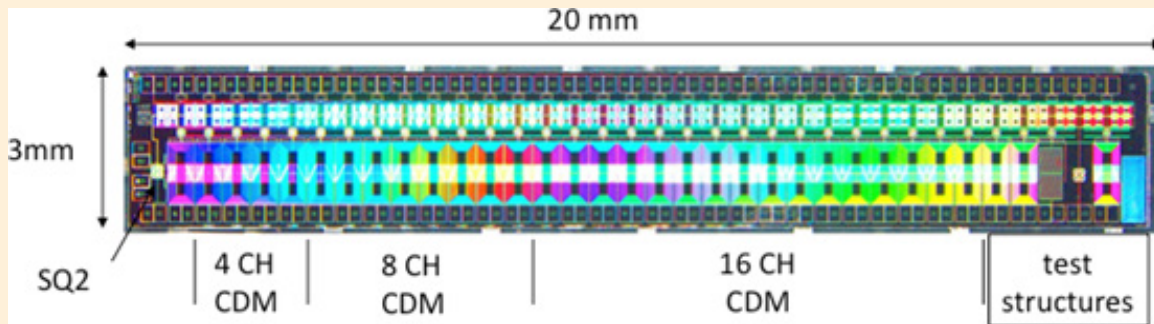


Figure 3.2–5. This annotated photograph shows the layout of a CDM chip that incorporates 4-, 8-, and 16-row CDM readouts.

is a more advanced version of CDM than the flux-coupled version, with potential advantages. In particular, if the switches can be integrated onto the same chip as the detectors, there could be many fewer wires between the detector chip and the readout, making it much easier to house the detector and shield it from environmental effects such as varying external magnetic fields (see **Section 3.2.3.7** on focal plane assembly). I-CDM is currently being researched, and appears to have good potential for applications with arrays of TES bolometers in which the currents needing to be switched are relatively small. For X-ray microcalorimeters, in which the TES current is much larger, it is not clear whether I-CDM is realizable in the near future. If it can be realized, I-CDM is an attractive alternative to TDM and flux-coupled CDM.

There is yet another type of TES readout with great potential for the future—the “microwave” readout (Mates et al. 2008). This is also currently being developed for bolometer applications in which the readout requirements are easier to meet. In this type of readout, a large number of TESs are elements of micro-resonator circuits, including unshunted, non-hysteretic radio frequency (RF) SQUIDs, that are attached to the input of a single high-electron-mobility transistor (HEMT) amplifier. Each high-quality (Q) TES-resonator is at a slightly different frequency, and a large number of these resonators may be read out by combining them, uniformly spaced in frequency, by the large bandwidth (~5 GHz) HEMT amplifier. Multiplexing factors of ~1000 may be achievable using this approach, and perhaps even greater if CDM approaches can also be integrated with this type of readout. For this decade, it is unlikely that this technology will reach the TRL needed to consider baselining it for an X-ray astrophysics mission. But this approach remains an exciting alternative for reading out much larger arrays of TESs (and magnetically coupled microcalorimeters) in the future.

3.2.3.5 Hydras

Some degree of thermal multiplexing can be engineered into microcalorimeter arrays through the use of position-sensitive detectors. The basic element of such arrays is a macropixel (which may be continuous or made of interconnected discrete elements) read out by one or more thermometers. The element is designed such that the shape of the output temperature pulse depends on the location of absorption on the macropixel.

The main advantage of such devices is that they reduce the total number of electronic channels required to read out a given number of pixels. This reduction eases the requirements on the wiring and the number of readout channels. The associated increase in the complexity of the analysis electronics, from the added task of determining the subpixel event location, is minimal (Smith 2009).

In the “Hydra” design, one thermometer is coupled to discrete separate absorbers via varied thermal links. For example, a single TES with six differently coupled 0.3-mm absorbers has been tested at Goddard. Resolutions across the 6 pixels ranged from 5.4 eV to 7.8 eV; the layout and distinguishing pulse shapes are shown in **Fig. 3.2–6**.

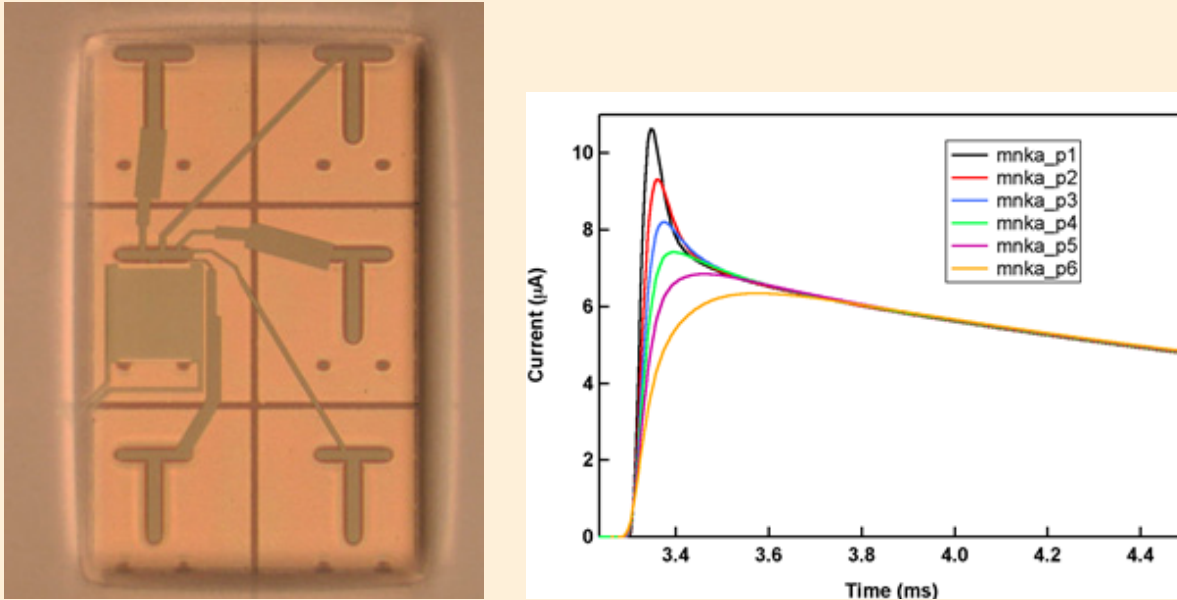


Figure 3.2–6 *Left:* This image of a 6-pixel macro-pixel, seen from the back (looking through the nitride membrane), shows six absorbers, a single TES, and the links between them. *Right:* This image shows the characteristic pulse shapes that distinguish the 6 pixels. Resolutions across the 6 pixels ranged from 5.4 eV to 7.8 eV. A single pixel of the same heat capacity and TES properties would have had a resolution of about 4 eV.

The distributed-absorber approach does come with a penalty of reduced energy resolution, however. The resolution will always be somewhat worse than that of a single pixel with the heat capacity and temperature sensitivity of the macro-pixel because decoupling parts of the absorber to introduce position variation introduces thermal fluctuation noise between parts of the absorber.

In the AXSIO baseline, the outer regions of the 40×40 pixel main array are assumed to be Hydras with single TESs attached to four absorbers and each absorber identical to those of the inner single pixels. The requirement for the Hydras is that the energy resolution for each pixel (absorber) is less than 6 eV. This main array is expected to be fabricated on a single silicon substrate, which is possible because the pixel size and therefore back etch are the same for the two regions.

3.2.3.6 Anti-Coincidence Detector

Observations of extended sources with low surface brightness (e.g., galaxy clusters out to the virial radius and potential warm-hot intergalactic medium WHIM filaments), require an anti-coincidence detector (ACD) to veto background interactions in the imaging spectrometer. The ACD of the *Suzaku* and *Astro-H* missions is a square cm silicon ionization detector with a thickness of 0.5 mm (Kilbourne et al. 2006; Kelley et al. 2007).

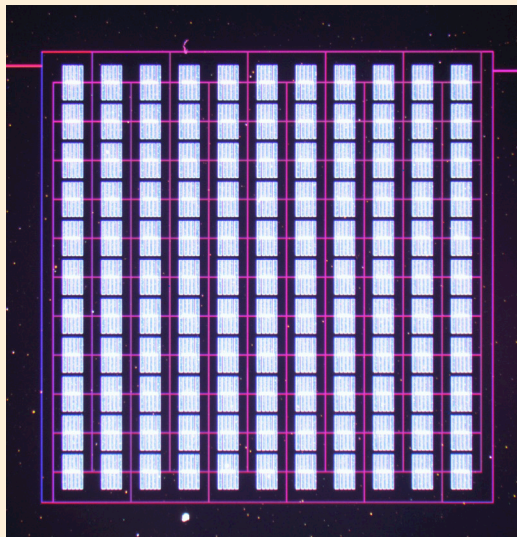


Figure 3.2-7. A proof-of-concept ACD for XMS, consisting of 121 TESs wired in parallel. Future iterations will cover the surface with four channels similar to this one. The prototype had a sensitivity threshold well below 6 keV, far below the level needed for detection of minimum ionizing particles, which will deposit 120 keV traversing 0.3 mm of Si.

The baseline for XMS is an ACD compatible with the TES SQUID readout, based on the detector technology used by the Cryogenic Dark Matter Search (CDMS). CDMS uses TESs to detect phonons created by particle interactions in large Si and Ge crystals (7.5 cm diameter \times 1 cm thick) [Akerib et al., 2006]. The CDMS approach uses four independent readout channels, each of which monitors \sim 1000 TESs that are wired in parallel. To increase the sensitive area, each TES is connected to phonon collection fins. In this scheme, particle interactions in the crystal create phonons that propagate quasi-ballistically to the crystal surface, where superconducting Al collection fins absorb them. Phonons with sufficient energy (greater than twice the superconducting Al band gap) break Cooper pairs, creating quasi-particles that then diffuse through the Al and are collected into the tungsten TESs, creating a signal [Akerib et al. 2006].

A proof-of-concept CDMS-style ACD using Mo/Au TESs has recently been fabricated. This first prototype (**Fig. 3.2-7**) features 121 TESs, in an 11×11 grid, wired in parallel. Each TES is $250 \mu\text{m}$ long by $2 \mu\text{m}$ wide and is connected to 8 Al $300 \mu\text{m}$ long by $50 \mu\text{m}$ wide collection fins. The prototype has a sensitivity threshold well below 6 keV, far below the level needed for detection of minimum ionizing particles, which will deposit 120 keV traversing 0.3 mm of Si. Characterization of this prototype to assess its efficiency and the uniformity of its response is in progress.

Improvements to the ACD design that improve the rejection of secondary particles must also be studied. A background simulation done for IXO (Lotti et al. 2012) projected that 86% of the unrejected background would come from electrons ejected from the surface of material very close to the TES array. When such an electron is ejected, the responsible primary cosmic proton is also scattered into the detector volume. The background will be reduced if more of these protons can be detected, but increasing the area of the ACD to capture these events would also increase the rate of triggers from events that interact only in the ACD, which would increase the dead time of the spectrometer. Adding some position sensitivity to the ACD would enable basic tests of whether the energy deposited and the track location are consistent with having the same origin as an event in the array. To the extent that the other constraints on the design of the focal-plane assembly (see **Section 3.2.3.7**) permit it, we must also

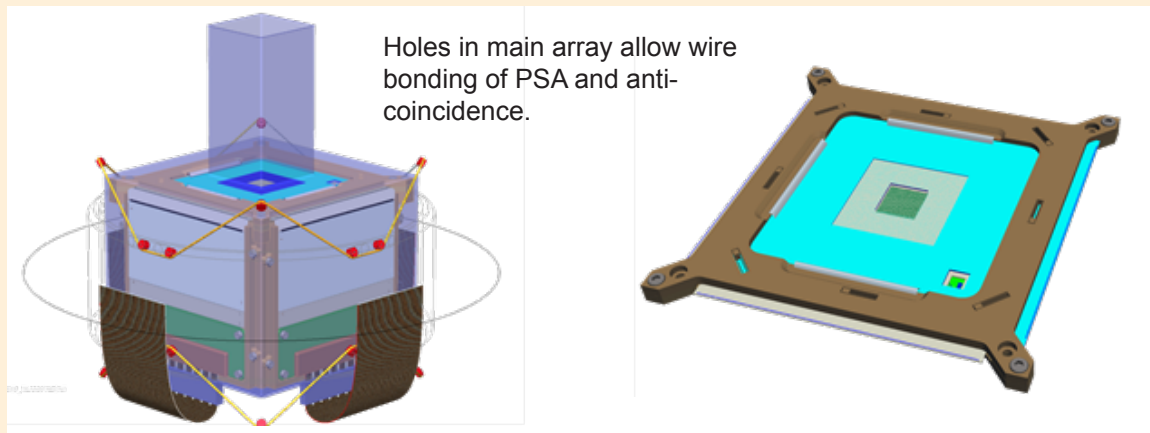


Figure 3.2-8. This image shows the SRON Netherlands Institute for Space Research (SRON)/Goddard design for the focal-plane assembly for IXO/XMS. Demonstrating a flight-worthy design of these electrical, thermal, and mechanical interfaces is an important aspect of TRL-6.

minimize the area of surfaces within line of sight of the spectrometer array by bringing those surfaces in as close as practical, and these surfaces must be coated with a low-Z material.

3.2.3.7 Focal-Plane Assembly

It is necessary to combine the core and outer regions of the main array with the PSA and the anti-coincidence into a focal-plane assembly (FPA) that fulfills detector requirements within the constraints of the cryogenic apparatus. These include the thermal, electrical, and mechanical integration of the detectors and read out. A verified design concept for packaging of the focal plane components is needed for the detector system to advance to TRL-6.

The most challenging requirements for the assembly are those on magnetic shielding, size, mass, and vibrational isolation. The Kevlar strings that suspend the lowest temperature stages of the FPA must rigidly support them without introducing unmanageable heat loads. These strings need to be sufficiently tensioned that microphonic vibrations from the rest of XMS, such as from the cryocooler, are not coupled to the detector, and also to ensure that the FPA will not break apart due to launch vibrations. These requirements are most easily met when the suspended mass is kept as small as possible. The extremely stringent magnetic shielding requirements also favor a compact design with superconducting and mu-metal shields that have large length-to-width aspect ratios, as detailed in Van Weers and Bandler (2010). Additionally, the size of the system ultimately affects the cooling power needed, and thus the overall size and mass of the XMS cryostat. Modularity and ease of assembly are important design goals that will be difficult to achieve in the required package size.

A number of separate technologies need to be matured for the XMS FPA. Some of these are expensive technologies that are already evolving independently from microcalorimeter technology, such as miniaturized connectors and techniques for fine-pitch wiring or bump-bonding electrical connections. Below is a list of some of the main FPA technologies that need to be developed:

1. High-density around-the-corner microstrip wiring.
2. Lightweight, modular, magnetic shielding (niobium and mu-metal shields).

3. Kinematic, multi-chip mounts.
4. Suspension system meeting mechanical requirements and with a suitable form factor.

3.2.4 TRL Demonstrations for X-ray Probe

The projected successful execution of the following demonstrations is based on already achieved component-level performance demonstrations, models, and analysis. Nevertheless, since the actual components assembled for the demonstrations will likely be slightly different from those that provided input to the models, the actual configuration of each of these demonstrations will in turn be modeled, and all performance metrics checked for consistency against the appropriate model. Each of these demonstrations is expected to be a long-running experiment, with the performance converging to the requirements of the milestone as non-fundamental limitations in the test platforms are addressed and as TES and multiplexer operating parameters are optimized. Once the required performance metric has been demonstrated in a single acquired spectrum, it will be repeated in at least two additional acquired spectra before the milestone is declared successfully reached.

3.2.4.1 Core Array Prototype (TRL-5) Demonstration (2014)

Demonstrate multiplexed (3 columns \times 32 rows) readout of 96 different flight-like pixels on a 0.30 mm pitch in a 32 \times 32 (or greater) array with > 95% of pixels achieving better than 3 eV resolution at 6 keV, using an analysis method consistent with the requirement of 80% live time at an X-ray rate of 50/s/pixel. Vibration testing of an array is required to validate the mechanical design of the pixels. Radiation testing of the detectors and readout is necessary to validate robustness in the space environment.

The details of this milestone depend on the mission concept, but meeting the *Athena* requirements (16 rows) is a minimum for this technology to be considered at TRL-5. For the current XMS, the demonstration should be done with 0.3 mm pixels and pushed to 32-row multiplexing.

3.2.4.2 Outer Array Feasibility (TRL-4) Demonstration (2014)

Demonstrate multiplexed (2 columns \times 8 rows) readout of 16 four-absorber devices with better than 6 eV resolution on all 64 pixels and fall times of <4 ms. The individual absorbers shall be at least 0.25 mm wide. Position discrimination within the four-absorber devices must be achievable to energy at least as low as 1.5 keV.

3.2.4.3 Outer Array Prototype (TRL-5) Demonstration (2015)

Demonstrate multiplexed (3 columns \times 32 rows) readout of 96 four-absorber devices with better than 6 eV resolution at 6 keV using an analysis method consistent with the requirement of 80% live time at an X-ray rate of 10/s/pixel, and position discrimination to energy at least as low as 150 eV.

3.2.4.4 Particle Veto Concept Demonstration (2013)

Demonstrate proof-of-principle one-sided anti-coincidence detector for particle veto and design a feasible scheme for its readout and integration behind the microcalorimeter array.

3.2.4.5 Particle Veto Prototype (TRL-5) Demonstration (2016)

Demonstrate particle veto prototype on a scale appropriate for size of focal-plane array with pulse time constant <50 microseconds, energy resolution better than 1 keV, and ability to reject >99.8% of minimum ionizing particle

interactions depositing <12 keV in the calorimeter array. (The particle veto is presumed to be TES-based, along the lines of detectors developed for dark-matter detection.)

3.2.4.6 Point-Source Array High Count Rate Feasibility (2013)

Demonstrate 2.5 eV resolution at 6 keV at a count rate of greater than 100 cps (unmultiplexed).

3.2.4.7 Point-Source Array Prototype (TRL-4) Demonstration (2015)

Demonstrate 2.5 eV resolution at 6 keV of close-packed PSA in a 2×4 multiplexed demonstration with x-rate count-rate capability of 300 cps, most likely integrating CDM readout.

3.2.4.8 Point-Source Array Prototype (TRL-5) Demonstration (2017)

Demonstrate 2×16 (32) readout of close-packed PSA with less than 2.0 eV energy resolution at a count rate capability of 300 cps.

3.2.4.9 Detector System Demonstration (TRL-6) (2019)

Demonstrate a system of integrated sensor and readout components. Electrical and thermal interconnects and staging are approaching a flight-worthy design, but a flight design is not fully realized. All pixels are biased though not read out, in order to validate the thermal design.

Table 3.2-1 shows the major milestones associated with the schedule and costs to reach TRL-6 for the X-ray calorimeter.

Table 3.2-1. X-ray Microcalorimeter Technology Development Tasks Schedule and FY13 Costs

Task	2013	2014		2015	2016	2017	2018	2019
Multiplexing		Optimized TDM multiplexers (Nov)	32-row multiplexer for CDM (June)					
Core Array		< 3 eV for up to 50 cps with 80% throughput on single pixel (Dec)	< 3 eV for all pixels in full size array (Mar)	3x32 readout with < 3 eV @ 6 keV with 0.3 mm pixels and TDM (TRL 5) (Aug)				
Point Source Array		2 eV @ 6 keV at >100 cps (Oct)		2x4 readout with < 2.5 eV @ 6 keV at >100 cps (TRL 4) (Feb)	2x16 readout with < 2 eV @ 6 keV at >100 cps (TRL 5) (Oct)			
Outer Array		Demonstrate ability to build single pixels & hydras on same array (Feb)	2x8 readout of 16 four-absorber devices with < 6 eV on all pixels (TRL 4) (Apr)	3x32 readout of 96 four-absorber devices with < 6 eV on all pixels (TRL 5) (May)				
Particle Veto	Proof-of-principle demo (June)					Prototype with >99.8% rejection of minimum ionizing particles (TRL 5) (Oct)		
Detector System	3x16 readout with < 3 eV @ 6 keV using TDM (Jan)				Verify that focal plane meets flight instrument thermal/mech requirements (May)			Integrated sensor and readout in flightworthy design (TRL 6) (Mar)
Budget Estimate	\$1.8	\$2.0M		\$2.2M	\$2.3M	\$3.0M	\$3.0M	\$3.0M

■ TRL 5 development
■ TRL 6 development
■ Risk reduction/performance margin increase
■ SAT/APRA already awarded
■ New funding required

3.3 Off-Plane X-ray Spectrometer (OP-XGS) Technology Development Roadmap

3.3.1 Driving Requirements

The driving requirements for the OP-XGS are a spectral resolving power >3000 ($\lambda/\Delta\lambda$) and effective area >1000 cm² over the 0.2–1.0 keV band. Recent developments in off-plane gratings have shown that these are reasonable requirements to achieve in the near future. To obtain this performance over the large band, the OP-XGS will utilize diffraction orders ~ 1 – 5 with zero order as a wavelength reference. The actual effective area of the spectrograph may be limited by the quantum efficiency of the charge-coupled device (CCD) camera at low energies, 0.2–0.4 keV (see **Section 3.5**). This limit is driven by minimizing the thickness of the optical blocking filters, a development currently in progress (see **Section 3.5.3.2**). The overall response is currently being addressed by developments in the grating groove profile.

3.3.2 Technology Description

Future X-ray observatories will necessitate large collecting area optics coupled with high-fidelity gratings to achieve the high throughput and high spectral resolution requirements at X-ray energies below 1 keV. The main goal of future spectrometer development efforts is to increase the technology readiness level of these systems by demonstrating a spectral resolution of >3000 ($\lambda/\Delta\lambda$) in soft X-rays using a high-throughput, high-fidelity array of aligned gratings. To achieve this goal, a spectrometer based on off-plane reflection gratings (Cash 1983, 1991; McEntaffer 2011) can be utilized. Such a spectrometer typically consists of an array of Wolter Type-1 optics (parabolic primary followed by a hyperbolic secondary) that focuses an X-ray beam over a focal length of several meters. The converging telescope beam is intercepted by an array of off-plane reflection gratings which disperse the spectrum onto a CCD camera.

The off-plane grating mount (**Fig. 3.3–1**) provides high efficiency for reflection gratings given the ideal illumination of the grooves combined with excellent packing geometry. Light intersects the gratings nearly parallel to the groove direction, thus limiting groove shadowing. A small fraction of light undergoes specular reflection to a zero order image while dispersed light forms an arc at the focal plane. The light exiting the grating is at the same shallow graze angle as the incident light thus allowing for close, efficient spacing between gratings. This configuration is also known as conical diffraction given the resulting cone of dispersion.

The diagram on the right of **Fig. 3.3–1** illustrates properties of off-plane gratings required to achieve future requirements—blazed profiles for efficiency, radial groove distribution for resolution, and precision alignment to enable both. An array of three representative gratings is projected from its position just aft of the optics onto the focal plane several meters away. Grating grooves are typically recorded with a periodic shape that resembles a sinusoid or square wave. Diffraction off such a surface occurs on each side of the specularly reflected beam at zero order. Subsequent processing of the grooves can “blaze” the profile allowing for diffraction to occur preferentially on one side of zero order, thus limiting the size of the readout array and increasing the signal-to-noise ratio in a given spectral feature. Furthermore, the angle of this blaze can be tailored to emphasize a specific wavelength and order. The blaze allows for efficient diffraction into high orders, thus concurrently optimizing throughput and resolution. Given that the off-plane array is placed into a converging beam from the telescope optics, the grating grooves must be arranged in a converging fashion to maintain a constant α over the surface and therefore a constant β at the focal plane; i.e., a spectral line free of grating induced aberration. Variable-line-spaced (VLS) gratings are common in spectrometers; however, the direction of varying groove density is typically orthogonal to the grooves. The high-resolution, off-plane geometry is unique in that it requires variable density in the groove direction. Finally, **Fig. 3.3–1** demonstrates the need for high-precision alignment within the array of gratings. The

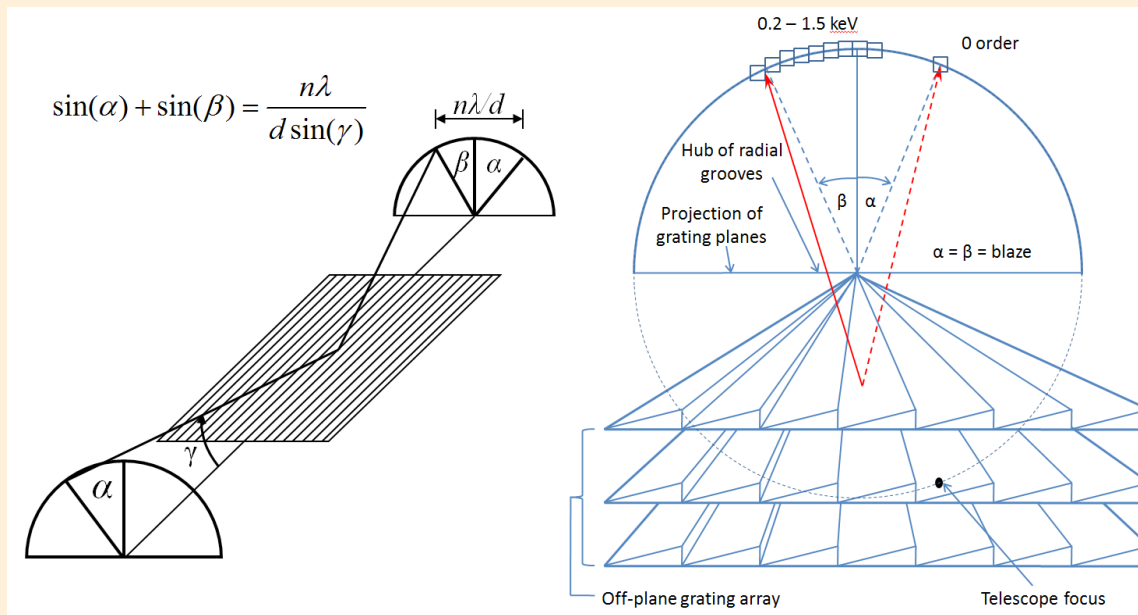


Figure 3.3–1. Left: The off-plane grating mount. **Right:** Three gratings, placed many meters from the focus are shown projected onto the focal plane to elucidate the nature of the arc of diffraction which is detected by an array of CCDs depicted as squares.

projection of each grating lies along the diameter of the circle that defines the arc of diffraction. Furthermore, the hub of all radially oriented grating grooves lies at the center of this circle. Given that the gratings typically lie several meters from the focal plane, these requirements lead to strict tolerances in the alignment of pitch (rotation about the direction orthogonal to the central groove) and yaw (rotation about the grating normal), respectively.

A precisely aligned array of VLS reflection gratings is currently being utilized in the Reflection Grating Spectrometer (RGS) onboard the *XMM-Newton* Observatory. The gratings that will be utilized in future X-ray spectrometers will be very similar in terms of size, mass, flatness requirements, alignment requirements, and interfacing. The major difference is that these gratings will be mounted rotated 90° with respect to the XMM RGS. Again, this offers increased throughput given that the gratings can be more tightly packed without occulting dispersed light. However, the grating fabrication process will be different in order to achieve the resolution requirements of future spectrometers. Additional heritage for reflection gratings has been accomplished through the use of X-ray spectrometers incorporating arrays of high-efficiency, modest resolution off-plane gratings on suborbital rocket flights (McEntaffer, Cash, & Shipley 2008; Oakley, McEntaffer, and Cash 2011). The most recent suborbital flights utilize many (134) thin ($125 \mu\text{m}$), replicated gratings in multiple ($2\times$) arrays. The technologies developed during XMM development, over the course of several suborbital rocket missions, and during the *Constellation-X* and subsequent IXO program have outlined a path for designing, fabricating, replicating, and aligning gratings that satisfy future observatory requirements. However, key steps still need to be taken in the laboratory to demonstrate these capabilities.

3.3.3 Status

The development of off-plane reflection grating technologies is progressing rapidly under the support of a NASA Strategic Astrophysics Technology grant and a NASA Roman Technology Fellowship (RTF). As detailed in the

following text, the technology has recently been advanced to TRL-4 with plans of obtaining TRL-5 under these programs.

3.3.4 Current TRL and Rationale

Currently, off-plane gratings have only been used in suborbital rockets and laboratory testing. These applications and results have achieved a TRL of 4 with medium-fidelity prototypes. Most importantly, a series of efficiency and resolution tests have recently been performed on next-generation off-plane gratings with the goal of meeting future performance requirements.

A novel method for grating fabrication has been identified and is currently being studied. Previous results from holographically ruled gratings have been promising for achieving high diffraction efficiency and resolving power via this fabrication method (McEntaffer et al. 2004; Osterman et al. 2004). However, holographic recording may be limited in its ability to approximate the necessary groove convergence. To circumvent this uncertainty and the significant cost associated with overcoming it, fabrication methods that use common semiconductor industry techniques are now being investigated. First, the grating profile is created using e-beam lithography to write a photomask that is subsequently reduced onto another resist coated wafer using deep-ultraviolet (UV) projection lithography to transfer the pattern into single crystal silicon. This grating is called the “pre-master” and is fabricated by LightSmyth Technologies. The groove pattern at this time is laminar (rectangular grooves) with a step-like radial approximation averaging 6000 grooves/mm. This pattern is then imprinted onto an off-cut silicon wafer, which is soon to become the master grating. Processing steps including reactive ion etching and anisotropic wet etching to transfer the pattern onto atomically smooth crystal planes resulting in a low-scatter, high-efficiency, blazed profile. This master grating can then be used in the same imprint device to produce many high quality replicas.

The initial steps of this chain have been accomplished, and the radial profile, high groove density pre-master has been procured. The efficiency and resolution tests on this pre-master have been performed to ensure quality at this early phase of the process and to provide confidence that the resulting master will be capable of achieving the performance goals. Diffraction efficiency tests were performed at the Berliner Elektronenspeicherring-Gesellschaft für Synchrotronstrahlung (BESSY) synchrotron light facility. The gratings were tested using 50 eV energy steps between 0.3 and 1.0 keV at graze angles of $\gamma = 1.5^\circ$ and 2.0° . The resulting efficiencies are shown in **Fig. 3.3–2**. These tests provide critical data on a grating fabrication process that appears to be even more promising than holographic lithography. At a graze angle of 1.5° , the grating diffracts upwards of 60% (absolute efficiency; i.e., inclusive of reflectivity) of incident light into usable spectral orders and does so without noticeable scatter. The grating routinely achieves 40% absolute efficiency over a wide range of energies at both graze angles. It is important to note that the grating was tested at $\alpha = 0$ (light parallel to the grooves). This led to a limitation on available orders at low energy, which results in only one or two measurable orders over a significant range of our bandpass for this configuration. Even so, diffraction efficiencies for these orders are quite high. Finally, the effect of the laminar profile is evident—there are large contributions to zero order, the +/- orders contain a nearly equal number of photons, and the diffraction pattern is quite regular and stable over a large range of energies. This signifies that the rectangular grooves are clean and well-shaped, which is corroborated by scanning electron microscope (SEM) imaging of the profile (**Fig. 3.3–3**).

The gratings have also been tested for spectral resolving power. This test was performed using the Stray Light Facility at Marshall Space Flight Center. The test utilized a slumped glass Wolter-1 telescope consisting of three aligned shells of optics produced by Goddard Space Flight Center. This telescope produced a <10 -arcsec half-power diameter (HPD) focus that was subapertured to ~ 1 arcsec in the dispersion direction. The high quality of the optics actually limited the ability to obtain theoretical resolutions given their ability to resolve the electron impact spot on the Manson X-ray source anode. However, even with this limitation a spectral resolution of 900 in 1st order for the Mg-K α line at 0.93 keV (**Fig. 3.3–4**), and > 1300 in 2nd order was achieved. These results can be projected to

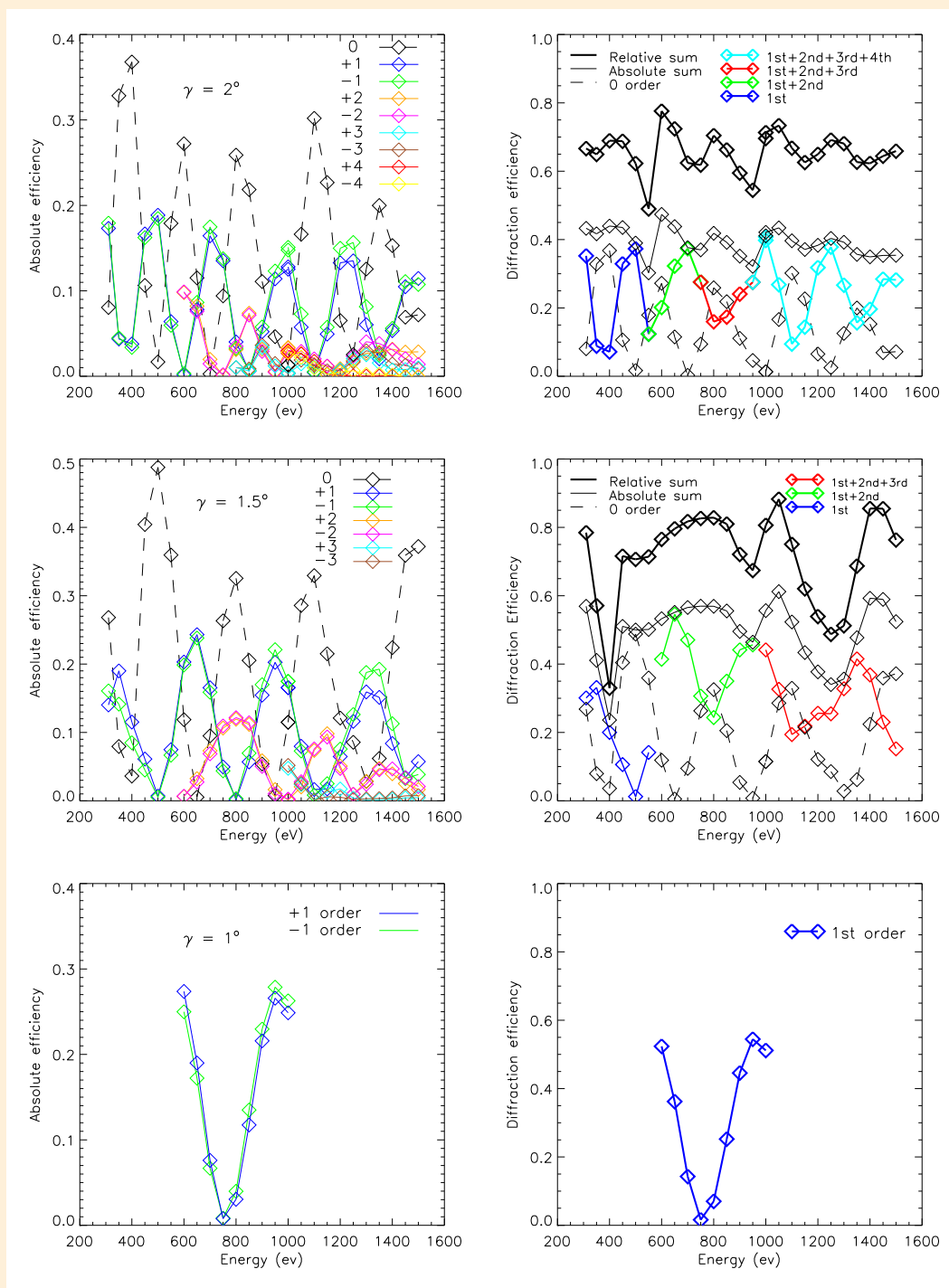


Figure 3.3–2. Measured diffraction efficiencies at graze angles of 2 (top row), 1.5 (middle row), and 1 (bottom row). Measurements of individual orders are shown in the left column as absolute efficiencies, which include the reflectivity of Au. Summed order efficiencies are shown in the right column. The thin, solid black line shows the total absolute efficiency of all orders, including zero order; the thick, solid black line shows the total relative efficiency which factors out the effect of the Au reflectivity.

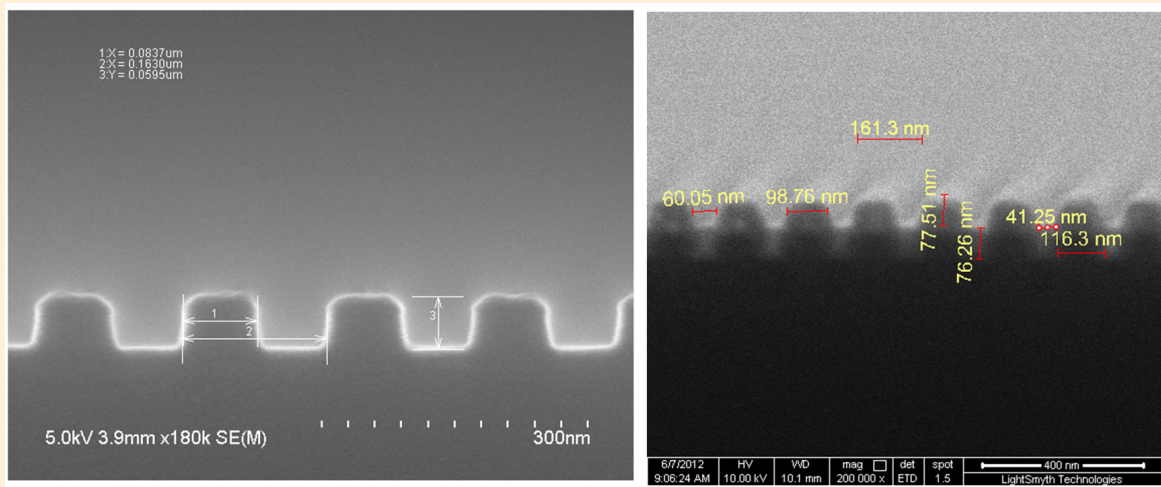


Figure 3.3–3 Scanning Electron Microscope images of the pre-master fabricated at LightSmyth. **Left:** Rectangular groove profile etched into the single crystal silicon substrate. **Right:** The silicon substrate appears black with an 80 nm coating of gold appearing gray.

higher order, assuming no limitations due to facility considerations. Calculations of theoretical resolutions, given the current system with an unresolved X-ray source, give resolution projections of >2500 in 3rd order and >3500 in 4th order for this ~1 keV line.

The requirements of future X-ray observatories translate to diffraction efficiencies of ~40% in usable spectral orders with resolutions above 3000. Recent test results show that this performance can be realized with this next generation of off-plane gratings. Currently, pre-masters are being imprinted using a nanoimprint device at Nanonex. The imprinted gratings are being processed for a blaze at the Microfabrication Facility at the University of Iowa. These blazed masters will be used for another round of performance testing scheduled in the coming months. Obtaining efficiency and resolution numbers consistent with future requirements using these gratings will further solidify a TRL of 4.

3.3.5 Steps to TRL-5

In the context of an OP-XGS, achieving TRL-5 requires thorough testing of an aligned grating module to meet the subsystem demonstration requirement. After achieving the performance requirements for our master gratings, the plan to raise the TRL to 5 includes five main steps: 1) blazed master fabrication; 2) substrate material trade study; 3) replication; 4) module mount/alignment development; 5) performance testing.

The methodology for fabricating blazed grating facets has been previously performed by Chang et al. (2004). The processing steps and necessary tools are in hand and are currently being used to develop the first blazed gratings. These gratings will undergo the same performance testing as the pre-master for throughput and spectral resolving power in the coming year.

The replication step is well in hand, given that replication via nanoimprinting has previously been demonstrated (Chang et al. 2004). Furthermore, this replication can occur onto a variety of substrate materials and shapes, which allows for much flexibility. The current plan is to perform a trade study between replication onto substrates

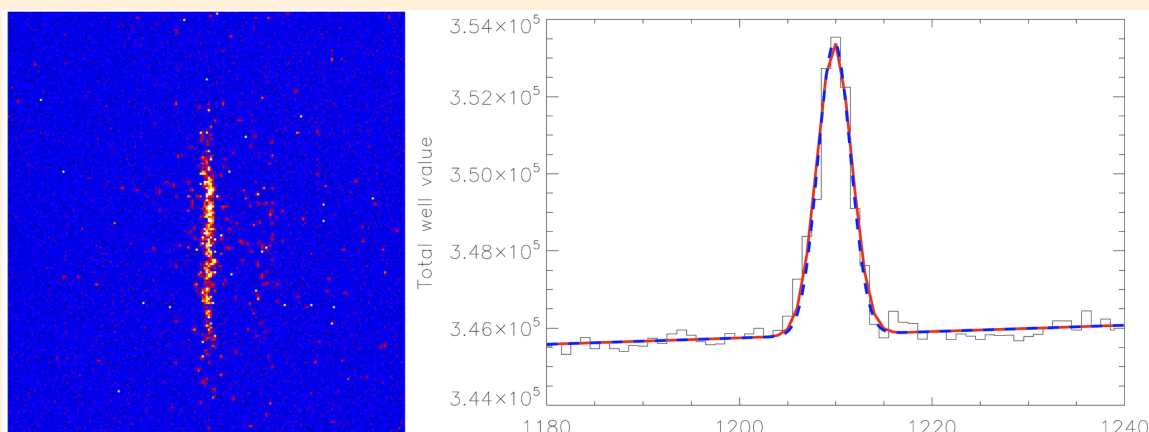


Figure 3.3-4. *Left:* Image of the first order Mg K α line. *Right:* Histogram of all CCD counts. The red line is a best fit Gaussian to the data with a FWHM of 0.011 Å ($R=900$).

composed of single-crystal silicon wafers or beryllium (Be). These results will feed into the substrate trade study which intends to optimize the substrates for manufacturability, and module integration. Given possible future telescope optic material choices, the substrate trade study materials (Si and Be) will optimize the grating array material for interfacing with the telescope optics and integration on future missions.

Much of this study depends on the fourth step of this process, module design and alignment. The alignment tolerances are dependent on the location of the grating array within the observatory, but can be on the order of a few arcseconds in the worst case. Previous alignment studies under the IXO program and discussions with the XMM RGS team have elucidated a path forward for off-plane grating alignment. Testing of a nanopositioning mount capable of meeting our alignment tolerances (**Fig. 3.3-5**) is currently under way. In practice, this mount will be able to incorporate any number of gratings aligned relative to one another. The alignment process involves mechanical confinement of the three linear degrees of freedom (these are the loosest tolerances) followed by a Shack-Hartmann sensor measurement of each grating to determine relative pitch and roll (see **Fig. 3.3-3**), and ends with X-ray alignment of the spectra to constrain yaw. Three closely spaced gratings will be aligned to match the three aligned mirror shells that are used during resolution testing. Performance testing of this system will take place before and after vibration testing to verify the subsystem at TRL-5.

Additionally, a monolithic mount that incorporates both the optics and the gratings will be considered. This is not a requirement for TRL-5 or -6 but may be a critical consideration given mission architectures that are dedicated to grating spectroscopy. In such a configuration, individual parabola-hyperbola-grating channels will be fabricated from the same material and co-aligned in a single mount channel by channel. This will greatly ease considerations dealing with thermal and mechanical interfacing as well as integration and alignment within the observatory. Such a design is intended to be used on an upcoming suborbital rocket mission (see **Section 3.3.9**).

3.3.6 OP-XGS TRL 5 Milestones

The empirical milestones used at each step of our TRL 5 development are outlined here. First, to ensure the fidelity of blazed master fabrication we will produce scanning electron micrographs and atomic force microscopy images to measure the groove shape, roughness, and uniformity. Repetitive imaging of the groove profile will quantify the repeatability and yield of the process. Second, the assessment of substrate material in our trade study will depend

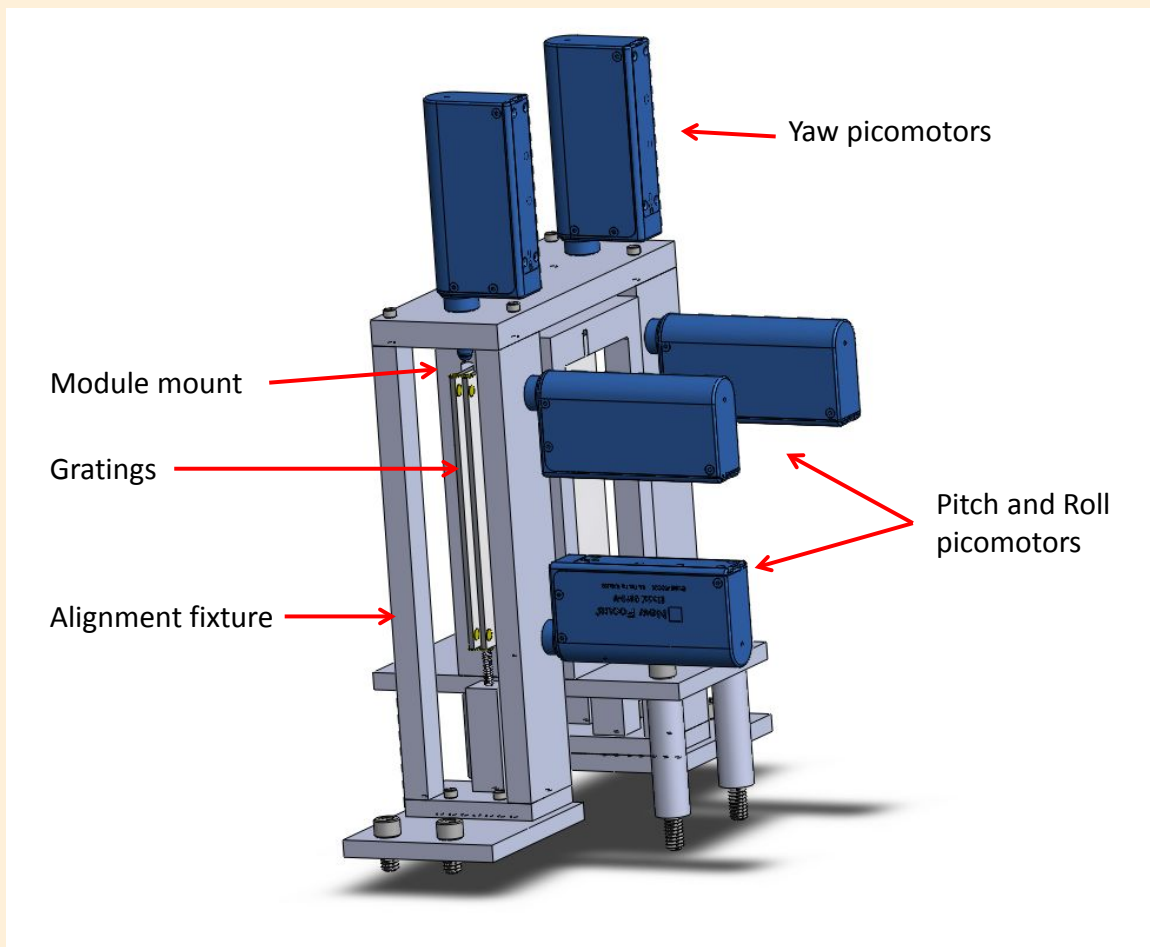


Figure 3.3–5. Nanopositioning alignment fixture for populating off-plane grating modules.

on manufacturability, cost, and ease of alignment. We will measure the surface figure of Be and Si substrates before and after alignment as well as the tightest achievable tolerances for each. This will be performed on several substrates within multiple modules. Third, our replication process will be assessed based on the ease of replication in our nanoimprint lithography machine between Be and Si substrates. We will measure the surface figure before and after replication to quantify induced figure error during the replication process, if any. These tests will be performed on multiple substrates of each material. Finally, the alignment methodology will be vetted through measurement of alignment tolerances achieved from our high-precision alignment mount. We will use a Shack-Hartmann sensor (SHS) to measure the relative attitudes of each grating as they are integrated into the module. We will sample closely spaced gratings as well as gratings placed at the limits of the module volume. The alignment mount and SHS provide 5 degrees-of-freedom knowledge. The sixth, grating yaw, will be measured during X-ray testing. Using nanoactuators on the alignment mount we will quantify the alignment accuracy in each degree of freedom for every mounted grating. The module will undergo throughput and spectral resolving power tests before and after environmental testing in order to verify the subsystem at TRL 5. These tests can be performed at least three times to verify module alignment repeatability. Furthermore, we will model performance predictions during TRL 6 development assuming higher fidelity components.

3.3.7 Steps to TRL-6

Given the previously stated developments, there are a handful of well-defined tasks that need to be accomplished to mature this technology to TRL-6. The developments of grating fabrication, replication, module design, and alignment directly influence TRL-6 developments by merely applying them at a larger scale. The current prototype grating size is 25×32 mm and will need to be a factor of $\sim 2\text{--}4$ larger in each of these dimensions for future observatories. Increasing the size will increase geometric efficiency, decrease complexity, ease alignment, decrease mass, and decrease power requirements. Depending on the observatory, not all of these benefits may be critical (such as mass or power), yet the design has the ability to be tailored. Therefore, the major technical challenges during this phase are: 1) the fabrication of a large-format master; 2) fabrication of a high-fidelity mount; 3) alignment of the large-format gratings; 4) performance testing of the assembly.

The fabrication of a large-format master has already undergone the design phase. The process has been discussed with LightSmyth Technologies, and the procedure to create large-format pre-masters up to $\sim 100 \times 100$ mm has been identified. Once the large pre-master is made. Techniques identical to those during TRL-5 development will be used to blaze and replicate these gratings. The substrate and module material will also follow those used in TRL-5. In fact, the substrate and module format used during TRL-5 will already be large enough to incorporate large-format masters and will merely receive tweaks to optimize performance. The same is true for the alignment methodology. The major difference for TRL-6 will be an identified observatory specification to fulfill. Once this is determined, the module design and alignment methodology will be reevaluated to verify their application.

The plan is to perform performance and environmental tests on a full-scale grating module with upward of a dozen aligned gratings. Verification of effective area and spectral resolving power on this module will firmly place the OP-XGS at TRL-6 once a specific architecture is identified.

3.3.8 OP-XGS TRL 6 Milestones

The ability to quantify measurable milestones assumes that a specific mission architecture has been defined, thus allowing for a definition of TRL 6, and therefore a definition of the performance requirements, and how they flow down into the grating spectrometer design. Nonetheless, grating efficiency, resolving power, and alignment will still be the driving requirements, and the empirical milestones to reach TRL 6 are outlined here. First, we will verify the quality of a large format master through repetitive performance testing of throughput and spectral resolving power to obtain a presumed 40% diffraction efficiency and 3000 resolution. These tests will be implemented on the master as well as several replicas to ensure performance at each level. Next, we will performance test an aligned module of gratings. This development leverages heavily from the milestones achieved and modeling performed in TRL 5 and follows the same testing scheme. The high fidelity module mount will be based on the TRL 5 demonstration module with alterations based on the mass, power, and interface requirements of the mission. The alignment methodology and measurements will verify placement of each grating in the module within tolerance. Again, we will measure grating placement in all six degrees of freedom for all mounted gratings. We will verify the effective area and spectral resolving power of the aligned, populated module before and after environmental testing to achieve TRL 6. These steps can be repeated on at least three modules to demonstrate repeatability of achieving predicted performance levels.

3.3.9 Rocket Test

As a risk reduction measure, the launch of an OP-XGS on board a suborbital rocket flight is planned. This payload will utilize an array of slumped glass Wolter-1 optics followed by an array of precision-aligned, high-fidelity gratings that disperse onto a high-quantum efficiency (QE) CCD camera, thus increasing the flight and system

level readiness of these spectrometers. The key steps for this program are: 1) integrating the findings of the RTF programs into the optics and grating module designs; 2) fabrication of flight components; 3) launch.

The findings from the TRL-5 and -6 developments greatly reduce the technical risk associated with fabrication of this rocket payload. The OP-XGS on board this mission will incorporate the same gratings as those developed, and stated previously, and similar optics. Furthermore, high-QE CCDs will be flown to complete a system-level demonstration. Given that this is a dedicated grating spectrometer mission, we intend to fly monolithic optics/gratings modules. However, each subsystem will be tested in the laboratory for individual performance during pre-flight calibrations. Developing and flight proving a full OP-XGS will significantly reduce the risk of future grating spectrometer mission integrations and implementations.

3.3.10 Schedule and Funding to TRL-5 and TRL-6

The schedule to TRL-5 follows the current schedule of the SAT and RTF grants. As described previously, the plan is to demonstrate a spectral resolution >3000 with high throughput on a set of aligned, medium-fidelity gratings in a medium-fidelity module mount. The final fabrication steps for the master gratings and the alignment mount are currently taking place. The blazed master gratings will be tested for throughput and resolution in 2013. The precision of the alignment mount will be tested during that same timeframe. Following these tests, 2–3 gratings will be aligned into the mount and tested with the optics module consisting of three aligned shells. Environmental and performance testing of this system will solidify a TRL of 5 by the end of the 2013 calendar year. Given that these are the goals already set forth in these current programs, no additional funding is required at this time.

The developments made during the SAT and RTF programs will provide the final details for the current roadmap to TRL-6. However, it is not the goal of these programs to reach TRL-6, so additional funding will be required for this development phase. As outlined previously, the tallest poles will be the fabrication of a large-format master grating, followed by alignment of many, closely packed gratings. However, much of that is due to cost, not technology. Upon definition of a specific mission architecture, we will be able to finalize grating parameters and tweak the current techniques to provide this capability. Assuming a mission program beginning in 2017, a schedule and estimated costs to reach TRL-6 is presented in **Table 3.3–1**.

Table 3.3-1. Off-Plane Gratings Technology Schedule and FY13 Costs

Task	2013	2014	2015	2016	2017	2018	2019	
Grating Fabrication	Blazed master fabrication and performance testing							
	Substrate trade study	Develop replication technique, performance test replicas	Replicate for module alignment testing and rocket payload					
	Design large format mask	Fabricate large format master						
Grating Alignment	Finish characterization of low fidelity module mount performance	Perform Module Fabrication/Alignment Methodology trade study	Fabricate medium fidelity grating mount and align 3 gratings					
	Design medium fidelity mount		Environmental and performance testing of medium fidelity mount – TRL5					
Grating Alignment		Design and fabricate monolithic mount	Tweak design and refabricate					
		Co-align 3 sets of parabola/hyperbola/grating channels	Co-align 3 sets of parabola/hyperbola/grating channels					
		X-ray performance tests	Environmental and Performance Testing					
Flight		Construction and flight of rocket with OP-XGS						
	Rocket Test	Receive input on grating fabrication, material, optical design	Receive input on module mount fabrication and alignment	Final Alignment and assembly	Rocket Launch			
TRL 6	Mission specific development	Preparation for TRL 6 demo per mission requirements						
Budget Estimate		\$1.1M	\$1.7M	\$1.6M	\$1.2M	\$1.9M	\$1.5M	

■ TRL 5 development
■ TRL 6 development
■ Risk reduction/performance margin increase
 New funding required

3.4 Critical-Angle Transmission X-ray Grating Spectrometer Technology Development Roadmap

3.4.1 Introduction

This section summarizes the technology status and development roadmaps for a Critical-Angle Transmission X-ray Grating Spectrometer (CATXGS). A brief description of the instrument and its heritage are provided in this introductory section. In the following **Section 3.4.2**, the current status of the XGS gratings are described, and the roadmap and schedule for bringing these to technical readiness for full instrument development are outlined. X-ray CCDs for the detector component of the CATXGS are described in **Section 3.5**.

3.4.2 CATXGS Description

The Critical-Angle X-ray Grating Spectrometer is a wavelength-dispersive high-resolution spectrometer offering spectral resolution $\lambda/\Delta\lambda \geq 3000$ (FWHM) and effective area on the order of 1000 cm² in the 0.3–1.0 keV spectral band.

The CATXGS relies on a novel optical element recently developed at MIT: the CAT grating. The CAT grating is a blazed X-ray transmission grating that provides high-dispersion spectroscopy with excellent efficiency over a broad spectral bandwidth, low mass and relaxed alignment tolerances (Heilmann et al. 2008). Recent accounts of the CATXGS optical principles, state of development, and configuration are given by Heilmann et al. (2009–2012).

The CATXGS is shown schematically in **Fig. 3.4–1**. Arrays of CAT gratings are located in two sectors behind the flight mirror assembly. The gratings are mounted tangent to the Rowland torus. They diffract X-rays through a range of angles near the grating blaze angle (~1.5 degrees) and the dispersed spectrum is recorded by a dedicated CCD camera, displaced from the mirror focus (F). Thus, the complete CATXGS instrument consists of a set of grating arrays and a readout subsystem. The CAT grating has high diffraction efficiency in many (up to 10) orders near the blaze angle, and the intrinsic energy resolution of the CCD detectors is used to separate the overlapping orders.

The CAT grating array mounting concept is shown in more detail in **Fig. 3.4–2**. Each grating array contains many individual grating membranes, and each membrane is secured within a facet frame. The individual CAT grating membranes, ~6×6 cm in size, are produced from conventional silicon-on-insulator (SOI) wafers using nanofabrication techniques. The grating bars within a membrane are fabricated in the 4–6 μm-thick SOI device layer, and are nominally 40 nm wide and 4–6 μm deep; the grating bar period is 200 nm. The grating bars are supported by a two-level structure fabricated in the silicon wafer along with the grating bars. The finer “Level-1” (L1) supports are fabricated in the SOI device layer; the coarser hexagonal “Level 2” (L2) supports are fabricated in the ~500 μm-thick SOI handle layer.

CATXGS Heritage

X-ray transmission gratings have a long flight history dating to the *Einstein Observatory* (HEAO-2), which operated from 1978–1981. The CATXGS is a direct descendant of the high-energy transmission grating (HETG) spectrometer, launched in 1999 and still operating successfully on the *Chandra X-ray Observatory*.

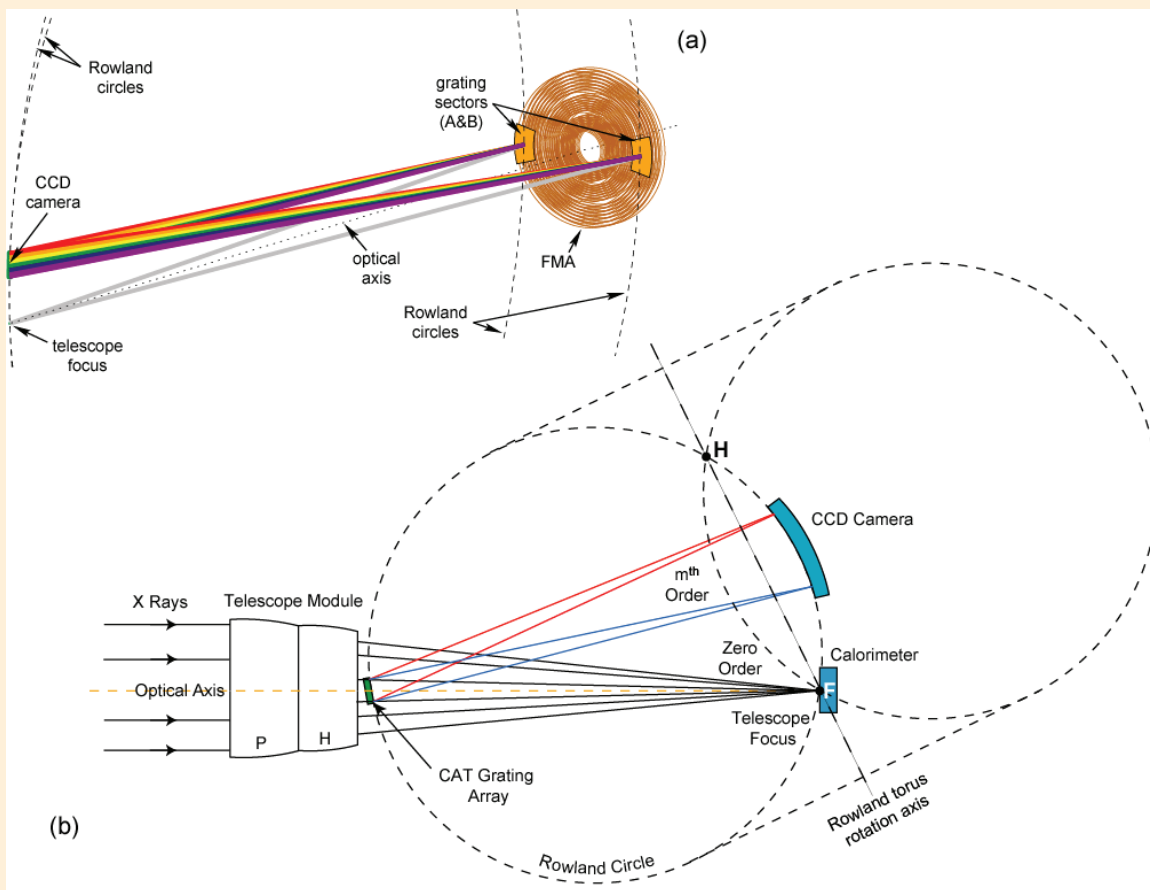


Figure 3.4-1. This schematic shows a CATXGS (not to scale). **(a)** Shown here is a perspective view of optical design, with X-rays incident onto the FMA from the right. **(b)** A side view of optical design is shown here. X-rays are focused by the telescope module onto the focus F. CAT gratings intercept a fraction of the X-rays and diffract them, predominantly at angles centered around the blaze direction. Representative paths for longer (red) and shorter (blue) wavelength rays diffracted in one order are shown. The CAT grating has high diffraction efficiency in many orders.

3.4.3 Technology Development Roadmap

3.4.3.1 Technology Status

Technology development is required for the CAT grating arrays. Test gratings with the required period (200 nm), bar-thickness (40 nm) and bar aspect ratio (150:1) have been successfully fabricated with a potassium hydroxide (KOH) wet-etch process and X-ray tested, showing 80–100% of the theoretically expected diffraction efficiency over most of the soft X-ray band, putting the technology at TRL-3. However, the wet-etch process suffers from trapezoidally broadening L1 supports, which significantly reduce the open area for CAT grating bars.

To solve the support broadening problem, a deep reactive-ion etch (DRIE) process has been developed that simultaneously etches CAT grating bars and L1 supports vertically into the device layer. A process that allows for the fabrication of large-area ($> 30 \times 30 \text{ mm}^2$) gratings with the full hierarchy of CAT gratings bars and L1 and L2 supports with $>60\%$ of open area was also demonstrated.

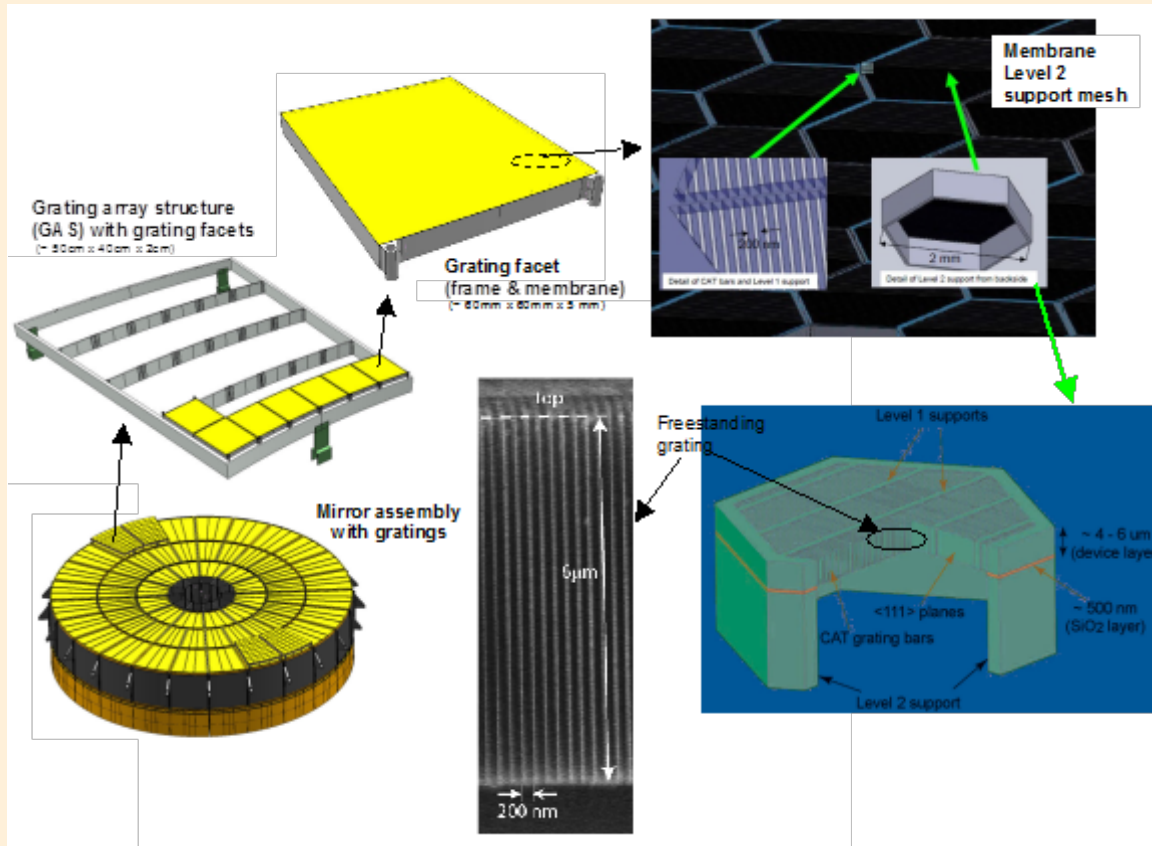


Figure 3.4-2 This image shows a CAT grating array and mounting concept and grating membrane structure.

3.4.4 Technology Development Tasks

The remaining steps for CATXGS technology development toward TRL-5 are to:

1. Optimize the deep reactive-ion etch (DRIE) and combine it with a short wet-etch polishing step to improve the CAT grating bar profile and sidewall roughness;
2. Demonstrate CATXGS resolving power in an imaging X-ray system;
3. Adapt alignment techniques originally developed for the *Chandra* Advanced CCD Imaging Spectrometer (ACIS) HETG spectrometer for use in aligning CATXGS grating membranes within an array;

These goals will be achieved by performing three technology development tasks. These are discussed in **Section 3.4.4.1**. **Fig. 3.4-4** shows the current schedule for performing these tasks.

3.4.4.1 Grating Fabrication Technology Development

Task 1: Combine and optimize dry- and wet-etch processes for high-efficiency, high-throughput, large-area ($> 30 \times 30 \text{ mm}^2$) CAT gratings. DRIE does not produce smooth enough CAT grating bar sidewalls. This task includes the development of a process, such as a short potassium hydroxide (KOH) polish, to smooth out the sidewalls and its integration into the existing process flow. Acquisition of a dedicated DRIE tool will accelerate DRIE process optimization. Verify success via X-ray diffraction efficiency measurements.

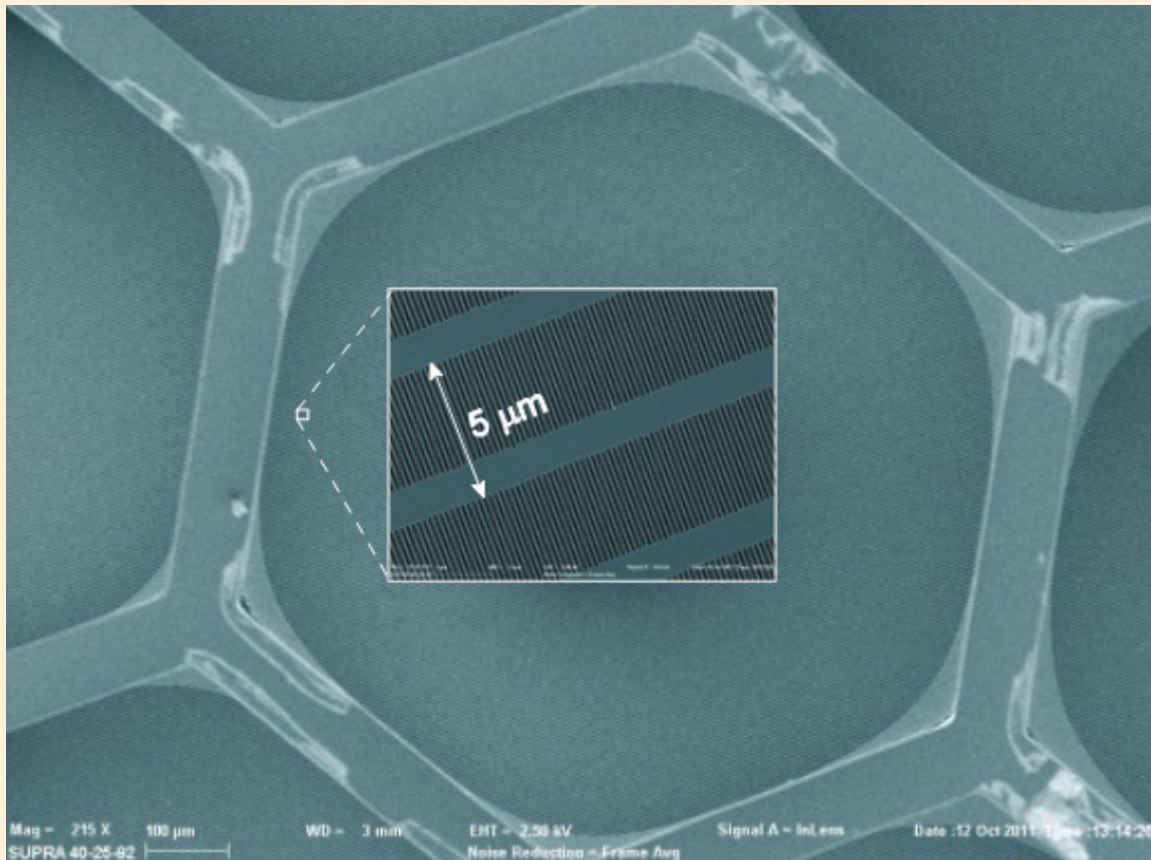


Figure 3.4–3 This scanning electron micrograph of the bottom of a 31×31 mm² deep reactive-ion etched CAT grating shows the hexagonal L2 mesh etched from the bottom and the much finer L1 supports etched from above. Inset: This zoomed-in view shows the L1 lines and the 200 nm-period CAT grating bars.

Task 2: Demonstrate CATXGS resolving power in an X-ray imaging system. After we have a high-quality large-area grating, measurements of resolving power will be performed by putting the grating in a converging X-ray beam, such as the one at the Marshall Space Flight Center (MSFC) Stray-light Test Facility (breadboard test—TRL-4). After multiple gratings are available, these measurements will be repeated (breadboard of grating array).

Task 3: Detailed facet/frame design, membrane integration, and alignment process development. Each grating membrane must be integrated with a facet frame so that it can be mounted in the grating array structure. The various grating facets must then be aligned with one another. This task will draw on the experience gained in assembling and aligning grating facets for *Chandra* HETG to develop the procedures required for a CATXGS.

This task will include fabrication, alignment and X-ray, and environmental testing of a brass board grating array structure (GAS) (see **Fig. 3.4–2**) partially populated with grating facets. Reaching TRL-5 (X-ray performance verification) for the brass board grating array is anticipated by the end of 2016.

Tasks, durations, and milestones from TRL-4 to TRL-5 (several of these tasks can be done in parallel with sufficient manpower):

1. Fabricate tens of high-quality large-area gratings (9 months)

2. Design and manufacture frames for gratings (4 months)
3. Design and build infrastructure for grating-to-frame alignment (9 months)
4. Environmental and X-ray tests of grating facets (i.e., gratings mounted to frames)—gated by tasks 1–2 (6 months)
5. Design and build brass board GAS (4 months)
6. Develop metrology to align and mount grating-facets to brass board GAS, align and mount—gated by tasks 1–5 (6 months)
7. X-ray and environmental tests of brass board GAS populated with grating facets—gated by tasks 1–6 (6 months)

TRL-6 will depend on mission specifics. It requires full-size gratings ($60 \times 60 \text{ mm}^2$) with the specified performance (diffraction efficiency averaged over grating area), integrated into frames of specified mass and obscuration, aligned and mounted into a prototype GAS of specified size, mass, and obscuration. TRL-6 will be demonstrated through environmental (vibration, thermal) and X-ray testing (effective area, resolving power) of the populated GAS, and can be achieved by the end of 2019.

Tasks, durations, milestones from TRL-5 to TRL-6 (several of these tasks can be done in parallel with sufficient manpower):

1. Scale up grating fabrication process to full-size gratings (12 months)
2. Redesign and manufacture frames for full-size gratings (4 months)
3. Scale up grating-to-frame alignment and integration for full-size gratings (6 months)
4. Environmental and X-ray tests of full-sized grating facets—gated by tasks 1–3 (6 months)
5. Design and build GAS prototype (6 months)
6. Develop scaled-up grating-facet-to-GAS alignment and integration steps—gated by tasks 1–5 (3 months)
7. X-ray and environmental tests of GAS populated with full-size gratings—gated by tasks 1–6 (6 months)

3.4.4.2 TRL 5 and 6 Demonstration

TRL 5 will be demonstrated through X-ray and environmental tests of a brass board GAS with aligned large area grating facets in a suitable facility such as the MSFC Stray Light Test Facility in combination with focusing optics of an appropriate focal length and X-ray detectors. Performance criteria will be spectral resolving power $R = \lambda/\Delta\lambda \geq 3000$ (based on diffraction line width, facility performance without gratings, and optical/ray-trace models) and effective area or relative GAS throughput (X-ray count rates in blazed diffraction orders normalized to incident flux on the GAS, measured at a few relevant wavelengths). The X-ray tests will be repeated before and after vibration, shock, and thermal cycling of the brass board GAS. TRL 6 will be demonstrated in similar fashion, except that performance criteria for resolving power (presumably $R > 3000$), effective area over a certain bandpass, and mass will be based on specific mission requirements. Grating facet size and GAS prototype design will also be mission specific, as well as focusing optic properties and detectors

3.4.5 CAT Gratings Schedule and Costs

Table 3.4-2 shows the major milestones associated with the schedule and costs to reach TRL-6 for the CAT grating.

Table 3.4-2. CAT Gratings Technology Development Schedule and FY13 Costs

Task	2013	2014	2015	2016	2017	2018	2019
Fabrication		Combine and optimize dry and wet etch processes for high efficiency, high throughput, large area (> 30 x 30 mm ²) CAT gratings	Scale up grating fabrication process to full-size grating	Design and build GAS prototype			
Performance Demonstration		Demonstrate CATXGS resolving power in an X-ray imaging system			Environmental & X-ray tests of full-sized grating facets		
Mounting		Detailed facet/frame design, membrane integration and alignment process development	Redesign and manufacture frames for full-size gratings	Develop scaled-up grating-facet to-GAS alignment and integration steps – gated by Tasks 1-5			
			Environmental & X-ray tests of grating facets	Scale up grating-to-frame alignment and integration for full-size gratings			
			Alignment verification and environmental test of brass board GAS	X-ray and environmental tests of GAS populated with full-size gratings – gated by Tasks 1-6			
Budget Estimate		\$1.25M	\$1.5M	\$1.5M	\$1.5M	\$1.0M	
		\$1.25M	\$1.0M				

 TRL 5 development
 TRL 6 development
 Risk reduction/performance margin increase
 SAT already awarded
 New funding required

3.5 Gratings Charge-Coupled Device (CCD) Detector Technology Development Roadmap

3.5.1 Introduction

This section summarizes the technology status and development roadmaps and schedule for enhanced charge-coupled device (CCD) detector as part of an X-ray grating spectrometer. X-ray CCD detectors have a rich flight heritage, having flown on at least six high-energy astrophysics missions since their first use on the *ASCA* satellite, launched in 1993. The CCDs discussed here are similar to those currently in use on the *Suzaku* mission and descend directly from those now operating on *Chandra*. Existing X-ray CCD technology adequately meets the requirements for a gratings detector assuming the gratings themselves can meet specific requirements on throughput and efficiency. The technology development discussed here would increase the throughput of X-ray gratings systems at longer wavelengths or lower energies, creating margin that could be used to relax requirements on the grating technologies described in **Sections 3.3** and **3.4**.

3.5.2 Technology Development Roadmap

3.5.2.1 Technology Status

The CCD devices used in the IXO XGS design were enhanced versions of those currently operating on *Chandra* and *Suzaku* that have the X-ray detection efficiency and spectral resolution required for large effective area gratings detectors. Like all X-ray CCDs, they require optical blocking filters (OBF) to reject out-of-band “optical” (i.e., ultraviolet, visible, and near-infrared) radiation that would otherwise degrade detector performance. These filters inevitably absorb X-ray photons as well, reducing system throughput. The IXO XGS requirement was 1000 cm² of effective area across the entire 0.3–1.0 keV band. Absorption effects from the OBF forced a design where this requirement was just met at lower energies, while the actual effective area at higher energies was significantly larger. Sensitivity to optical light can be minimized in X-ray photon-counting systems by reducing the CCD integration period, since this minimizes the number of incident optical photons per readout for a given optical flux. By increasing X-ray CCD readout speed, the minimum integration time can be reduced, which in turn reduces the required OBF thickness. To further minimize OBF thickness, the filters will be deposited directly on the CCDs.

3.5.3 Technology Development Tasks

For application to X-ray gratings, current detectors themselves are at TRL-5. The remaining steps of the detector system towards TRL-5 are to enhance the CCD readout system to maximize low-energy detection efficiency by directly depositing the OBF and increasing the readout speed of the system. This latter development task requires both slight modifications to the detector itself and changes to the readout electronics, which would need to be implemented with radiation-hardened electronics. Two approaches have been identified for this final step, one of which involves recently developed CCD technology, currently at TRL-3, that offers some attractive advantages for X-ray gratings.

These technology development tasks are discussed in **Section 3.5.3.1**. **Table 3.5–1** shows the current schedule for performing these tasks.

3.5.3.1 Technology Development Tasks

Task 1: *Develop directly deposited thin-film optical blocking filters.* As previously noted, thin film OBFs are required to avoid CCD performance degradation in the presence of stray light in the ultraviolet (UV), visible, and near-infrared (IR). The X-ray opacity of the OBF must be minimized to achieve the required system detection efficiency in the X-ray band ($0.3 \text{ keV} < E < 1.0 \text{ keV}$). Moreover, the higher readout rate of X-ray CCDs (Task 2) will reduce the required optical opacity, and should make it possible to employ thinner OBFs than have been used on previous missions. Finally, the relatively large area ($\sim 50 \text{ cm}^2$ per camera) of the X-ray gratings focal planes renders free-standing filters problematic.

Directly deposited blocking filters have been used successfully on previous missions—notably the XMM-Newton Reflection Grating Spectrometer—and there is laboratory experience with relatively thick (aluminum+parlylene $\sim 200 \text{ nm}$ total thickness) directly deposited OBFs. However, a directly deposited filter as thin as those contemplated for X-ray gratings ($< 50 \text{ nm}$) with the back-illuminated X-ray gratings devices has not yet been demonstrated. A NASA SAT program was begun in July, 2012 to demonstrate directly deposited blocking filters. This technology is expected to be demonstrated by July, 2014.

Task 2: *Increase detector readout speed.* The baseline CCD detector for the X-ray gratings, the MIT Lincoln Laboratory CCID41, is a 1024×1024 pixel frame transfer device with four output nodes. Front- and back-illuminated versions of these detectors are successfully operating on the *Suzaku* mission; the X-ray gratings will use back-illuminated devices. The CCID41 is a direct descendant of the CCID17, currently operating in *Chandra's* ACIS instrument. The primary difference between the CCID41 and CCID17 is the presence of a charge injection register on the former. This feature has proven effective in mitigating the effects of radiation exposure and would be retained for the X-ray gratings.

On the *Chandra* and *Suzaku* missions, the readout speed of the devices is slower (100 kHz and 42 kHz per node, respectively) than required for X-ray gratings, which is to operate at 500 kHz per node or more. As previously noted, faster readout reduces optical contamination of each X-ray event, allowing thinner OBFs, and therefore providing better low-energy X-ray detection efficiency. The readout speed requirement for the X-ray gratings is 15 frames/s.

Two detector development paths are being considered to meet this requirement. The first, most direct path involves two modifications of the existing CCID41 to reduce power consumption and maintain noise performance at the higher speed. The two design modifications for this path are:

1. Addition of metal ‘straps’ to the parallel transfer gate busses and electrodes to minimize gate impedance, voltage drop, and power consumption during readout. This change has been successfully implemented on other Lincoln Laboratory devices. Since the X-ray gratings detectors are back-illuminated, the additional strapping will not affect detection efficiency.
2. Replacement of the existing, on-chip Metal-Oxide-Semiconductor Field-effect Transistor (MOSFET) output source-follower with a higher responsivity Junction Field-effect Transistor (JFET) device to maintain low noise performance at the higher readout speed. The JFET amplifier has already been demonstrated in the laboratory on a small test detector. A factor of two increase in responsivity is expected.

A second, parallel development path will be developed that exploits the substantial advances in detector fabrication, readout amplifier design, and CCD architecture that have occurred in the decade since the CCID41 was developed. In particular, single-level polysilicon transfer gates now allow operation with much lower clock swings (3.3 V vs. 10 V) and a 10-fold reduction in clock power consumption, and multicell, multiplexed output

architectures offer improved readout speed with no compromise in noise performance, and nearly an order of magnitude improvement in radiation tolerance. Such advanced architecture CCDs (AACCD) are also compatible with integrated (on-chip) complementary metal-oxide semiconductor (CMOS) analog signal processing that offer corresponding reductions in power consumption of analog signal processing chains. Successful development of the AACCD would enable an X-ray gratings instrument with lower mass, less power consumption, and lower cost than one relying on modified CCID41s.

Each of these development paths requires modification of existing device designs and fabrication of test devices, and subsequent performance and environmental testing. In the case of the CCID41, production of a single, dedicated development lot, followed by a suitable X-ray and radiation-tolerance test program will be sufficient to demonstrate the necessary enhancements. This could be accomplished in 21 months. In the case of the AACCD branch, two fabrication/test cycles are planned. The first of these (Cycle 1) would confirm the X-ray performance of a small-scale AACCD device, and the second (Cycle 2) would produce a full-scale detector. Given interest of other Government agencies in this technology, Cycle 1 could be completed, in collaboration with other programs at Lincoln, within 24 months. Cycle 2 would require an additional 24 months.

Development of the enhanced CCID41 and the AACCD in parallel through AACCD Cycle 1 is planned. If the performance, radiation tolerance, and other engineering and cost advantages of the AACCD, relative to the CCID41, are sufficient to justify it, Cycle 2 of AACCD development would take place. If not, the enhanced CCID41 for the X-ray gratings would be selected. This decision would also determine the approach to Task 3 (described next). At the completion of this task, the CAT-XGS detectors would have achieved TRL-6.

Task 3: *Develop low-power, radiation-tolerant detector electronics.* The basic architecture for CCD control and readout electronics has been demonstrated on a number of previous missions and is well understood. Given the relatively large number of parallel output channels (64 for the enhanced CCID41 approach; 80 for the advanced CCD architecture approach) and the higher readout rates, it is desirable to reduce power and mass requirements for the readout electronics by integrating components, where possible. The two CCD development paths described previously drive two distinct electronics development paths. Depending on the outcome of Task 5, one or the other of these paths will be followed.

Enhanced CCID41s would require development of radiation-tolerant application-specific integrated circuits (ASICs). Members of the CCD detector team have already demonstrated that elements of the analog signal chain can be integrated with the analog-to-digital conversion function in ASICs (Nakajima et al. 2009). This implementation requires further development to demonstrate adequate noise performance at CCD readout rates, and to achieve the necessary radiation tolerance (>54 krad Si for a 10-year mission). Following this approach would entail building on existing ASIC designs to develop a CCD readout ASIC that meets the X-ray gratings requirements for noise performance and radiation tolerance. Three iterations of the design/fabricate/test cycle are anticipated to be required. The performance of the final ASIC design would be measured with devices from the detector development lot described in Task 2, and radiation tolerance would be demonstrated. This ASIC development effort would be completed in 30 months.

Alternatively, the AACCD allows the signal processing electronics to be integrated with the detectors themselves using a three-dimensional (3-D) circuit integration process (e.g., Suntharalingam et al. 2007, and references therein). In the 3-D process, separate wafers containing detectors and electronics, respectively, are integrated in a vertical stack by means of precision alignment and oxide bonding.

Electrical connections between the wafers are then made by means of extremely small conductive plugs. The result is illustrated in **Fig. 3.5–1**, which shows a scanning electron microscope (SEM) cross-section of a 3-D imager. Unlike conventional hybrid (or “bump-bonded”) vertical integration, this oxide-bonded wafer-scale approach can

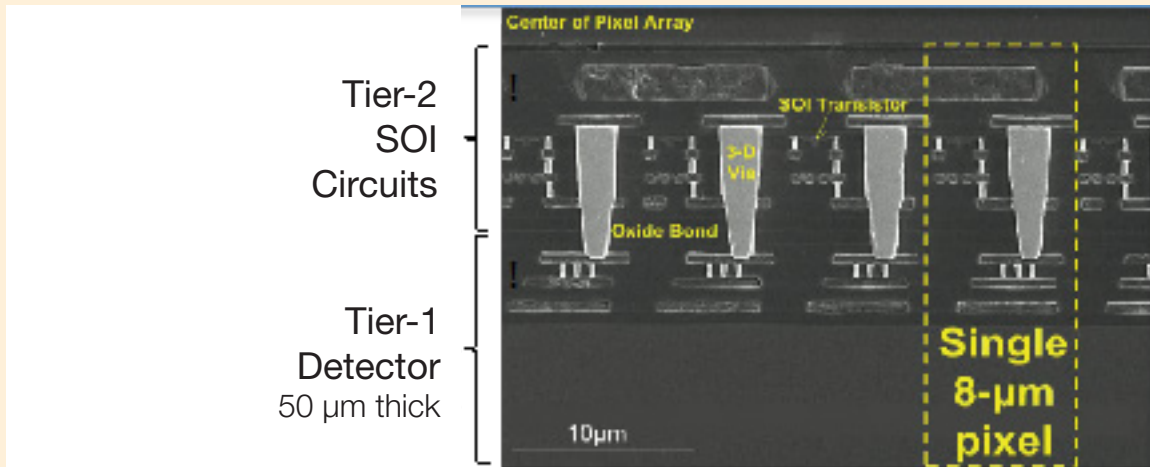


Figure 3.5-1 This SEM cross-section of integrated imaging detector and readout circuitry is fabricated with MIT Lincoln Laboratory 3-D circuit integration technology.

realize pixels smaller than $5\ \mu\text{m}$, has been shown to extend to three-circuit layers, and is fully compatible with the post-integration hydrogen-passivation anneals that are critical for dark current suppression in silicon detectors.

This 3-D technology offers the benefits of SOI CMOS circuitry. Radiation hardness in SOI CMOS is improved over bulk CMOS because the transistors occupy a smaller volume of silicon and because carriers created in the bulk wafer by energetic particles cannot flow into the active circuits. SOI circuits have also been shown to be less prone to single-event-upset damage than bulk CMOS technologies.

Development of on-chip electronics for the AACCD would require at least two design/fabricate test cycles of the electronics ‘tier’, followed by 3-D integration with the AACCD detector tier produced in Task 2. It is estimated that this effort could be completed in 36 months.

3.5.4 CCD Detector Subsystem and Readout

Table 3.5-1 shows the major milestones associated with the schedule and costs to reach TRL-6 for X-ray CCD gratings detectors.

3.5.5 TRL 5 and 6 Demonstration

CCD detectors are currently at TRL 5, as detectors meeting all requirements except readout speed and directly-deposited optical blocking filter (OBF) are now functioning in orbit (e.g., on Suzaku). The integrated detector/OBF component will reach TRL with the demonstration of required X-ray and optical performance, stability, and robustness to thermal cycling as part of a current Strategic Astrophysics Technology effort that is on schedule for completion by July 2014. Demonstration of TRL 6 for the detectors will require design and fabrication and packaging of a test-lot of detectors incorporating (existing) high-speed parallel clock and low-noise preamplifier designs already demonstrated on other (non X-ray) devices. Exit criteria for TRL 6 include demonstration with these detectors of required X-ray spectral resolution, detection efficiency, and optical light rejection, for the given specific mission requirements, at the required frame rate and after suitable thermal vacuum, vibration, and (non-ionizing) radiation exposure.

Table 3.5-1. CCD Grating Detector Technology Development Schedule

Task	2013	2014	2015	2016	2017	2018	2019	
Blocking Filters	Develop directly-deposited thin film optical blocking filters							
Readout Speed			Increase Detector readout speed (TRL 6)					
CCD Development			Develop advanced architecture CCDs					
				Fabricate & test high-speed CCDID41B or advanced CCD		Demonstrate TRL 6		
Low Power Rad Tolerant ASICs			ASIC design, fabrication and test (2 iterations to TRL 5)				Demonstrate TRL 6	
Budget Estimate	\$0.25M	\$0.5M	\$1.0M	\$1.5M	\$1.5M	\$1.0M		
		\$0.75M					\$1.0M	

TRL 5 development
 TRL 6 development
 Risk reduction/performance margin increase
 SAT already awarded
 New funding required

High-speed ASICs similar to those required have been qualified for flight on Astro-H. These devices must be modified to perform with slightly lower noise, higher speed, and better radiation tolerance to meet XGS requirements. Exit criteria for TRL 6 will include demonstration of required noise performance with TRL 6 CCDs operating at required speeds and after suitable thermal vacuum, vibration, and radiation exposure.

An alternative development path via the advanced architecture CCD (AACCD) would require demonstration of a modest-scale test device with the required X-ray performance and readout speed with bench analog electronics to achieve TRL 4, followed by fabrication and X-ray performance demonstration of a similar device with (3-D) integrated analog processing electronics to achieve TRL 5. TRL 6 would require fabrication of full-scale CCDs with integrated electronics, and demonstration of required X-ray spectral resolution, quantum efficiency and optical light rejection at the mission-specific required frames rates and after suitable thermal-vacuum, vibration and radiation exposure

3.6 Technology Development Costs—Summary

Table 3.6-1 shows the cost by technology area and by year of the activities described in the previous section. It includes funding that has already been awarded through the PCOS SAT program through FY2014. Of the \$62M required to complete the entire program, \$12M has already been awarded. Thus the additional total needed over the seven years through FY2020 is \$50M.

The technology and the funding profile included in this report assume that an X-ray Probe-class mission will be selected, and that it will include both a calorimeter spectrometer and a grating spectrometer. The values in **Table 3.6-1** therefore represent an estimate of the maximum required. It should be noted that decisions will be made over the next three years that could allow for a reduced level of funding or a less aggressive funding profile. These possible decision outcomes include: (1) ESA selecting *Athena+* as their L2 mission for a 2028 launch; (2) the NASA study team putting forward a single-instrument probe-class mission; (3) NASA not selecting the X-ray Probe-class mission; or (4) neither *Athena* nor the X-ray probe is selected. The ramifications of these decisions on the funding profile are summarized in turn below.

Decision 1: *Athena+* is selected as L2 (no earlier than November 2013)

Possible U.S. contributions to *Athena+* include any or all of the technologies described in this roadmap: optics, a calorimeter spectrometer (in whole or in part), and a grating spectrometer. Because ESA will require all technology for its L2 mission to attain TRL-5 by 2018, it will be essential to continue aggressively funding at least those technologies for which ESA has expressed an interest.

While ESA is funding the development of a baseline mirror technology (silicon pore optics, or SPO), it should be noted that the slumped glass represents a viable alternative, and thus a risk reduction measure. This is recognized by ESA, which is funding slumped glass development in Europe. Continued funding of the slumped glass mirror technology development is necessary even if ESA states no interest in using it, as this work forms the basis for the advanced optics work that could lead to a sub-arcsecond mirror for a late 2020's mission, as described in **Section 4**.

If *Athena+* is selected as L2, it will not be launched before 2028. It is possible that NASA will still select an X-ray probe. Such a probe might be a precursor mission to *Athena+*, with a more modest calorimeter and mirror, or it could complement *Athena+* by providing a large-area grating spectrometer (*Athena+* currently carries no grating spectrometer). Thus, it is anticipated that a FY14 Probe-class mission study will take place even if *Athena+* has been selected.

Decision 2: X-ray Probe is descoped to a single instrument (2015)

It is possible that the Probe-class mission study team will recommend that a grating spectrometer not be accommodated due to cost constraints. In that case, the development of the gratings and CCD detector technologies assume a lower priority than the mirror and the calorimeter.

Decision 3: X-ray Probe is selected (mid-2015)

The funding profile includes the development of both grating technologies through TRL-6. If the X-ray probe is selected for a 2017 start, its aggressive development schedule will require an instrument AO to be released as soon as possible after the 2015 selection. Thus, funding of only the selected grating technology would need to continue at high priority after 2016.

Decision 4: Neither *Athena+* nor the X-ray Probe is selected (mid-2015)

In this scenario, the goal of the technology development shifts to having all key technology at TRL 5 in time to support a proposal to the 2020 decadal survey for a strategic X-ray observatory that performs the IXO science,

in direct response to the recommendation in NWNH. All of the technology development should continue to TRL 5 to fulfill the NWNH recommendation.

The NWNH report found that it is critical to sustain development of these technologies, which will form the foundation of more advanced technologies needed for missions that will be proposed for the 2020 Decadal.

Table 3.6-1. Total FY13 Costs for the X-ray Astrophysics Probe Technology Development

Technologies	FY 13 (\$M)										Total Costs
	FY 2013	FY 2014	FY 2015	FY 2016	FY 2017	FY 2018	FY 2019	FY 2020			
Mirror Technology	\$1.90	\$2.30	\$2.30	\$4.00	\$4.00	\$4.00	\$0.00	\$0.00	\$0.00		\$18.50
Off Plane Grating	\$1.10	\$1.70	\$1.60	\$1.20	\$1.90	\$1.50	\$1.50	\$0.00	\$0.00		\$10.50
CAT Gratings	\$1.25	\$2.25	\$1.50	\$1.50	\$1.50	\$1.00	\$0.00	\$0.00	\$0.00		\$9.00
CAT Detectors	\$0.25	\$1.25	\$1.00	\$1.50	\$1.50	\$1.00	\$0.00	\$0.00	\$0.00		\$6.50
Micro-Calorimeter	\$1.80	\$2.00	\$2.24	\$2.30	\$2.40	\$3.00	\$3.00	\$3.00	\$3.00		\$19.94
SAT Already Awarded	\$5.20	\$6.05									\$11.25
New Funding	\$1.10	\$3.45	\$8.6	\$10.5	\$11.3	\$10.5	\$4.5	\$3.0	\$3.0		\$53.0
Totals	\$6.30	\$9.50	\$8.64	\$10.50	\$11.30	\$10.50	\$4.50	\$3.00	\$3.00		\$64.24
Technologies	Required Funding to Reach TRL 5					Additional Funding to Reach TRL 6					
Mirror Technologies	\$4.20					\$14.30					
Off Plane Gratings	\$4.40					\$6.10					
CAT Gratings	\$6.50					\$2.50					
CAT Detectors	\$2.50					\$4.00					
Micro-Calorimeter	\$10.74					\$9.00					
Totals FY 13 (\$M)	\$28.34 (\$11.25 already awarded)					\$35.90					

■ SAT already awarded
■ New funding required

■ TRL 5 development
■ TRL 6 development
■ Full reduction / performance margin increase

4 Longer-term Technology Needs

4.1 Introduction

The technology described in the previous section is critical for a near term X-ray Probe-class mission to start this decade designed to address NWNH science questions. In this section a small number of related but more advanced and potentially more capable technologies are briefly described. These technologies are less developed than the ones in the previous section but are advancements to the core capabilities recommended by NWNH for IXO and potentially could be matured sufficiently for inclusion in a mission that starts in the early 2020's. The relation between these technologies and those in the previous section is that those in the previous section are an essential prerequisite (optics and calorimeters) and/or the less developed technologies might eventually supersede those in the previous section (APS detectors supplanting CCDs).

The development timescale of these technologies is less constrained than those in the previous section, and a substantial investment needs to be made to bring them to comparable TRL. They are discussed in this technology roadmap because of their potential to replace the current technologies. Unlike the better-developed technologies, the ones described in this section are more appropriately currently funded through NASA's APRA program.

Some of the technologies described are parallel with one another, e.g., there are three or four different optics technologies. It is not obvious that any of these technologies will work at the desired levels. It may be necessary to employ hybrid approaches by combining technologies or to develop new approaches. Pursuing multiple technologies simultaneously improves the chances of success. Last, it should be noted that the following list of technologies is not all-inclusive and will have uses beyond the particular objectives stated here. No attempt is made to provide a development timescale or recommended funding needs, which will be discussed in a future report.

4.2 Optics Technology

Several technologies are described for developing lightweight sub-arcsec imaging grazing incidence optics. All the grazing incidence approaches can be married together in various combinations should that be necessary, so besides being competitive, they are also complementary.

4.2.1 Adjustable Optics

Adjustable X-ray optics is a technique whereby the shape of the mirror is adjusted or corrected after fabrication in order to reduce figure error. Two technologies to implement this approach are described below.

4.2.1.1 Thin film piezoelectric bimorph mirrors

In this approach, a strain introduced in a thin ($\sim 1 \mu\text{m}$) film of the piezoelectric material lead zirconate titanate (PZT) is used to deform a thin mirror, allowing for the correction of figure errors. After first depositing a continuous ground electrode, the PZT film is deposited also as a continuous layer on the back surface of 0.4 mm thick thermally formed glass segments of Wolter-I or Wolter-Schwarzschild grazing incidence mirrors. A pattern of independently addressable electrodes is lithographically printed on top of the PZT, defining the individual piezo actuator cells. Ultimately, a layer of zinc oxide will be deposited over the electrode layer, followed by the lithographic printing of integrated piezo cell control electronics and resistive strain gauges. A schematic cross section of the mirror design is shown in **Fig. 4.2–1(a)**, with a photo of a conical test mirror in **Fig. 4.2–1(b)**. When a DC voltage, typically

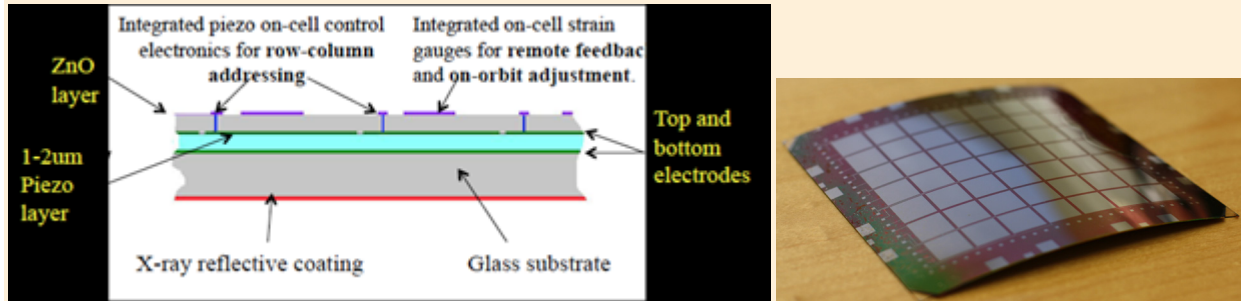


Figure 4.2-1 (a) Left – Schematic cross-section of thin piezoelectric film X-ray mirror. A low DC voltage applied across the top and bottom electrodes (green) produces a strain in the piezo film (light blue) parallel to the mirror surface (both in the plane of the page and out of the page). This produces localized bending in the structure, primarily over the extent of the individual top electrode. **(b) Right** – a test cylindrical mirror, 10 cm x 10 cm, with 49 piezo cells each 1 cm². The electrode side is facing up

< 10 volts, is applied to an electrode, a strain parallel to the mirror surface is produced in the PZT layer. This produces localized bending of the mirror (akin to the bending of a bimetallic strip under a temperature change), called an influence function (after the terminology used in VIS/IR active optics). Because the strain is parallel to the mirror surface, no heavy, large rigid reaction structure is needed. This enables the mirrors to be lightweight and thin, allowing dense packing of Wolter shells to achieve large X-ray collecting area. The integrated on-cell control electronics enables the use of row-column addressing, in use for many years in the LCD display industry.

Using calibrated influence functions, one for each piezo cell on the mirror, and standard optimization methods, a set of voltages for each cell is found that minimizes the existing mirror figure errors. Figure errors can be measured after mirror segment alignment and mounting, so that the correction can account for mirror fabrication errors, gravity release errors, and also mounting induced errors in the thin mirrors. The figure would be corrected once, on the ground, at the time of assembly. In principle, on-orbit figure corrections can be made to account for unexpected thermal conditions or some other ground-to-orbit change, via the use of the pre-calibrated strain gauges. The figure is corrected basically once, hence the term adjustable optics, as opposed to active optics.

The major advantage of this technology approach is that figure correction can account for not only mirror fabrication errors, but also mounting errors (which can be significant for thin lightweight optics), gravity release, and unanticipated environmental effects occurring on-orbit or at launch. Some other [non-adjustable] approaches do not account for mounting errors, and no other approaches can correct for changes from ground to orbit.

Working piezo films and electrode patterns have been deposited on the backside of thermally formed thin conical glass mirror segments (**Fig. 4.2-1(b)**) (Wilke 2013). The system is deterministic: measured influence functions are repeatable and agree with modeled influence functions to within the metrology noise (Cotroneo 2012). Computer simulations using modeled influence functions and representative mounted mirror data are consistent with correcting ~ 7 arc sec HPD Wolter-I mirror pairs to < 0.5 arc sec HPD (Aldcroft 2012).

Significant technology development is still required. The objective of the current work is to produce an aligned, mounted, figure corrected pair of mirror segments at the 0.5 arc sec level. Continuing efforts are required to (1) optimize the shape and pattern of the electrodes to optimize the shape of the influence functions, (2) verify PZT lifetime via real-time testing (accelerated life tests indicate lifetimes of > 10²–10³ years), (3) improve PZT stability via the use of dopants, (4) develop flight-like mounting and optimize the mounting constraints (which also affect the shape of the influence functions), and (5) complete the development of the ZnO transistor technology for the integrated on-cell electronics.

4.2.1.2 Magneto-strictive adjustable optics

This is an approach to mirror figure modification that can be applied to thin walled ($\sim 100\text{--}400$ micron thickness) optics to improve the near net shape of the mirror as well as the mid-frequency ($\sim 2\text{--}10$ mm length scales) ripple. It involves sputter deposition of a magnetic smart material (MSM) film onto a magnetically hard material (one that retains a magnetic field, e.g., the material in hard disk drives). The MSM material exhibits strains about 400 times stronger than ordinary ferromagnetic materials. The deformation process involves a magnetic write head which traverses the surface, and under the guidance of active metrology feedback, locally magnetizes the surface to impart strain where needed.

Experiments have been conducted using 0.14 mm thick electroformed Ni test mirrors 20 mm long by 5 mm wide, and glass test samples 0.1 mm thick (Ulmer 2012). Changes in curvature corresponding to a deflection of about 6 μm over 20 mm are seen in the Ni with a 1 μm thick MSM film. Deflections of ~ 0.86 μm over 20 mm are seen in 145 μm thick glass beams with a 0.11 μm thick MSM film (Jay 2010). This suggests sufficient stress can be produced in the Ni mirror approach and perhaps in glass of the requisite 0.2 mm to 0.4 mm thickness (necessary for handling and mounting), to be determined by further testing.

The advantage of this approach is that in principle, with no predefined actuator cells, the Nyquist limit for error correction is limited by the size of the magnetic field “write” head, and the structural mechanics (i.e., enough stress generated to produce large enough deflections as a function of mirror substrate material, thickness, error length, and MSM thickness). These experiments are in their earliest phase, the Ni results are promising, and alternative, and/or thicker, MSM’s might increase the available range of error correction in glass.

4.2.2 Differential Deposition

An alternative approach to figure correction is termed ‘Differential Deposition’ (Ramsey et al 2011) and utilizes physical vapor deposition to coat the inside of a mirror shell to smooth out figure imperfections. The inside of the mirror is first measured and compared with the desired figure profile to determine a ‘hit map’—this hit map represents the coating profile that must be applied to effect the correction. The desired coating profile is obtained by translating the mirror shell over a precisely defined ‘beam’ of sputtered material, using a computer simulation to derive an appropriate velocity profile. The process is shown schematically in **Fig. 4.2–2**.

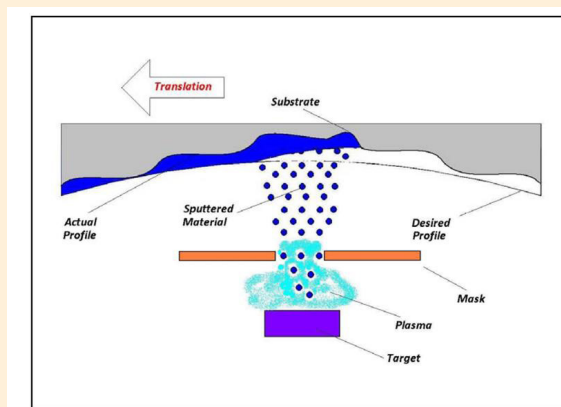


Figure 4.2–2. Differential deposition process

The attraction of the differential deposition technique is that it can be used on any type of optic, segmented or full shell, and potentially on both unmounted and mounted mirror shells. It can also be used to potentially correct a

wide range of spatial scales and has heritage in that it has been used to correct synchrotron optics down to sub-micro-radian-level slope errors.

Simulations show that in principle extremely high angular resolution, below 1 arcsec, can be achieved using differential deposition. In practice, there are sources of errors that could affect the level of improvement. These include variations of the sputtered beam profile along the length of the mirror shell, particularly for short-focal-length mirrors that have large tapers, and beam nonuniformities and temporal variations. Additional sources of error include positional inaccuracies in the registration of the masks with respect to the mirror shells, uncertainties in the metrology (particularly for full-shell optics), and stress effects due to the applied coatings. In simulations, the latter two are found to be the dominant source of errors.

Proof of concept of differential deposition has been demonstrated on small-scale optics, and larger coating systems are being assembled. In parallel, investigations of stress control in suitable coating materials are underway. A complementary approach to differential deposition is also being pursued in which the substrate is moved past a mask at a constant velocity while the mask aperture width is varied (using in-vacuum electronic actuators) in accord with the ‘hit map’. In principle, multiple mask apertures can then be arranged along a line perpendicular to the direction of motion in order to simultaneously correct surface height errors in two dimensions over an entire segmented shell during each pass. Differential erosion is also being investigated, in which material is removed from the substrate using a collimated ion beam, again with electronically adjustable apertures. The optimum surface error correction procedure may involve a combination of both differential deposition and differential erosion.

4.2.3 Silicon Optics

Another approach to making arc-second-class X-ray optics is to utilize existing polishing technology, capable of fabricating mirrors with sub-arc-second angular resolution, as demonstrated by *Chandra*. Existing polishing technology, however, has two drawbacks that must be addressed before it can be used for future high throughput and high angular resolution X-ray astronomical telescopes. The first is that it is only appropriate for fabricating thick and therefore heavy mirrors, the second that it is time-consuming and expensive.

To address the first drawback single crystal silicon replaces the usual glass or glass ceramic as the mirror substrate material (Zhang 2011). In a single crystal every atom is properly located on its lattice point, and as such, is at its lowest energy state and free of internal stress. This lack of internal stress makes it possible for a thick and heavy mirror to be fabricated and then light-weighted while preserving the figure, provided that surface and sub-surface damage caused by the light-weighting process is properly removed (Zhang 2012). **Figure 4.2–3** shows an experimental result that demonstrates the validity of this approach.

While there is no doubt that polishing can meet any reasonable angular resolution requirement, there is much development needed to meet the schedule and cost requirements of polishing the $\sim 10^3$ m² mirror surface area necessary for a future mission. Fortunately polishing technology has advanced by leaps and bounds in the fifteen years since the *Chandra* mirrors were made. Although these advances have been exclusively targeted for making normal incidence mirrors, they can be readily adapted to making grazing incidence X-ray mirrors. Modest and consistent investment in this area in coming years would enable the reduction in the fabrication time and cost to levels comparable to those of replication processes on a per unit mirror area basis.

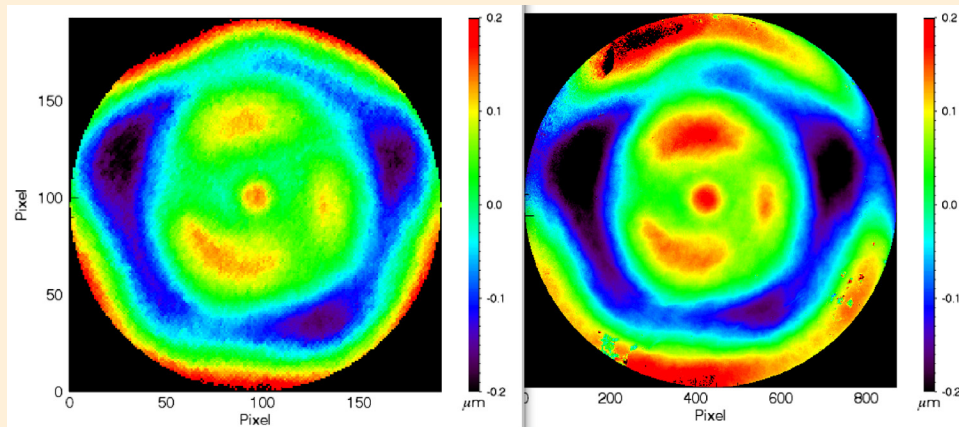


Figure 4.2-3. The image on the left is from a flat single crystal silicon mirror 100mm in diameter and 25mm thick. The image on the right is from the same mirror after it has been light-weighted to 0.40mm thickness, a factor of more than 60 reduction. The differences between these two images show that the figure is preserved at the sub-arc-second level. The similarities between them demonstrate the validity of making extremely lightweight mirrors by polishing and light-weighting single crystal silicon, which is abundantly and inexpensively available because of the semiconductor industry.

4.2.4 Ion Implantation

Implanting high-energy ions into a substrate imparts sub-surface compressive stresses while leaving the surface largely undamaged. The stress causes deformation of the substrate figure, and is controllable by changing the number of ions implanted. This allows precise modification of the mirror figure, using a low-cost and fast process.

Experiments have shown an approximately linear relationship between implant dose and stress, in both glass and silicon, over a large range of implant doses. Significant reduction of spherical curvature in silicon substrates has also been demonstrated in these experiments. In addition to spherical curvature, other figure errors could be corrected by implanting in various dose patterns on the front and back surfaces of the substrate. Modeling suggests ion implantation could reduce figure errors substantially.

Ion implantation could also be used for figure correction after a reflective coating has been applied. Monte Carlo simulations suggest a 20 nm Iridium layer would have little effect on the implant depth profile; and X-ray reflectivity measurements of D-263 substrates before and after implantation suggest micro-roughness is not significantly affected by ion implantation. Ion implantation is therefore a promising method of correcting figure errors that arise both from slumping or other substrate shaping processes, and from reflective coatings.

4.3 Detector Technology

4.3.1 Calorimeters and Read-out Electronics

Section 3.2 described the roadmap to bring the technical readiness level of micro-calorimeter arrays to TRL-6 with the capabilities needed for the focal planes envisaged for mission concepts such as an X-ray probe. In the longer term, there remains tremendous potential for a more advanced micro-calorimeter array, with a much wider field-of-view, utilizing pixels with higher energy resolution and angular resolution. **Figure 4.3-1** shows a plot of the largest number of TES pixels in a fully instrumented array as a function of time over the past 16 years, and extrapolates

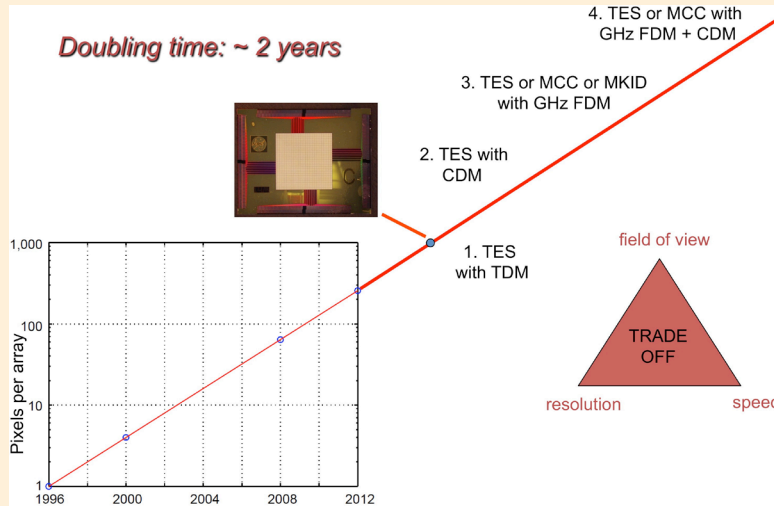


Figure 4.3–1. This figure shows the Moore's Law plot for the number of TESs in a fully functioning instrument, and extrapolates the current rate of evolution for the next couple of decades.

to predict the number of TESs one might reasonably expect in micro-calorimeter arrays with continued research funding. The doubling time for the number of pixels is ~2 years. Even at this rather modest development rate, it is not unreasonable to expect arrays with hundreds of thousands of TESs to be developed over the next two decades. Evolving the Hydra concept described in **Section 3.2.3.5** so that ~10–30 pixels can be read out by a single TES and incorporating these into the new multiplexed readout schemes means that mega-pixel micro-calorimeter arrays are very realizable. Hydras with 9 absorbers attached have already been demonstrated.

As indicated on **Figure 4.3–1**, the number of TESs that it will be possible to read out will be highly dependent upon the evolution of new multiplexing technologies. There will be a very natural evolution of these. The current time-division multiplexing (TDM) will evolve to code-division multiplexing (CDM) (Stiehl 2012) involving similar switching speeds (bandwidth) and electronics as TDM but with a more efficient use of the bandwidth to provide more densely packed information within the available bandwidth. The readout will evolve next to frequency domain multiplexing (FDM) in the GHz frequency range (Mates 2008), the first demonstrations of which have already begun. Finally it will be possible to integrate the CDM approach with GHz FDM to potentially read out hundreds of thousands of TES signals with each readout channel.

With further development, the energy resolution capabilities of micro-calorimeters will continue to improve. It is likely that higher than 1 eV energy resolution (FWHM) will eventually be achievable while measuring 6 keV photons. Magnetically coupled micro-calorimeters (MCCs) are one of the leading new micro-calorimeter technologies being developed with this potential (Bandler 2012). This type of detector appears to have greater energy resolution potential than TESs for a given temperature of operation. It incorporates a non-dissipative (no heat generated) read-out and therefore has potential for producing very large arrays without encountering limits from large amounts of heat being generated within the array. New modes of operation for TESs also hold great potential for improved energy resolution. The use of magnetically tuned TESs (Sadleir 2013) could lead to TESs also having sub-eV energy resolution across the X-ray band. Another low temperature detector technology under development with high energy resolution potential and very high multiplexing potential is the microwave kinetic inductance detector (MKID) (Mazin 2008). For this type of device to demonstrate high energy resolution with X-rays, uniform thermalization of super-conducting absorbers is necessary, something that has so far proven experimentally challenging.

As depicted by the triangle in **Fig. 4.3–1**, there will always exist a trade off between micro-calorimeter energy resolution, field-of-view (number of pixels being multiplexed), and X-ray count rate capability. Depending upon the application, these capabilities can be optimized for different regions of this triangle, and there remains a large amount of research needed to reach the limits of this large phase space of capabilities.

4.4 Gratings Technology

4.4.1 Reflection Gratings

The near-term Off-Plane X-ray Grating Spectrometer (OP-XGS) technology development is discussed in **Section 3.3**. These near-term developments work toward producing high throughput grating arrays capable of achieving spectral resolving powers of at least 3000 ($\lambda/\Delta\lambda$). A long-term technology roadmap for the OP-XGS must drive toward higher spectral resolving power while maintaining sensitivity.

Advances in X-ray optics point to the possibility of arc-second class optics. Fully utilizing the high angular resolution would enable higher spectral resolving power given that the line spread function (LSF) is dependent on the telescope focus. However, to maintain the fine focus, the gratings must not introduce any aberrations due to imprecise groove profiles or poor alignment. At a resolving power of 3000, current technologies are capable of sculpting the appropriate groove profile and aligning the gratings within an array with adequate accuracy. Going to higher resolving power will require finer control on the distribution and shape of the grooves. The OP-XGS utilizes radial, blazed gratings. The groove density increases along the groove direction to produce a converging, radial profile that matches the convergence of the telescope beam. This results in a subtle change in density over the typical size of a grating (~100 mm), which is currently being approximated by a series of progressively increasing density sections of parallel grooves (McEntaffer 2013). This approximation may not suffice for higher resolving power. The major technologies necessary to increase the fidelity of the groove profile are available through the semi-conductor industry. Electron beam lithography has made large improvements in feature size control over the last decade to go from tens of nanometers to just a few nanometers per feature. If this technique can produce sub-nanometer features in the next ten years then the required groove profile for ultra-high spectral resolving power can merely be written into the grating substrate. It is necessary to continue following the developments of various lithographic techniques and understanding their utility in production of X-ray diffraction gratings. As for alignment, the current technologies are not being pushed to their limits to achieve necessary tolerances. A factor of 2–3 increase in resolving power can still be met with these methods. However, projections for an order of magnitude improvement in resolving power, if desirable, will require an improvement in grating attitude control. This can be met through a combination of finer substrate figure control and higher resolution alignment stage control.

4.4.2 Transmission Gratings

CAT grating and spectrometer technology development for a “Probe-class” X-ray mission has already been described in **Section 3.4**. With arcsecond-class angular resolution it is conceivable to build transmission grating spectrometers with resolving power of $R = \lambda/\Delta\lambda = 10,000$. Transmission gratings are well positioned to take advantage of improved telescope angular resolution due to their relative alignment insensitivity and undistorted 0th order transmission (available to other focal plane instruments), and of increased aperture sizes due to their low mass. However, resolution limiting terms that can be ignored for $R = 3000$ spectrometer designs will have to be revisited and tightened. Examples are aberrations that can be corrected through grating period chirp, undesired variations from the ideal grating period, precision of alignment methods, and alignment stability. Further technology development will therefore be required in variable-period patterning, grating facet stress control and alignment, as well as assembly. Resolving power can be increased with larger blaze angles. This could be achieved

through coating of CAT gratings with high-Z materials via atomic layer deposition, which is another area of future technology development.

4.4.3 Silicon Detectors – Active Pixel Sensor Instrument (APSI)

In order to obtain a large field of view and excellent spatial resolution, while simultaneously obtaining moderate spectral resolution, large-format silicon sensors with small pixels are required. At present, CCDs are the state-of-the-art choice for this application. However, the next generation of detectors will need several characteristics that can not be achieved by current or planned CCDs: (1) a large numbers of pixels (>10 Mpixels) to achieve desired resolution over large FOV, (2) very fast readout (<10 ms equivalent frame rates) to avoid pile-up from large collecting area missions of the future, (3) more radiation hardness (> 100 krad) than current CCDs to avoid degradation of detectors over nominal mission lifetimes, and (4) lower operating power than current CCDs to enable realistic power budgets for large format detectors. All of these requirements suggest active pixel sensors (APS) as Si detectors to replace CCDs as the standard for large format X-ray detectors. Active pixel sensors can be optimized for the grating detectors that capture the dispersed X-ray spectrum and separates overlapping orders, with a pixel size and speed well matched to the grating dispersion and expected counting rates.

Currently, several groups are working on three distinct approaches to active pixel sensor development, using either bulk monolithic CMOS technology or hybrid CMOS technology. Each of these efforts is to develop a technology that can achieve all the requirements simultaneously.

5 Technology Development Management

It is to be noted that this document does not represent an official response to NASA Procedural Requirements for technology development plans set for in documents: 7120.5e, Space Flight Program and Project Management; 7500.2, NASA Technology Commercialization Policy, or 7500.1, NASA Technology Commercialization Process for Technology Utilization. This document is not intended to be of sufficient detail to support an official project formulation technology development management effort; i.e., this document is not intended to be a mission specific Technology Development Plan, which will be needed if an X Ray Probe class mission is selected in 2015.

The technology development roadmaps discussed in this document are sufficient in detail to estimate cost and schedule required for all the technologies to reach TRL 6 by 2020.

The following paragraphs discuss management of these technologies during their lifetime in the SAT program, and if selected as part of a mission, their lifetime as a mission-specific directed technology development effort.

Technology development management shall be in accordance with the PCOS Technology Management Plan (TMP), Document 440-PLAN-0012. In summary, both competed (e.g., SAT development) and directed technology development for the mission (study or project) will be matured with oversight from the PCOS PO in accordance with the TMP. As noted in **Section 2**, SAT development is expected prior to an X-ray mission selection, whereas directed technology development follows mission selection.

SAT development is managed by the PO and incorporates a set of reporting and assessment that includes kickoff and annual status presentations and bi-monthly and mid-year written reports.

Directed technology development would be managed by the X-ray Astrophysics Probe Project Manager (PM), who shall provide the PO with a technology development report annually. For directed technologies, the Technology Management Board (TMB) makes recommendations to the PM regarding future funding and/or other next step actions.

In both the SAT and directed technology development environments, progress of the technologies through the TRL maturation process is assessed by the TMB. The TMB consists of senior members from the PCOS PO and NASA HQ, together with subject matter experts. This assessment includes verification that the technology is at a specific TRL level, including readiness to advance to the next TRL. The TMB may also recommend future actions in support of the development efforts. For SAT projects, the TMB makes recommendations to HQ regarding future funding based on progress as gauged by completion of identified milestones and the quality of the results.

The techniques required to mature technologies to TRL-4 and TRL-5 are mostly generic, i.e., they can be developed without specific reference to a particular mission or mission design. For TRL-6 demonstration, however, specific mission and/or mission subsystem design information and modeling may be necessary to derive the proper environmental conditions necessary to achieve successful TRL-6 demonstration. In the event such information is available, specific mission design data will be used during TRL-6 testing; however, if specific mission information is unavailable, document GSFC-STD-7000, General Environmental Verification Specification, will be used as the source document for environmental loads for TRL-6 demonstration; data will be selected from the document for TRL-6 testing that would envelop expected environments for the mission. If an X-ray Astrophysics Probe-class mission is selected in 2015, the PM team will develop a mission-specific TDP that expands on the approaches outlined in this document. The TDP will comply with the standards defined in NPR 7120.5.

The Project TDP milestones shall be quantifiable and represent steps to achieving higher TRL. Completion of the milestones initiates a TRL peer review by the TMB where the technology developer is asked to present and justify the TRL achievement. TRL definition is per NPR 7120.8, Appendix J, and TRL achievement evidence needs to be supported by data, be reproducible, quantitative, and objective.

6 Risk Management

While under SAT auspices, risk management of the technology development efforts is the responsibility of the SAT PIs. The means and methods of the PIs' risk management approach is governed by their home institutions' policies and the accepted SAT proposal.

When technology development transitions from supported by SAT to directed funding, risk management becomes the responsibility of the Project Office. Risk management in this case will be in accordance with NASA NPR 7120.5e, NASA Program and Project Management Processes and Requirements Document, and NASA NPR 8000.4 Risk Management Procedures and Guidelines.

7 Conclusions

The NWNH Decadal Survey report, and the subsequent X-ray Mission Concepts Study report, identified the highest priority for X-ray astrophysics is large-area, high-resolution imaging spectroscopy. This TDR establishes a path for the technology development necessary for either a Probe-class mission selected in 2015 or for re-submission to the 2020 Decadal, which identifies the technology drivers, their funding requirements, and the associated schedule. This roadmap meets one of the Decadal's requirements regarding IXO, specifically that:

“Because of IXO’s high scientific importance, a technology development program is recommended this decade with sufficient resources—estimated to be on the order of \$200M—to prepare IXO for favorable consideration in the next survey in 2020.”

The primary technology needs are lightweight optics, high spectral resolution microcalorimeter arrays, high-throughput and high-resolution gratings, and their associated detectors. Thanks to long-term NASA-funded efforts, these key X-ray technologies have the promise of reaching flight readiness within this decade. This TDR identifies the steps required for each key technology, noting which steps are gates for future progress.

The funding requirements fit within the projected NASA Astrophysics Division's technology budget for the remainder of the decade. We note, in particular, that the anticipated future costs for these technology development efforts (\$62M, of which \$12M has already been committed) are well below the \$200M estimated from NWNH. This reduction is the result of three main factors. First, all of the key technologies have continued to advance from their status at the time of IXO's submission to the Decadal review. In some cases, TRLs have advanced by a full step, significantly decreasing the remaining effort required. Second, completely new technologies, such as the small-pixel TES detectors described herein for the Point Source Array, have allowed new approaches that reduce complexity, risk, and cost. Third, the requirements for the probes are, in some cases, substantially less stringent than the IXO requirements (e.g., AXSIO's 10-arcsec angular resolution versus IXO's 5 arcsec).

The schedule for development of all of these technologies has been devised to support a mission selection in 2015. It also retains flexibility to adjust for other possibilities, such as an ESA selection of *Athena+* or a decision not to build a Probe-class X-ray mission but rather to prepare for a high-TRL submission to the 2020 Decadal.

A brief description of relevant longer-term technologies that are not yet at or near TRL-4, but might achieve that status within a few years, has been included. In some cases, such technologies hold out promise of substantial risk or complexity reduction, as with the PSA. In other cases, such as high-resolution lightweight optics, significant improvements are possible that would allow a future mission to restore IXO science goals for the study of the high-redshift universe.

This report concludes that modest funding over the course of the next few years will advance these technologies to the level required for a mission start in 2017.

Acknowledgements

This document could not have been prepared without significant support from a large number of contributors. In particular, we would like to thank the following people for their efforts:

Simon Bandler (UMCP/NASA/GSFC)

Mark Bautz (MIT)

Abe Falcone (PSU)

Ralf Heilmann (MIT)

Richard Kelley (NASA/GSFC)

Caroline Kilbourne (NASA/GSFC)

Randall McEntaffer (U-Iowa)

Brian Ramsey (NASA/MSFC)

Paul Reid (CfA)

Mark Schattenburg (MIT)

Mel Ulmer (Northwestern U)

William Zhang (NASA/GSFC)

Acronyms

AAAC	Astronomy and Astrophysics Advisory Committee
AACCD	Advanced Architecture CCDs
ACIS	Advanced CCD Imaging Spectrometer
ADAP	Astrophysics Data Analysis Program
AEGIS	Astrophysics Experiment for Grating and Imaging Spectroscopy
AFTA	Astrophysics Focused Telescope Assets
AGN	Active Galactic Nuclei
AIP	Astrophysics Implementation Plan
ALD	Atomic Layer Deposition
AO	Announcement of Opportunity
APEX	Astrophysics Explorer
APRA	Astrophysics Research and Analysis program
ASCA	Advanced Satellite for Cosmology and Astrophysics
ASIC	Application Specific Integrated Circuits
Athena	Advanced Telescope for High Energy Astrophysics
ATP	Astrophysics Theory Program
AXSIO	Advanced X-ray Spectroscopic Imaging Observatory
BESSY	Berliner Elektronenspeicherring-Gesellschaft für Synchrotronstrahlung
BPA	Board on Physics and Astronomy
CAA	Committee on Astronomy and Astrophysics
CADR	Continuous Adiabatic Demagnetization Refrigerator
CAT	Critical-Angle Transmission
CATXGS	Critical-Angle Transmission X-ray Grating Spectrometer
CCD	Charge-Coupled Device
CDM	Code Division Multiplexing
CMB	Cosmic Microwave Background
CMOS	Complementary Metal-Oxide Semiconductor
COPAG	Cosmic Origins Program Analysis Group
COR	Cosmic Origins
CST	Community Science Team
CTE	Coefficient of Thermal Expansion
DOE	Department of Energy
DRIE	Deep Reactive-Ion Etch
DRM	Design reference Mission
DRS	Disturbance Reduction System
DSIAC	Decadal Survey Implementation Advisory Committee
EDM	Electric Discharge Machining
ESA	European Space Agency
EX	Explorer-class
ExEP	Exoplanet Exploration
ExoPAG	Exoplanet Exploration Program Analysis Group
FINESSE	Fast Infrared Exoplanet Spectroscopy Survey Explorer
FMA	Flight Mirror Assembly
FPA	Focal Plane Assembly

FWHM	Full Width Half Maximum
FY	Fiscal Year
GAO	Government Accountability Office
GAS	Grating Array Structure
GO	Guest Observer
GSFC	Goddard Space Flight Center
GUSSTO	Galactic/extragalactic ULDB Spectroscopic/Stratospheric THz Observatory
HEAO-2	High-Energy Astrophysical Observatory-2 (Einstein Observatory)
HEMT	High Electron Mobility Transistor
HETG	High-Energy Transmission Grating
HPD	Half-Power Diameter
HQ	Headquarters
HRMA	High Resolution Mirror Assembly
HST	Hubble Space Telescope
I-CDM	Current-Steering CDM
IR	Infrared
IXO	International X-ray Observatory
JAXA	Japanese Space Agency
JDEM	Joint Dark Energy Mission
JFET	Junction Field-effect Transistor
JPL	Jet Propulsion Laboratory
JUICE	Jupiter Icy moon Explorer
JWST	James Webb Space Telescope
L1	Level 1
L2	Level 2
LISA	Laser Interferometer Space Antenna
LSST	Large Synoptic Survey Telescope
MIDEX	Medium-class Explorer
MIT	Massachusetts Institute of Technology
MO	Mission of Opportunity
MOSFET	Metal-Oxide-Semiconductor Field-effect Transistor
MSFC	Marshall Space Flight Center
MUX	Multiplexer
N-CAL	Notional Calorimeter Mission
N-WFI	Notional Wide-Field Imager
N-XGS	Notional X-ray Grating Spectrometer
NAC	NASA Advisory Council
NASA	National Aeronautics and Space Administration
NICER	Neutron star Interior Composition Explorer
NISP	Near Infrared Spectrometer Photometer
NIST	National Institute of Standards and Technology
NODIS	NASA Online Directives Information System
NPR	NASA Procedural Requirements
NRC	National Research Council
NRO	National Reconnaissance Office
NSF	National Science Foundation
NWNH	New Worlds, New Horizons (Astro2010 Decadal Report)
OBF	Optical Blocking Filters

OMB	Office of Management and Budget
OPG	Off-Plane Grating
OPXGS	Off-Plane X-ray Grating Spectrometer
OSS	Origins of Solar Systems program
PAG	Program Analysis Group
PATR	Program Annual Technology Report
PCOS	Physics of the Cosmos PDR Preliminary Design Review
PhysPAG	Physics of the Cosmos Program Analysis Group
PI	Principal Investigator
PM	Project Manager
PO	Program Office
PSA	Point Source Array
Q	Quality (factor of a resonator)
QE	Quantum Efficiency
RF	Radio Frequency
RFI	Request for Information
RGS	Reflection Grating Spectrometer
ROSES	Research Opportunities in Space and Earth Sciences
RTF	Nancy Grace Roman Technology Fellowship program
SAG	Study Analysis Group
SAT	Strategic Astrophysics Technology
SDT	Science Definition Team
SEM	Scanning Electron Microscope
SMART-X	Square Meter Arcsecond-Resolution Telescope for X-rays
SMD	Science Mission Directorate
SMEX	Small-class Explorer
SOFIA	Stratospheric Observatory for Infrared Astronomy
SOI	Silicon-on-Insulator
SPICA	Space Infrared Telescope for Cosmology and Astrophysics
SPO	Silicon Pore Optics
SQUID	Superconducting Quantum Interface Device
SRON	SRON Netherlands Institute for Space Research
SSB	Space Studies Board
ST-7	Space Technology 7
STDT	Science and Technology Definition Team
TCAN	Theory and Computational Networks program
TDM	Time-Division Multiplexing
TDP	Technology Development Plan
TDR	Technology Development Roadmap
TES	Transition-Edge Sensor
TESS	Transiting Exoplanet Survey Satellite
TMB	Technology Management Board
TMP	Technology Management Plan
TRL	Technology Readiness Level
ULDB	Ultra-long Duration Balloon
UV	Ultraviolet
VLS	Variable-Line-Spaced
WASP	Wallops Arcsecond Pointer

WFIRST	Wide Field Infrared Survey Telescope
WHIM	Warm-Hot Intergalactic Medium
XGS	X-ray Grating Spectrometer
XMM	X-ray Multi-Mirror Mission.
XMS	X-ray Microcalorimeter Spectrometer
XRT	X-Ray Telescopes

Chemical Elements

Be	Beryllium
Bi/Au	Bismuth Gold
KOH	Potassium Hydroxide
Mo/Au	Molybdenum Gold
SiC	Silicon Carbide

Units

Å	angstrom
arcmin	arcminutes
arcsec	arcseconds
C	Celsius
cm	centimeters
cm ³	cubic centimeters
cps	counts per second
E	energy
eV	electron volt
f	frequency
F	focus
g	grams
Hz	Hertz
GHz	Gigahertz
K	Kelvin
keV	kiloelectron volt
kg	kilogram
krad (Si)	kilorads
m	meters
m ²	square meters
mK	milli-Kelvin
mm	millimeters
ms	microseconds
nm	nanometers
ns	nanoseconds
RF	radio frequency
trpw	sampling rate
T _c	Critical Temperature
μm	microns (micrometers)
V	voltage

References

- Akerib D.S., et al., 2006, “Limits on spin-dependent WIMP-nucleon interactions from the Cryogenic Dark Matter Search”, *Phys. Rev. B* 73, 011102
- Aldcroft, T.L., et al., 2012, “Simulating correction of adjustable optics for an X-ray telescope,” *SPIE Proc.*, 8503, 85030F
- Astro2010 Decadal Report, “New Worlds, New Horizons”, NRC Press
- Bandler, S. R., et al., 2008, “Performance of TES X-ray Microcalorimeters with a Novel Absorber Design”, *J. of Low Temp. Phys.* 151 1-2 (2008) 400
- Bandler, S. R., et al., 2010, “High Spectral Resolution, High Cadence, Imaging X-ray Microcalorimeters for Solar Physics”, *Proc. SPIE* 7732, 773238, 2010
- Bandler, S. R., et al., 2012, “Advances in Small Pixel TES-based X-ray Microcalorimeter Arrays for Solar Physics and Astrophysics”, submitted to IEEE proceedings of Applied Superconductivity conference, Portland, 2012
- Bandler, S.R., *et al.*, 2012, “Magnetically Coupled Microcalorimeters”, *Journal of Low Temperature Physics* Volume: 167 Issue: 3-4 Pages: 254-268 DOI:10.1007/s10909-012-0544-4
- Cash, W., 1983, “X-ray spectrographs using radial groove gratings”, *Appl. Opt.*, 22, 3971
- Cash, W., 1991, “X-ray optics. II - A technique for high resolution spectroscopy”, *Appl. Opt.*, 30, 1749
- Chan, K.-W. et al., 2010 , “Mounting and alignment of IXO mirror segments,” *SPIE*, Volume 7732, pp. 77323Q-77323Q-11
- Chan, K.-W. et al., 2011 , “Metrology of IXO mirror segments,” *SPIE*, Volume 8147, 39
- Chang, C-H, et al. 2004, “High fidelity blazed grating replication using nanoimprint lithography”, *J. Vac. Sci. Tech. B.*, 22(6), 3260
- Chervenak, J. A., et al., 1999, “Superconducting Multiplexer for Arrays of Transition Edge Sensors”, *Appl. Phys. Lett.*, 74, 4043-4045
- Chervenak, J. A., et al., 2012, “Fabrication of Microstripline Wiring for Large Format Transition Edge Sensor Arrays”, *J. Low Temp. Phys.* (on-line first) DOI 10.1007/s10909-012-0552-4
- Cotroneo, V., *et al.*, 2012, “Adjustable grazing incidence x-ray optics based on thin PZT films,” *SPIE Proc.* 8503, 850309
- Craig, W.A. et al., 2011 , “Fabrication of the NuSTAR flight optics,” *Proc. SPIE*, Vol. 8147, pp. 81470H-81470H-14

- Eckhart, M. E., et al., 2012, “Kilopixel X-ray Microcalorimeters Arrays for Astrophysics: Device Performance and Uniformity”, *J. Low Temp. Phys.* 167, 732-740
- Evans, T. C. et al., 2010 , “Arc-second alignment and bonding of International X-Ray Observatory mirror segments, “ *SPIE*, Vol. 7732, pp. 77323Z-77323Z-11
- Freeman, M. D. et al., 2010 , “Advances in the active alignment system for the IXO optics, “ *SPIE*, Vol. 7732, pp. 773243-773243-7
- Heilmann, R. K., Ahn, M. Gullikson, E. M. and Schattenburg, M. L., 2008, “Blazed high-efficiency x-ray diffraction via transmission through arrays of nanometer-scale mirrors.” *Optics Express* 16: 8658
- Heilmann, R. K., Chen, C. G., Konkola, P. T. and Schattenburg, M. L., 2004, “Dimensional metrology for nanometer-scale science and engineering: Towards sub-nanometer accurate encoders.” *Nanotechnology* 15: S504-S511
- Heilmann, R.K., Ahn, M., Bautz, M. W., Foster, R., Huenemoerder, D., Marshall, H., Mukherjee, P., Schattenburg, M., Schulz, N. and Smith, M., 2009, “Development of a critical angle transmission grating for the International X-ray Observatory.” *Proc. SPIE* 7437
- Irwin, K. D., et al., 2010, “Code-division Multiplexing of Superconducting Transition-edge Sensor Arrays”, *Supercond. Sci. and Technol.* 23, 034004
- Jay, J.-P., *et al.*, 2010, “Direct and inverse measurement of thin films magnetostriction,” *J. Magnetism and Magnetic Mat.*, **322**, 2203.
- Kelley RL, et al., 2007, “The Suzaku high resolution X-ray Spectrometer”, *PASJ* 59, S77
- Kilbourne, C. A., et al., 2006, “Analysis of the Suzaku/XRS background”, *Nucl. Instr. and Meth. A* 559, 620
- Kilbourne, C. A., et al., 2008, “Multiplexed Readout of Uniform Arrays of TES X-ray Microcalorimeters Suitable for Constellation-X”, *Proc. SPIE* 7011, 701104
- Kilbourne, C. A., 2010, “Noise Budget for the X-Ray Microcalorimeter Spectrometer (XMS) Core Array”, NASA/GSFC document ID IXO-TN-001141, NTRS ID 20100026671. http://ntrs.nasa.gov/archive/nasa/casi.ntrs.nasa.gov/20100026671_2010028449.pdf
- Kilbourne, C. A., & Doriese, W., 2010, “Technology Development Plan for the Baseline Detector System of the X-Ray Microcalorimeter Spectrometer (XMS) of the International X-Ray Observatory (IXO)”, NASA/GSFC document ID IXO-PLAN-001084, NTRS ID 20100027322. http://ntrs.nasa.gov/archive/nasa/casi.ntrs.nasa.gov/20100027322_2010028450.pdf
- Lehan, J. P. et al., 2009 , “Progress toward a complete metrology set for the International X-ray Observatory (IXO) soft x-ray mirrors, “ *SPIE*, Vol. 7437, 24
- Lotti S, et al., 2012, “Estimate of the impact of background particles on the X-Ray Microcalorimeter Spectrometer on IXO”, *Nucl. Inst. and Meth. A*, 686, 31-37
- Mates J.A.B., *et al.*, 2008, “Demonstration of a multiplexer of dissipationless superconducting quantum inter-

ference devices”, *Appl. Phys. Lett.* **92**, 023514

Maula, J. et al., 2010, “Atomic layer deposition (ALD) for optical nanofabrication,” SPIE Vol. 7591, 18

Mazin, B.A. *et al.*, 2008, “Optical/UV and X-ray Microwave Kinetic Inductance Strip Detectors,” Proceedings of LTD-12, *J. Low Temp. Phys.*, vol **151**, pp. 537-543, 2008

McEntaffer, R. L., Osterman, S. N., Cash, W., Gilchrist, J., Flamand, J., Touzet, B., Bonnemason, F., Brach, C., 2004, “X-ray performance of gratings in the extreme off-plane mount”, Proc. SPIE, 5168, 492

McEntaffer, R. L., Cash, W., Shipley, A., 2008, “Off-plane reflection gratings for Constellation-X”, Proc. SPIE, 7011, 6

McEntaffer, R. L., et al., 2011, “Development of off-plane gratings for WHIMex and IXO”, Proc. SPIE, 8147, 52

McEntaffer, R.L., *et al.*, 2013, “First results from a next-generation off-plane X-ray diffraction grating”, *Exp. Astro.*, 10.1007/s10686-013-9338-1

Mates, J. A. B., et al., 2008, “Demonstration of a Multiplexer of Dissipationless Superconducting Quantum Interference Devices”, *Appl. Phys. Lett.* **92**, 023514

Nakajima, H., Matsuura, D., Anabuki, N., Miyata, E., Tsunemi, H., Doty, J., Ikeda, H., Takashima, T. and Katayam, H., 2009, “Performance of an Analog ASIC Developed for X-ray CCD Camera Readout System Onboard Astronomical Satellite.” *IEEE Transactions on Nuclear Science* **56**: 747-751

Oakley, P., McEntaffer, R. L., & Cash, W., 2011, “A suborbital payload for soft X-ray spectroscopy of extended sources”, *Exp. Astro.*, **31**, 23

Osterman, S. N., McEntaffer, R. L., Cash, W., & Shipley, A., 2004, “Off-plane grating performance for Constellation-X”, Proc. SPIE, 5488, 302

Ramsey, B., et al. 2011, “Improving X-ray Optics Through Differential Deposition”, White Paper submitted in response to the PCOS X-ray RFI

Sadleir, J.E., *et al.*, 2013, “Magnetically Tuned Superconducting Transition-Edge Sensors,” *IEEE Trans. on Appl. Sup.*, Issue: 99, 1 DOI: 10.1109/TASC.2013.2251391

Saha, T. et al., 2011, “Grazing incidence wavefront sensing and verification of x-ray optics performance,” SPIE, Vol. 8147, pp. 814717-814717-12

Smith, S. J., et al., 2009, “Implementation of Complex Processing Algorithms for Position-sensitive Microcalorimeters”, *Nucl. Inst. & Meth. in Phys. Res. A* **602**, 537–544

Smith, S. J., et al., 2011, “Small Pitch Transition-Edge Sensors with Broadband High Spectral Resolution for Solar Physics”, *J. Low Temp. Phys.* **167** 168–175

Stiehl, G. M., et al., 2012, “Code-Division Multiplexing for X-ray Microcalorimeters”, *Appl. Phys. Lett.* **100**, 072601

Suntharalingam, V., Rathman, R., Prigozhin, G., Kissel, S. and Bautz, M., 2007, “Back-illuminated, three-dimensionally integrated CMOS image sensors for scientific applications.” Proc. SPIE 6690

Ulmer, M.P., *et al.*, 2012, “Progress report on using magneto-strictive sputtered thin films to modify the shape of an x-ray telescope mirror,” SPIE Proc. **8503**, 85030C

Van Weers H. and Bandler S.R., 2010, “Focal Plane Assembly Trade-off Report”, SRON document ID SRON-XMS-RP-2010-008

Wilke, R.H.T., *et al.*, 2013, “Sputter Deposition of PZT Piezoelectric Films on Thin Glass Substrates for Adjustable X-Ray Optics,” *Appl. Opt.* **52**, 14, 3412

Zhang, W.W. et al., 2003, “Development of mirror segments for the Constellation-X observatory,” SPIE, Vol. 4851, pp. 503-518

Zhang, W.W. et al., 2011, “Lightweight and high angular resolution x-ray optics for astronomical missions,” SPIE, Vol. 8147, pp. 81470K-81470K-12

Zhang, W. W., et al. 2011, “Next Generation X-ray Optics: High-resolution, Light-weight, and Low- cost”, White Paper submitted in response to the PCOS X-ray RFI

Zhang, W. W., et al., 2012, “Next generation astronomical x-ray optics: high angular resolution, light weight, and low production cost,” SPIE Proc. Vol. 8443, p. 84430S